POLARIZATION MODE DISPERSION EMULATION AND THE IMPACT OF HIGH FIRST-ORDER PMD SEGMENTS IN OPTICAL TELECOMMUNICATION SYSTEMS

VITALIS MUSARA

Submitted in fulfillment of the requirements for the degree of

PHILOSOPHIAE DOCTOR

in the Faculty of Science at the Nelson Mandela Metropolitan University

December 2009

Promoter: Prof Andrew W. R. Leitch

Co-promoter: Dr Lorinda Wu

DECLARATION

I, **Vitalis Musara**, declare that this thesis is my own original work and that it has not been presented and will not be presented to any other institution for a similar or any other degree award.

Signature: ……

DEDICATION

To God and my wonderful wife Golebaone Nunu Podise Musara.

ACKNOWLEDGEMENTS

Sincere gratitude extended to Professor Andrew Leitch, promoter, and Doctor Lorinda Wu, co-promoter, for their motivation, guidance and unlimited support during my research project.

Acknowledgements extended to all members of the Nelson Mandela Metropolitan University (NMMU) Physics Department, especially the technical support staff of Dan O'Connor and Len Compton for their support.

Thanks to the NMMU Fibre Optics Group members for their support, motivation and fruitful discussions.

I am also thankful to the Telkom staff based at the Sidwell Exchange in Port Elizabeth for their advice and support towards field work data collection, which was made possible by Telkom South Africa.

Special thanks to Run Zhang of Boston Applied Technologies for excellent product support.

Financial support from Telkom South Africa Ltd, Ingoma Communications Services (Pty) Ltd, Hezeki Contracting (Pty) Ltd, MCT Telecommunications (Pty) Ltd, the National Research Foundation (NRF), the African Laser Centre (ALC) and the Technology and Human Resources for Industry Program (THRIP) is gratefully appreciated, as are scholarships that I received from the NRF and NMMU.

Lastly, special thanks to my beloved wife Golebaone Nunu, family and friends for their encouraging and unwavering support during the project.

Vitalis Musara

December 2009 *(email:Vitalis.Musara@nmmu.ac.za)*

CONTENTS

DECLARATION.....ii

DEDICATION.....iii

ACKNOWLEDGEMENTS.....iv

SUMMARY.....ix

ABBREVIATION LIST.....xi

CHAPTER 1 Introduction.....1

CHAPTER 2 Polarization effects in lightwave systems

2.1 Polarization mode dispersion.....4
2.1.1 Definition of PMD.....4
2.1.2 Factors influencing PMD.....5
I. Intrinsic perturbation.....5
a. Geometric asymmetry (imperfection) of the core.....5
b. Internal stress.....5
II. Extrinsic perturbations.....6
a. Temperature.....6
b. Wind and fibre movement.....7
c. Stress and strain.....7
d. Cabling and spooling effects.....7
III. Mode coupling.....8
2.1.3 PMD equations.....9
I. The frequency domain PMD vector equations.....10
a. The Principal states model.....10
b. PMD equation (after Gisin and Pellaux 1992).....11
II. The time domain PMD vector equation.....13
a. Time evolution PMD vector.....13
III. The spatial domain PMD vector equations.....13
a. Concatenated rules for PMD.....13
b. The PMD evolution or dynamic equations.....15
2.1.4 PMD statistics.....15
I. The FO-PMD statistics.....16
II. The SO-PMD statistics.....18
2.1.5 The autocorrelation function.....19
I. The frequency ACF.....20
II. The time ACF.....21
2.1.6 PMD compensation and mitigation.....22
2.1.7 Systems impairments due to PMD.....23
I. First-order PMD.....23
a. Pulse broadening and signal degradation.....23
b. Intersymbol interference.....24
c. Power penalty.....25
d. Bit error rate and Q-factor.....26

e. Bit rate and span limitation....26
f. Outage probability....27
II. Second-order PMD....28

2.2 Polarization dependent loss....28
2.2.1 Definition of PDL and its origins....29
2.2.2 Implications of PDL and its mitigation....30

2.3. PMD and PDL interaction....30
2.3.1 Combined effects of PMD and PDL....30
2.3.2 PMD and PDL interaction evolution equations....31

CHAPTER 3 Aspects of polarization mode dispersion emulation
3.1 The need for PMD emulation....33

3.2 Requirements for a PMD emulator....33
3.2.1 Autocorrelation function....33
3.2.2 FO-PMD statistics....34
3.2.3 Higher-order PMD statistics....34
3.2.4 Stability....34
3.2.5 Low loss....34
3.2.6 Simplicity....35

3.3 PMD Emulator components and tools....35
3.3.1 Optical delay component....35
I. Polarization maintaining fibres....35
II. Birefringent crystals....36
III. Delay line....37
3.3.2 Polarization orientation control components....38
I. Acrobat polarization rotator....38
II. Faraday rotator....38
III. Lithium niobate polarization controller....39
IV. Fibre-squeezer polarization controller....40
V. Polarization switch....40
3.3.3 Simulation....40

3.4 Types of PMD emulators....41
3.4.1 Fixed birefringent sections and polarization orientations....42
3.4.2 Rotatable birefringent sections or polarization orientations....43
3.4.3 Uniform scattering of polarization orientations....46
3.4.4 Tuneable birefringence and fixed polarization orientations....47
3.4.5 All elements tuneable....49
3.4.6 Both fixed birefringent sections and rotatable polarization orientations....50

3.5 Limitations of PMD emulators....51

CHAPTER 4 Measurement techniques
4.1 The frequency domain technique....53
4.1.1 The JME for PMD measurement....54
4.1.2 The JME for PDL measurement....56

4.2 The time domain interferometry method.....57
4.2.1 Michelson interferometer.....57
4.2.2 The General interferometry technique.....59

CHAPTER 5 Characterising deployed fibres for PMD
5.1 PMD measurements.....62
5.1.1 PMD variation with wavelength and time in buried fibres.....64
5.1.2 PMD variation with time in aerial fibres.....68
5.2 Monitoring the state of polarization of light in optical fibres.....69

CHAPTER 6 PMD emulator design and implementation
6.1 PMD emulators with fixed birefringent sections and polarization orientations.....73
6.1.1Emulator with increase in both FO- and SO-PMD.....74
6.1.2 Emulator with inverse trend in FO- and SO-PMD.....77
6.1.3 Emulator with fixed FO-PMD but varying SO-PMD.....80
I. Operational principle of the PMD emulator.....81
II. PMD emulator characteristics.....82
III. The impact of the high first-order PMD segment on PMD statistics.....84

6.2 Tuneable delay element.....86

6.3 Emulator with fixed birefringent sections and rotatable polarization orientations.....89
6.3.1 Emulator design and its operation.....89
6.3.2 PMD characteristics of the emulator with wavelength.....93
6.3.3 PMD characteristics of the emulator with time.....98

6.4 Emulator with fixed birefringent sections plus tuneable delay element and rotatable polarization orientation.....100
6.4.1. Design considerations for the emulator.....100
6.4.2. Characteristics of the PMD emulator.....103

6.5 Impact of PDL in PMD emulators.....106

CHAPTER 7 Impact of a high first-order PMD Section in optical network systems
7.1 Impact of a HiFO-PMD section on PMD.....110
7.1.1 FO- and SO-PMD.....111
7.1.2 GINTY interferogram and JME spectrum in the presence of a HiFO-PMD section.....112

7.2 Impact of a HiFO-PMD section on the output SOP.....115

7.3 Impact of a HiFO-PMD section on system performance.....119

CHAPTER 8 Conclusions
8.1 Deployed fibre characterisation.....124

8.2 PMD emulators.....125

8.2.1 Emulator with an increase in both FO- and SO-PMD.....125
8.2.2 Emulator with inverse trend in FO- and SO-PMD.....125
8.2.3 Emulator with fixed FO-PMD but varying SO-PMD.....125
8.2.4 Tuneable delay element.....126
8.2.5 Emulator with fixed birefringent sections and rotatable polarization orientations.....126
8.2.6 Emulator with fixed SO-PMD and varying FO-PMD.....126

8.3 The impact of PDL in PMD emulators.....127

8.4 The impact of a HiFO-PMD section in optical network systems.....127

APPENDIX I Poincaré sphere and Stokes parameters.....129

APPENDIX II Polarization-optical time domain reflectometry method.....132

APPENDIX III Specifications of components used in experimental work.....134

APPENDIX IV Research outputs of the author.....135

REFERENCES.....137

SUMMARY

In this study, focus is centred on the measurement and emulation of first-order (FO-) and second-order (SO-) polarization mode dispersion (PMD). PMD has deleterious effects on the performance of high speed optical transmission network systems from 10 Gb/s and above. The first step was characterising deployed fibres for PMD and monitoring the state of polarization (SOP) light experiences as it propagates through the fibre. The PMD and SOP changes in deployed fibres were stochastic due to varying intrinsic and extrinsic perturbation changes. To fully understand the PMD phenomenon in terms of measurement accuracy, its complex behaviour, its implications, mitigation and compensation, PMD emulation is crucial.

This thesis presents emulator designs which fall into different emulator categories. The key to these designs were the PMD equations and background on the PMD phenomenon. The cross product from the concatenation equation was applied in order to determine the coupling angle β (between 0^o and 180^o) that results in the SO-PMD of the emulator designs to be either adjustable or fixed. The digital delay line (DDL) or single polarization maintaining fibre (PMF) section was used to give a certain amount of FO-PMD but negligible SO-PMD. PMF sections (birefringent sections) were concatenated together to ensure FO- and SO-PMD coexist, emulating deployed fibres. FO- and SO-PMD can be controlled by altering mode coupling (coupling angles) and birefringence distribution.

Emulators with PMD statistics approaching the theoretical distributions had high random coupling and several numbers of randomly distributed PMF sections. In addition, the lengths of their PMF sections lie within 20% standard deviation of the mean emulator length. Those emulators with PMD statistics that did not approach the theoretical distributions had limited numbers of randomly distributed PMF sections and mode coupling. Results also show that even when an emulator has high random mode coupling and several numbers of randomly distributed PMFs, its PMD statistics deviates away from expected theoretical distributions in the presence of polarization dependent loss (PDL). The emulators showed that the background autocorrelation function (BACF) approaches zero with increasing number of randomly mode coupled fibre sections. A zero BACF signifies that an emulator has large numbers of randomly distributed PMF sections and its presence means the opposite. The availability of SO-PMD in the emulators made the autocorrelation function (ACF)

asymmetric. In the absence of SO-PMD the ACF for a PMD emulator is symmetric. SO-PMD has no effect on the BACF.

Polarization-optical time domain reflectometry (P-OTDR) measurements have shown that certain fibre sections along fibre link lengths have higher FO-PMD (HiFO-PMD) than other sections. This study investigates the impact of a HiFO-PMD section on the overall FO- and SO-PMD, the output state of polarization (SOP) and system performance on deployed fibres (through emulation). Results show that when the wavelength-independent FO-PMD vector of the HiFO-PMD section is greater than the FO-PMD contributions from the rest of the fibre link, the mean FO-PMD of the entire link is biased towards that of the HiFO-PMD section and the SO-PMD increases ($\beta \neq 0^o$ or 180^o) or remains fixed ($\beta = 0^o$ or 180^o) depending on the coupling angle β between the HiFO-PMD section and the rest of the fibre link. In addition, the FO-PMD statistics deviates away from the theoretical Maxwellian distribution. However, experimental results show that the HiFO-PMD section has negligible influence on the SO-PMD statistical distribution.

An increase in the amount of FO-PMD on a HiFO-PMD section reduces the output SOP spread to a given minimum, in this study the minimum was reached when the HiFO-PMD $\geq$ 35 ps. However, the outcome of the output SOP spread depends on the location of the HiFO-PMD section along the fibre link length. It was found that when the HiFO-PMD section introduces SO-PMD, the bit error rate (BER) is much higher compared to when it does not introduce SO-PMD.

Keywords: *birefringence, first-order polarization mode dispersion, second-order PMD, polarization dependent loss, PMD emulation, optical fibre.*

ABBREVIATION LIST

ACF	autocorrelation function
ASE	amplified spontaneous emission
BACF	background autocorrelation function
BER	bit error rate
CD	chromatic dispersion
DDL	digital delay line
DGD	differential group delay
DWDM	dense wavelength division multiplexing
DOP	degree of polarization
EDFA	erbium doped fibre amplifier
FO-PMD	first-order polarization mode dispersion
FWHM	full-width at half-maximum
GINTY	General Interferometry Technique
HiBi	high birefringence
HiFO-PMD	high first-order PMD
HWP	half waveplate
JME	Jones matrix eigenanalysis
NRZ	non-return to zero
PC	polarization controller
PCD	polarization-dependent chromatic dispersion
PCM	pulse coded modulation
PDF	probability density function
PDL	polarization dependent loss
PMD	polarization mode dispersion
PMF	polarization maintaining fibre
P-OTDR	polarization optical time domain reflectometry
PSP	principal state of polarization
SMF	single mode fibre
QWP	quarter wave-plate
RMS	root mean square
SOP	state of polarization
SO-PMD	second-order PMD
WDM	wavelength division multiplexing

CHAPTER 1

INTRODUCTION

The first and second Industrial Revolution from the late 18th century to the early 19th century revolutionised the way human beings work by introducing machines and new organisational forms. According to John Chambers, Chief Executive Officer (CEO) of Cisco Systems Inc, we are now in the Information Age – The third Industrial Revolution (FitzGerald and Dennis 2002). The Third Industrial Revolution is centred on revolutionising the way people work through networking and information (data, voice and video) communication.

A study conducted by the University of Minnesota in the United States of America, reports that internet traffic has been increasing to the point of almost doubling every year since 1990 (Odlysko 2003). Modern telecommunication companies are up to date with the exponential growth of bandwidth consumption and have turned to higher data transmission mechanisms through exploiting improved semiconductor laser sources (Hayashi *et al.* 1970) together with advanced low-loss optical fibre networks (Kapron *et al.* 1970). These optical transmission system technologies, lasers and fibres, were first implemented for telecommunication in the 1970's although the feasibility of using optical fibres had been seriously studied in the mid 1960's.

Optical fibres revolutionised telecommunication network companies such as Sprint in the mid 1980s because of their advantages as transmission media. Up to date modern telecommunication companies are based upon optical technologies, with the optical fibre forming the backbone of their physical layer. Initially optical telecommunication systems were severely restrictive due to factors such as high signal attenuation (~ 1000 dB/km), multimodal dispersion, chromatic dispersion and nonlinearity. To solve these problems, there have been advances in technologies such as the replacement of traditional single mode fibres with dispersion-shifted single mode fibres, replacing analogue transmitting signals with pulse coded modulation (PCM), advent of erbium doped fibre amplifiers (EDFAs), design of chromatic dispersion compensators and specialised manufacturing methods to reduce attenuation to as low as < 0.2 dB/km. Some of these innovative inventions together with optical components (e.g. isolators, splitters, polarizers, multiplexers/demultiplexers and circulators) paved the way for wavelength division multiplexing (WDM) and dense

wavelength division multiplexing (DWDM) applications. These applications are some of the high speed data communication technologies that have emerged in order to address the growing bandwidth demand, though they also had or have their shortcomings such as non-linear effects.

Having overcome the challenges posed by multimode dispersion, attenuation, chromatic dispersion and non-linear effects, a phenomenon known as polarization mode dispersion (PMD) arose which to date still provides a complex challenge in high speed long-haul data transmission, 10 Gb/s and above (Nelson *et al.* 2004). PMD effects are linear electromagnetic propagation phenomena occurring in single-mode fibres. PMD has been known in the research community since the late 1970's (Rashleigh and Ulrich 1978). Much of the world's legacy fibre was deployed before PMD became a major concern. PMD is more of a major issue in old G.652 fibres (< 1996) than in newer G.652, G.653, G.655 fibres (Gregory 2006). With the evolution of specialised manufacturing techniques, PMD in present day manufactured telecommunication grade fibre is kept very low at ≤ 0.1 ps/km$^{1/2}$.

Legacy fibres provide more serious challenges; therefore there is a need to strategise for PMD mitigation and/or compensation as well as accurate PMD monitoring. In order to achieve the former and latter, there is a need for accurate PMD emulation under a controlled laboratory environment. The PMD emulator should be able to mimic the stochastic PMD behaviour experience in deployed fibres. PMD emulators comprise a number of concatenated delay (or birefringent) sections since an optical fibre link is modelled using hundreds to thousands of briefringent fibre sections. PMD is classified as first-order and higher-order (second-order PMD upwards).

Initially at low bit rates, first-order PMD (FO-PMD) was of concern (Rashleigh and Ulrich 1978) and this led to the design of FO-PMD emulators (Williams 1999a, Lima *et al.* 2001, Raja and Arabasi 2003, Muga *et al.* 2005). A continued increase in data transmission speeds led to higher-order PMD making a significant contribution. This has also led to the design of second-order PMD (SO-PMD) and other higher-order PMD emulators (Phua and Haus 2002, Bogoni *et al.* 2002, Lee *et al.* 2003). The coexistence of FO- and SO-PMD in optical network systems led to emulator designs mimicking the two PMD regimes (Dal Forno *et al.* 2000, Mimura *et al.* 2003, Zeng 2003, Hauer *et al.* 2004). A PMD emulator with a single birefringent section provides FO-PMD only, that with two concatenated birefringent sections

emulates for FO- and SO-PMD only, and when there are more than two concatenated sections the emulator is able to emulate for FO-, SO- and other types of higher-order PMD.

The PMD in deployed fibres is known to evolve in a stochastic pattern due to unpredictable extrinsic perturbations (i.e. environmental changes, vibrations and human interactions) with time and non uniform intrinsic perturbations (i.e. core asymmetry and internal stress) experienced along the fibre length. Therefore, accurate PMD emulation (like compensation) is easier in stable secured buried fibres than in unstable exposed aerial fibres. Emulation (like compensation) should occur within the picosecond time scale; although in practise it can be difficult to realise due to limitations in the electronic speed of its components. A tuneable PMD emulator (Yan *et al.* 2003) can be able to emulate the PMD of different fibre links or fibre plants. The purpose of this thesis is therefore to bring about an understanding of the complex nature and effects of PMD to the telecommunication industry and research groups through novel PMD emulator designs. This would contribute to future adaptive PMD compensation designs which are expected to be more effective.

The work presented in this thesis is organised as follows: Chapter 2 gives an overview of polarization mode dispersion (PMD) and polarization dependent loss (PDL). Chapter 3 focuses on the principles behind PMD emulation, and discusses various PMD emulation techniques proposed and demonstrated in literature. Chapter 4 pays particular attention to PMD measurement techniques; both the frequency and time domain measurement techniques are discussed. Chapter 5 contains experimental field results of this study from deployed buried and aerial fibres in Port Elizabeth, South Africa; this also involves PMD statistical analysis. Chapter 6 will focus on several experimental PMD emulator designs and implementations produced in this study. Chapter 7 will involve looking into the impacts of a high first-order PMD (HiFO-PMD) section in optical network systems through the use of the Virtual Photonics Inc. (VPI) simulation software (Version 8). Chapter 8 then wraps up with conclusions of the vital findings of this study.

CHAPTER 2

POLARIZATION EFFECTS IN LIGHTWAVE SYSTEMS

This chapter gives an overview of polarization mode dispersion (PMD) to enable an understanding into its measurement, statistical characteristics, implications and the effective design of PMD emulators. Polarization dependent loss (PDL) is also briefly discussed due to its effects on the performance of PMD emulators. The reader is referred to Appendix I with regard to information on the state of polarization of light.

2.1 Polarization mode dispersion

This section will focus on the various aspects of first-order and second-order polarization mode dispersion (PMD). It includes the PMD definitions, its mathematical expressions within the frequency and time domain, factors causing and affecting PMD, PMD statistics and the autocorrelation function (ACF) as a tool to quantify PMD. Furthermore, insight will be given into PMD compensation and mitigation, and system impairments due to PMD. Lastly, insight will also be given into understanding polarization dependent loss (PDL) and its interaction with PMD in optical network systems.

2.1.1 Definition of PMD

In this study, PMD will be addressed for first-order (FO) and second-order (SO) only, although it extends to other higher orders (third order and above). PMD is defined to first-order as the relative disparity in arrival time between the two polarization modes, pointing along the unit Stokes vector (Poole and Wagner 1986) (this will be shown in Eq. (2.1)). The propagation time difference between the fastest and slowest polarization is called the differential group delay (DGD); it is the magnitude of the FO-PMD vector. In this study, the DGD will be referred to as FO-PMD. To second-order, PMD is defined as the variation of the FO-PMD (DGD) and principal states of polarization (PSPs) with optical frequency (Zalevsky and Eckhouse 2004) (this will be shown in Eq. (2.3)), corresponding to the two components of the SO-PMD vector: the polarization-dependent chromatic dispersion (PCD) and PSP-depolarization, respectively. PCD causes pulse compression or broadening (Poole and Giles 1988) and PSP-depolarization results in the reduction in the degree of polarization (DOP) of propagating signals (Nelson *et al.* 1999). The next subsection looks at the factors influencing PMD.

2.1.2 Factors influencing PMD

The main cause of PMD is birefringence, which is complicated by mode coupling. A multitude of factors affect birefringence and mode coupling over time and with wavelength resulting in PMD being a statistical phenomenon as highlighted in Section 2.1.4. These factors are classified either as intrinsic or extrinsic perturbations. Therefore, to improve the measurement accuracy of PMD, PMD should be monitored over a prolonged time frame and wide wavelength range. An understanding of the PMD behaviour due to the influence of these factors acts as a guide in the design of PMD emulators presented in Chapter 6 and 7. Some of the factors promote the state of polarization (SOP) change for propagating light. Deployed fibres and emulators in this study will be also characterised using SOPs.

I. Intrinsic perturbations

Intrinsic factors are those that are present in the fibre right from the manufacturing stage. These are: the asymmetric nature of the core, impurities and internal stress due to manufacturing imperfections.

a. Geometric asymmetry (imperfection) of the core

Assuming the fibre has a core that is perfectly circular (symmetric) throughout its entire length, the resulting PMD would be null. However, in reality due to manufacturing imperfections during the fibre drawing process the core is asymmetric in nature, resulting in two orthogonal principal states of polarization (PSPs) axes to be shown in Fig. 2.2 (a). This means if a single pulse of light is launched into the input of the fibre, it is decomposed into two distinct modes. The PSP axes have independent refractive indices, thus each of the two modes experiences a unique group velocity. This results in differences in arrival time of the pulses at the fibre end, best known as DGD (or FO-PMD). The difference between the refractive indices possessed by the two orthogonal axes is known as birefringence. In addition to this delay, each pulse is subject to chromatic dispersion during propagation. Due to improvements in the manufacturing techniques, modern fibres typically have PMD coefficients of $\leq$ 0.1 ps/km$^{1/2}$ or less as compared to legacy fibres that possessed PMD coefficients around 0.5 ps/km$^{1/2}$ or greater.

b. Internal stress

The inhomogeneous structure of the core region is caused by impurities and dopants. Such a core structure results in asymmetrical transverse stress to be frozen into the fibre during

manufacturing due to different thermal contractions of different materials present in the fibre. This internal stress also introduces birefringence (Rashleigh 1983).

II. Extrinsic perturbations

Extrinsic factors are those which induce birefringence and mode coupling in a fibre after it has been manufactured. These factors may include temperature, wind, humidity, strain and stress, movement, cabling and installation (see Fig. 2.1).

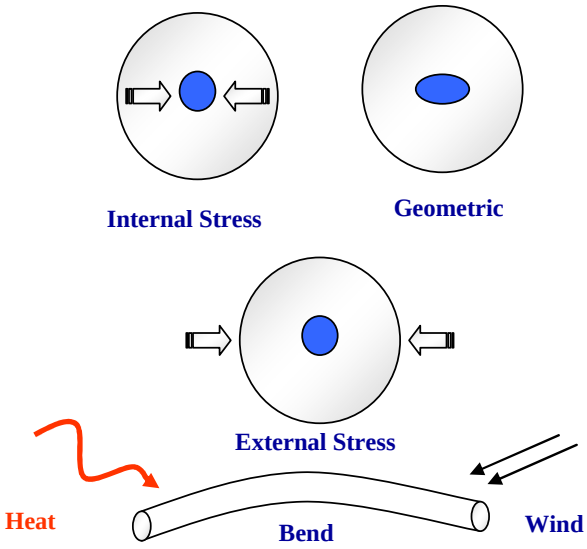

Fig. 2.1: Some of the internal and external perturbation causing and affecting PMD.

a. Temperature

Temperature enhances thermal expansion or contraction and internal stress of the fibre, as well as of the buffer or coating (De Lignie 1994). Several researchers (Hakki 1996, Cameron *et al.* 1998, Willner *et al.* 2004) have cited temperature as the major factor affecting PMD, leading to the design of temperature controlled PMD emulators (Hauer *et al.* 2004). However Gouronnec *et al.* (1995) suggested through experiments that temperature has little influence. Previous work by Poole *et al.* (1991) showed greater FO-PMD variation occurring during sunset and sunrise when temperature changes are high. The degree of FO-PMD change during the night is much less. This was experimentally proven by Cameron *et al.* (1998) who placed bare fibre on shipping spools in a climate chamber and cycled the temperature. They observed that the FO-PMD fluctuation rate is correlated to the rate of change of temperature. This explains why temperature fluctuations are of more influence in exposed aerial fibres (Cameron *et al.* 1998) than secured buried fibres (Allen *et al.* 2003). Van Antwerpen *et al.*

(2002) of the NMMU Fibre Optics Research Unit also showed that the FO-PMD of a bare fibre exhibits greater fluctuations when temperature change is sharp and the opposite when temperature gradient approaches null. The laboratory environment in which PMD emulator designs in this study were implemented had a fairly stable room temperature.

b. Wind and fibre movements

Temperature fluctuations cannot exist in isolation on exposed aerial fibres; this coexist with wind which enhances fibre galloping movements (Tomita *et al.* 1988) or oscillations (Wuttke *et al.* 2003), bends and strain on the optical fibre. Strain and bends affect the birefringence of the fibre, while fibre movements or oscillations affect the SOP of the propagating light signal. When the fibre moves out of its original plane, the SOP can change significantly due to either the geometric phase effect, fibre birefringence or both (Schinn 2003). Tomita and Chiao (1986) also agree that the SOP change is caused by a change in Berry phase (known as the geometric phase effect). The geometric phase effect occurs when the elliptical SOP of light rotates without a change in the geometry of the fibre and on the DOP of the light (Schinn 2003). Lefevre (1980) equates effects on the SOP due to the pendulum motion of the fibre cable to be similar to a twist in a mechanical polarization controller. In this study polarization rotators (half waveplates (HWPs)) are used to effect SOP changes in PMD emulators.

c. Stress and strain

External forces such as pressure and weight if exerted on the fibre result in fibre stress, which induces birefringence (Mabrouki *et al.* 1998). Twisting the fibre induces birefringence directly proportional to the twist rate (Rashleigh 1983). Bending of the fibre puts the outer part of the fibre cross section under strain, which then exerts lateral pressure on the inner compressed part of the fibre resulting again in induced birefringence.

d. Cabling and spooling effects

In order to protect and secure optical fibres for easy handling, transportation and installation, quite a number of fibre links are bundled to make a single fibre cable and then spooled. Gisin *et al.* (1991) showed through the use of the interferometric technique that there are significant increases in the FO-PMD after cabling. This also strongly agrees to findings by De Lignie *et al.* (1994), who used the fixed analyser technique (Poole and Favin 1994) to measure FO-PMD. The increase in FO-PMD is attributed to increased coupling lengths found in the cabled fibre compared to bare fibre. However, Gallagher *et al.* (1995) showed that the FO-PMD of a

spooled bare fibre is higher than that of a relaxed cabled fibre. They believed that the relaxed cabled fibre has nominal winding tension as compared to the bare fibre wound under tension on a shipping spool. The higher tension in the spooled bare fibre induces more birefringence which increases the FO-PMD.

Gaillard *et al.* (1995) showed that bare fibres with high FO-PMD increased FO-PMD values after cabling. The bare fibres were loosely spooled to ensure nominal tension during measurement. Therefore cabling was assumed to introduce extra strain on the fibre generating birefringence thus increasing the FO-PMD. By contrast, Van Antwerpen (2004) showed that a well designed cabling process has negligible effect on the PMD of loose tube design cables. Li *et al.* (2000) also showed that few cabled fibres increased in PMD after installation. Therefore spooling can potentially induce PMD depending on the tightness and the size of the diameter of the drum. Ulrich *et al.* (1980) found that bending or spooling the fibre induces birefringence, which is inversely proportional to the square of the bend radius. The emulator design to be presented in Section 6.3 consists of spooled PMFs although their spooling radius ($\geq$ 6.75 cm) is large and does not affect the PMD of the PMFs.

III. Mode coupling

The variation of the factors stated in Section 2.1.2 II over time and distance can also result in mode coupling. Mode coupling sites enhance optical energy exchange; thus some energy can be transferred from one orthogonal polarization mode to the other. During propagation, the PSP frequency rotation couples the two input orthogonal modes, therefore energy can always be found on both output PSPs even when only one of the two orthogonal axes is excited at the input end (Francia *et al.* 1998). The mode coupling phenomenon is known to complicate PMD according to Gisin (1994) where it introduces multiple polarization modes, where each fibre segment splits the input signal into two signals. If the axes of one fibre segment are directly aligned to the opposite axis of the next fibre segment, the fast mode would be slowed and the slow mode would have increased group velocity. Mode coupling is also known at times to reduce the overall FO-PMD of a fibre link. That is why in modern single mode fibres, mode coupling is intentionally introduced through fibre twisting and during the manufacturing process through bidirectional fibre spinning (Rashleigh 1983).

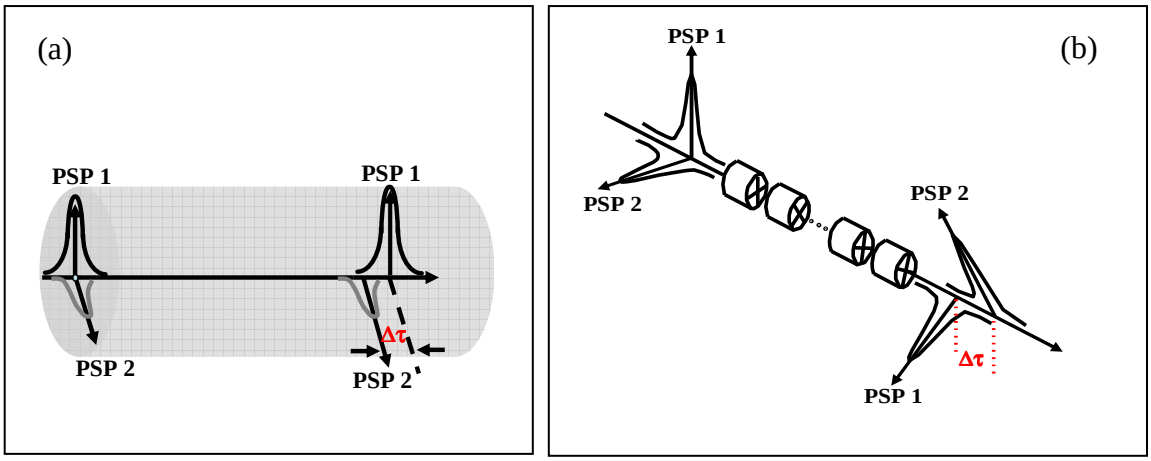

Fig. 2.2: Schematic illustration of (a) birefringence and (b) mode coupling in a fibre. PSP stands for the principal state of polarization.

The fibre itself is modelled to constitute hundreds (if not thousands) of concatenated birefringence fibre segments as illustrated in Fig. 2.2 (b). In order to mimic the optical fibre, PMD emulators comprising several PMFs segments were designed (Chapter 6). The sites where the segments concatenate are called the mode coupling sites and the distance between adjacent sites is known as the coupling length. When the fibre length is far less than the coupling length, mode coupling is negligible and when the fibre length is far greater than the coupling length there is random mode coupling. The next subsection gives insight into PMD representations.

2.1.3 PMD equations

The PMD phenomenon is best understood from PMD vector equations. This subsection gives emphasis to equations that act as vital guides for the design of PMD emulators presented in this study. Since PMD measurements fall into the time and frequency domain (see Chapter 4), the PMD vector equations presented in this subsection will also fall into these domains. However, PMD varies with the fibre length leading to an additional category for the PMD called the spatial domain. Therefore the PMD equations presented in terms of this subsection are classified as frequency, time and spatial domains.

I. The frequency domain PMD vector equations

a. The Principal States model

The Principal States Model, originally developed by Poole and Wagner (1986) is still commonly used today for the frequency domain characterisation of PMD. This model can also be used for PMD time domain characterisation. Using the Principal States Model, FO-PMD can be characterised by the reduced three-component Stokes vector (Kogelnik *et al.* 2002):

$$\vec{\tau}\ (\omega) = |\vec{\tau}| \cdot \vec{q} = \Delta\tau \cdot \vec{q} \qquad (2.1)$$

where ω is the angular frequency, $\Delta\tau$ is the magnitude of the FO-PMD vector otherwise known as the DGD (or FO-PMD τ) and $\vec{q}$ is the unit Stokes vector pointing in the direction of the principle state of polrization (PSP) of a fibre system. Since the FO-PMD vector varies with angular frequency, this means if the signal bandwidth increases, higher-order terms of PMD have to be taken into account. Thus a Taylor-series expansion of the FO-PMD vector Eq. (2.1) with $\Delta\omega$ about the carrier frequency ω_0 allows an interpretation of higher-order PMD (Gleeson *et al.* 1997):

$$\vec{\tau}(\omega_0+\Delta\omega) = \vec{\tau}(\omega_0) + \vec{\tau}_\omega(\omega_0)\Delta\omega + \frac{1}{2}\vec{\tau}_{\omega\omega}(\omega_0)\Delta\omega^2 + \ldots \qquad (2.2)$$

The second term on the right-hand side of Eq. (2.2), a derivative, describes the SO-PMD vector and is given by:

$$\vec{\tau}_\omega = \frac{\partial\vec{\tau}}{\partial\omega} = \frac{\partial\Delta\tau}{\partial\omega}\cdot\vec{q} + \Delta\tau\cdot\frac{\partial\vec{q}}{\partial\omega} = \Delta\tau_\omega\cdot\vec{q} + \Delta\tau\cdot\vec{q}_\omega = \vec{\tau}_{\omega||} + \vec{\tau}_{\omega\perp} \qquad (2.3)$$

The first term in Eq. (2.3), $\frac{\partial\Delta\tau}{\partial\omega}\vec{q}$, is parallel to $\vec{\tau}$ and describes polarization-dependent chromatic dispersion (PCD) $\Delta\tau_\omega$. The second term in Eq. (2.3), $\Delta\tau\frac{\partial\vec{q}}{\partial\omega}$, is orthogonal to $\vec{\tau}$ and describes PSP-depolarization $\vec{q}_\omega$ of the transmitted signal. Because $\vec{q}\cdot\vec{q}_\omega = 0$, the SO-PMD vector is naturally expressed as a sum of parallel $\vec{\tau}_{\omega||}$ and perpendicular $\vec{\tau}_{\omega\perp}$ vector

components relative to the FO-PMD vector as illustrated in Fig. 2.3. For a detailed geometric interpretation of second-order PMD the reader is referred to Karlsson (2006).

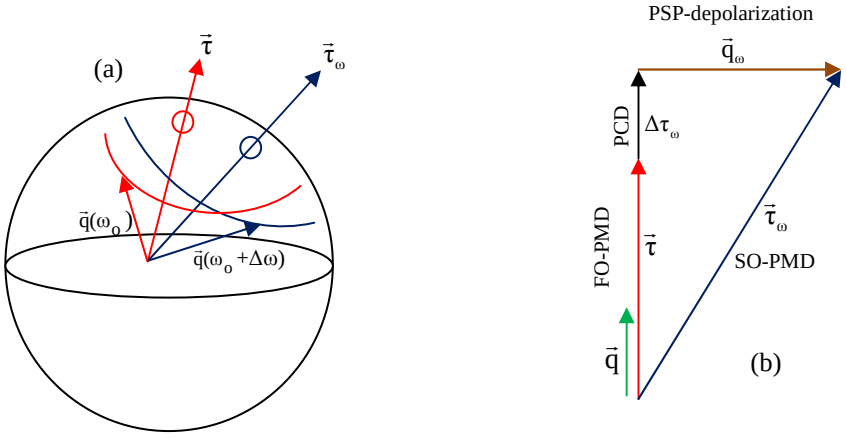

Fig. 2.3: Vector illustration of the effect of first-order (FO) and second-order (SO)-PMD on the output-state of polarization.

b. PMD equation (Gisin and Pellaux 1992)

Consider a concatenation of N fibre sections as in Fig. 2.4. The delay τ_n and direction $\vec{e}_n$ (denoting a unit vector) in each fibre section are assumed to be wavelength-independent. Chromatic dispersion is also not taken into account. In order to compute the principal states corresponding to this concatenation, the evolution operator U_ω^N through the N sections is

$$U_\omega^N = \exp\left(-i\tau_N\omega\vec{e}_N\sigma\right)...\exp\left(-i\tau_2\omega\vec{e}_2\sigma\right)\times\exp\left(-i\tau_1\omega\vec{e}_1\sigma\right) \qquad (2.4)$$

where the incoming SOP $\vec{m}_{in}$ is such that the corresponding outgoing SOP $\vec{m}_{out}$ is independent of the angular frequency ω to first- order and σ represents Pauli matrices.

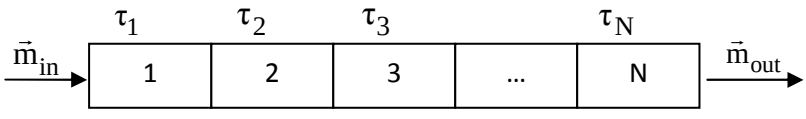

Fig. 2.4: A model, as a block diagram, of an optical fibre with N number of concatenated fibre sections.

The directions of $\vec{m}_{in}$ and $\vec{m}_{out}$ define the incoming and outgoing principal states on the Poincaré sphere. Since $m_{out}\sigma = \pm iU_{\omega}^{N}\left(\partial/\partial\omega\right)U_{\omega}^{N\dagger}$ and using the fact that $U_{\omega}^{N} = \exp\left(-i\tau_N\omega e_N\sigma\right)U_{\omega}^{N-1}$ (as from Eq. (2.4)), a recursion formula for the outgoing principal states after N sections is:

$$\vec{m}_{out}^{N}\sigma = \tau_N\vec{e}_N\sigma + \exp\left(i\tau_N\omega\vec{e}_N\sigma\right)\, m_{out}^{N-1}\sigma\, \exp\left(-i\tau_N\omega\vec{e}_N\sigma\right) \tag{2.5}$$

Through the application of the Pauli matrices $\sigma;\sigma_x=\begin{pmatrix}0 & 1\\ 1 & 0\end{pmatrix},\sigma_y=\begin{pmatrix}0 & -1\\ 1 & 0\end{pmatrix},\sigma_z=\begin{pmatrix}1 & 0\\ 0 & -1\end{pmatrix}$, equation (2.5) reduces to:

$$\begin{aligned}\vec{m}_{out}^{N}\sigma = \tau_N\vec{e}_N\sigma \; &+ \left(m_{out}^{N-1}\times\vec{e}_N\right)\vec{e}_N \; + \cos\left(2\tau_N\omega\right)\left[m_{out}^{N-1}-\left(m_{out}^{N-1}\times\vec{e}_N\right)\vec{e}_N\right] \\ &- \sin\left(2\tau_N\omega\right)\vec{e}_N\times m_{out}^{N-1}\end{aligned} \tag{2.6}$$

When N = 1, Eq. (2.6) gives $\vec{m}_{out}^{1}\sigma = \tau_1\vec{e}_1$ and the principal states are the eigenmodes. This ($\vec{m}_{out}^{1}\sigma = \tau_1\vec{e}_1$) compares well to equation (2.1), thus $\vec{m}_{out}^{N}\sigma$ is the FO-PMD vector. When N = 2, Eq. (2.6) becomes:

$$\begin{aligned}\vec{m}_{out}^{2}\sigma = \tau_2\vec{e}_2 \; &+ \tau_1\left(\vec{e}_1\cdot\vec{e}_2\right)\vec{e}_2 \; + \cos\left(2\tau_2\omega\right)\tau_1\left(\vec{e}_1-\left(\vec{e}_1\cdot\vec{e}_2\right)\vec{e}_2\right) \\ &- \sin\tau_1\left(2\tau_2\omega\right)\vec{e}_1\times\vec{e}_2\end{aligned} \tag{2.7}$$

For two fibre sections the principal states depend on the frequency ω, but the delay between the principal modes is independent of ω. When N > 3 the delay between the principal modes depends on the frequency ω and so too does the PSPs.

The standard deviation $\delta(\tau)$ of the delays the light experiences after propagating over N fibre sections is equal to the magnitude of the FO-PMD vector of that link, given as:

$$\left(\delta(\tau)\right)^2 = \left(\tau\right)^2 = \langle\langle\left|\vec{m}_{out}^{N}\sigma\right|^2\rangle\rangle_{\omega} \tag{2.8}$$

where $\langle\langle ... \rangle\rangle_{\omega}$ denotes the average over ω and $\left| \right|$ the magnitude. Therefore the derivative of the FO-PMD vector ($\vec{m}_{out}^{N}\sigma$) with respect to frequency gives the SO-PMD vector. The PMD vector equations in this section were used by Wegmuller *et al.* (2002) and Zeng (2003) to guide them through their emulator designs, and the same applies for this study.

II. The time domain PMD vector equation

a. Time evolution PMD vector

The variation of ambient parameters, such as humidity, temperature and stress, affect the distribution of birefringence along optical fibres. Thus the SOP at a fixed frequency and a fixed point in the fibre may change with time. This results in the time evolution of the FO-PMD vector $\vec{\tau}$ equation which is equivalent to that of the FO-PMD evolution equation (Hui *et al.* 2004):

$$\frac{\partial\vec{\tau}}{\partial t} = \vec{T}_{\omega} + \vec{T}\times\vec{\tau} \qquad (2.9)$$

where $\vec{T}_{\omega}$ represents the time evolution of the FO-PMD (or DGD) and $\vec{T}\times\vec{\tau}$ describes the time evolution of the PSP in a short time interval. $\vec{T}$ is the time evolution vector.

III. The spatial domain PMD vector equations

a. Concatenation rules for PMD

Deployed optic fibre links are modelled to constitute hundreds if not thousands of birefringence elements concatenated to each other. This is the basis on which PMD emulators are built (see Chapters 6 and 7), wherein birefringent sections are joined to each other. In order to track the PMD vectors as more and more sections are added, there is need to gain more insight into the concatenation rules (Gordon *et al.* 2000, Poole *et al.* 1991, Galtarossa and Menyuk 2005). The concatenation rules can also be used in analysing how the PMD vectors grow with fibre length and for statistical PMD modelling (Nelson and Jopson 2004). These rules can be used as a guide to designing multi-section PMD compensators. The concatenation rule was first derived by Gisin and Pellaux (1992).

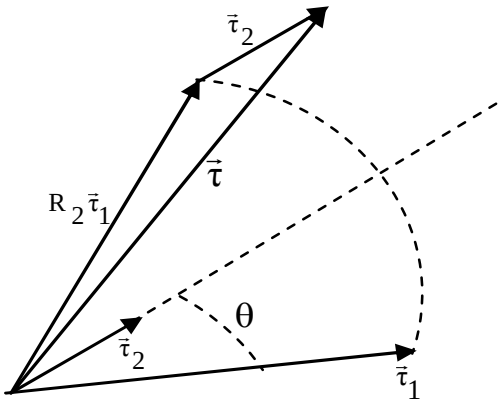

Fig. 2.5: Representation of the concatenation of two vectors (see Eq. (2.10)).

The geometrical interpretation of the concatenation rules for two concatenated birefringent fibre sections is shown in Fig. 2.5. The FO-PMD cumulative vector is expressed as:

$$\vec{\tau} = \vec{\tau}_2 + R_2\vec{\tau}_1 \tag{2.10}$$

where $\vec{\tau}_1$ and $\vec{\tau}_2$ are the FO-PMD vectors of the first and second birefringent sections and R_2 is the rotational matrix of the second section. The SO-PMD expression comes from the frequency derivative of Eq. (2.10):

$$\vec{\tau}_\omega = \vec{\tau}_{2\omega} + R_2\vec{\tau}_{1\omega} + R_{2\omega}\vec{\tau}_1 \tag{2.11}$$

But since $\vec{\tau}_1 = R_2^\dagger\left(\vec{\tau} - \vec{\tau}_2\right)$ from Eq. (2.10), Eq. (2.11) simplifies to:

$$\vec{\tau}_\omega = \vec{\tau}_{2\omega} + R_2\vec{\tau}_{1\omega} + \vec{\tau}_2\times\vec{\tau} \tag{2.12}$$

where $R_2^\dagger$ is the transpose of the rotational matrix of the second birefringent section. These concatenation equations, equations (2.10) and (2.12), can be extensively applied to fibres with more than two sections. For more information with regard to the former, the reader is referred to Nelson and Jopson (2004) and Damask (2005).

b. The PMD evolution or dynamic equations

There are two main ways to derive the PMD dynamic equations, one by Gisin *et al.* (1992) and Gordon *et al.* (2000), and the other by Poole *et al.* (1991). In this section focus is on the work of Poole *et al.* (1991). The established precession rules in length and frequency for an arbitrary state are (Poole *et al.* 1991):

$$\frac{\partial \vec{s}}{\partial z} = \vec{\beta} \times \vec{s} \tag{2.13a}$$

$$\frac{\partial \vec{s}}{\partial \omega} = \vec{\tau} \times \vec{s} \tag{2.13b}$$

where $\vec{s}$ is a 3-D Stokes vector and $\vec{\tau}$ is the cumulative FO-PMD vector up to z, $\vec{\beta}$ is the local birefringence vector (the local birefringence per unit length is $\beta = \omega \Delta n / c$). Taking the frequency derivative of Eq. (2.13a) and the length derivative of Eq. (2.13b) yields $\frac{\partial^2 \vec{s}}{\partial z \partial \omega} = \vec{\beta}_\omega \times \vec{s} + \vec{\beta} \times \vec{s}_\omega$ and $\frac{\partial^2 \vec{s}}{\partial \omega \partial z} = \vec{\tau}_z \times \vec{s} + \vec{\tau} \times \vec{s}_z$. The left hand sides of the derivatives are equal under the assumption of continuity of the function $\vec{s}(z,\omega)$. By using the vector identity $(\vec{\beta} \times \vec{\tau}) \times \vec{s} = \vec{\beta} \times (\vec{\tau} \times \vec{s}) - \vec{\tau} \times (\vec{\beta} \times \vec{s})$, this results in the FO-PMD vector $\vec{\tau}$ evolution equation:

$$\frac{\partial \vec{\tau}}{\partial z} = \vec{\beta}_\omega + \vec{\beta} \times \vec{\tau} \tag{2.14}$$

The SO-PMD vector $\vec{\tau}_\omega$ evolution equation is derived from Eq. (2.14) as:

$$\frac{\partial \vec{\tau}_\omega}{\partial z} = \vec{\beta}_{\omega\omega} + \vec{\beta} \times \vec{\tau}_\omega + \vec{\beta}_\omega \times \vec{\tau} \tag{2.15}$$

The frequency-dependent evolution of the states of polarization in optical fibres can be described by the vector equation (2.13b).

2.1.4 PMD statistics

The unpredictable variation of extrinsic and intrinsic perturbations (Section 2.1.2) with time and fibre length makes PMD statistics stochastic about some average value, either with

wavelength or time. This means that the PMD of optical systems with time and wavelength is unpredictable; therefore one must resort to statistical analysis. The statistical property of PMD that attracted initial interest was the mean FO-PMD (Andresciani *et al.* 1987). Thus all PMD measurement techniques currently in use in the telecommunication industry require an averaging procedure in order to determine the overall PMD of a fibre link (Gisin *et al.* 1996).

Most if not all work done has been focused mainly on FO- and SO-PMD statistics, which is likely due to the FO- and SO-PMD vectors being known to be statistically dependent on each other (Damask 2005, Galtarossa and Menyuk 2005). However, Phua and Haus (2002) concluded that FO-PMD can be more accurately characterised than SO-PMD. Understanding the nature and characteristics of PMD is a key step towards the construction of effective PMD emulators and compensation techniques. The PSP model facilitated the investigation into the statistical properties of PMD. The statistical characterisation of PMD include the probability densities of FO- and SO-PMD, the scaling of the PMD phenomena with changes in the mean FO-PMD, various correlation functions, and characteristics associated with the accuracy of PMD measurements (Gisin *et al.* 1996). The probability densities for both FO- and SO-PMD in most situations have asymptotic tails extending to unacceptable large impairments best known as outage probability events. This subection looks into the FO- and SO-PMD statistics only.

I. The FO-PMD statistics

The FO-PMD vector comprises of three vector components which have independent Gaussian distributions with zero mean and identical variance (Foschini and Poole 1991). This means generating three independent Gaussian random variables and taking their root square sum (RSS) results in a Maxwellian distributed variable. Through implementing the PSP model the probability density function (PDF) of FO-PMD has been proven to be Maxwellian. The SOPs represented on the Poincaré sphere denote PSP time evolution as a Brownian motion (Curti *et al.* 1990).

The probability density function of the FO-PMD in long fibres has been proven to be Maxwellian over time and wavelength (Dal Forno *et al.* 2000, Karlsson *et al.* 2000), whilst its vector components show a Gaussian distribution (De Angelis *et al.* 1992, Brodsky *et al.* 2004). The probability density of the FO-PMD was the first PMD density to draw attention (Poole *et al.* 1991). Field measurements have proved the relevancy of the FO-PMD PDF for a

very large number of fibre sections, random mode coupling under certain conditions. This has led researchers to design and simulate PMD emulators which reproduce FO-PMD statistics approximating the Maxwellian distribution (Dal Forno 2000, Lizé *et al.* 2004, Khosravani *et al.* 2001, Yan *et al.* 2003). However, Elbers *et al.* (1997) argues using Monte-Carlo simulations that FO-PMD statistics approximate better to the Rayleigh distribution than the Maxwellian distribution even though they possessed the same mean value.

Mathematical proof by Gisin and Pellaux (1992) showed that, for an ideal fibre with infinite random mode coupling and no polarization dependent loss (PDL), the mean FO-PMD at one wavelength measured over a sufficiently long period of time will provide the same result as the mean FO-PMD at a fixed time measured over a sufficiently large wavelength range. Studies however have shown that not all fibre FO-PMD values approximate to the idealised Maxwellian distribution (Sunnerud *et al.* 2002, Musara *et al.* 2009).

The Maxwellian PDF of the FO-PMD, τ (Gisin *et al.* 1993, Curti *et al.* 1990) is given by:

$$\mathrm{PDF}_\tau = 8/\pi^2 \langle\tau\rangle \left(2\tau_i/\langle\tau\rangle\right)^2 \exp\text{-}\left(2\tau_i/\langle\tau\rangle\right)^2/\pi \qquad \tau_i \geq 0,\ i = 1, 2, 3, \ldots \qquad (2.16)$$

Using the Maxwellian PDF, the probability of τ exceeding a particular value can be found using:

$$P(\tau \geq X) = 1 - \int_0^X p(\tau)\, d\tau \qquad (2.17)$$

The Rayleigh PDF of the FO-PMD according to Elbers *et al.* (1997) is given by:

$$\mathrm{PDF}_\tau = \langle\tau\rangle/\alpha^2 \exp\text{-}\left(\langle\tau\rangle^2/2\alpha^2\right) \qquad \text{where} \qquad \alpha^2 = 8N/3\pi^3\tau_i \qquad (2.18)$$

Elbers *et al.* (1997) made some confusion which were laiter rectified by Galtarossa and Palmieri (1998). Galtarossa and Palmieri (1998) proved that the FO-PMD (or DGD) is Maxwellian while the PDF of pulse broadening is Rayleigh distributed. The Rayleigh and Maxwellian distributions are fitted on FO-PMD measurements and compared in Fig. 2.6.

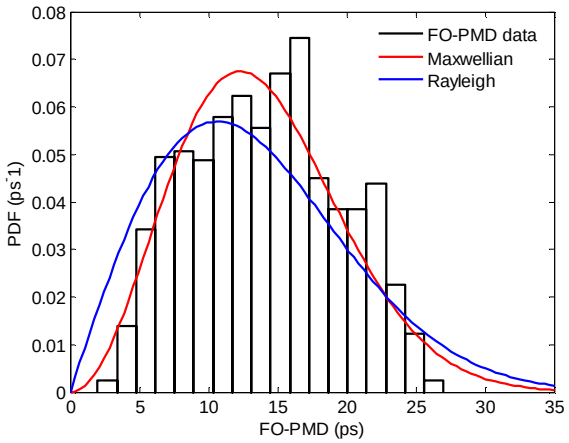

Fig. 2.6: Comparison of the Maxwellian and Rayleigh distribution fits on the FO-PMD statistics of a 28 km ITU-T G.652 deployed buried fibre link at the Telkom South Africa Sidwell exchange in Port Elizabeth.

The FO-PMD statistics obtained from the field and PMD emulators when the random mode coupling is large approaches the Maxwellian distribution best as compared to the Rayleigh distribution, for example see Fig. 2.6. Therefore this makes the Maxwellian distribution the only used theoretical PDF fit on PMD measurement in this study.

II. The SO-PMD statistics

Among all higher orders, SO-PMD has drawn significant attention; this is evident through the vast amount of literature on it (Nelson *et al.* 1999, Foschini *et al.* 1999, Phua and Haus 2002, Zalevsky and Eckhouse 2004, Musara *et al.* 2009b). SO-PMD is caused by random birefringence changes over the fibre length. The SO-PMD statistics are described by a probability density function first proposed by Foschini *et al.* (1999). For more information on the statistics of SO-PMD components, namely PCD and PSP depolarization, the reader is referred to Foschini *et al.* (2000), Foschini *et al.* (2001) and Forestieri (2003).

The PDF of the magnitude of the SO-PMD vector $\left|\vec{\tau}_{\omega}\right|$ is (Foschini *et al.* 1999):

$$\mathrm{PDF}_{\left|\vec{\tau}_{\omega}\right|} = \left(32\left|\vec{\tau}_{\omega}\right|_{\mathrm{i}}/\pi\langle\tau\rangle^{4}\right)\tanh\left(4\left|\vec{\tau}_{\omega}\right|_{\mathrm{i}}/\pi\langle\tau\rangle^{2}\right)\mathrm{sech}\left(4\left|\vec{\tau}_{\omega}\right|_{\mathrm{i}}/\pi\langle\tau\rangle^{2}\right),\ \left|\vec{\tau}_{\omega}\right|_{\mathrm{i}} \geq 0 \qquad (2.19)$$

where i is equal to 1, 2, 3, …

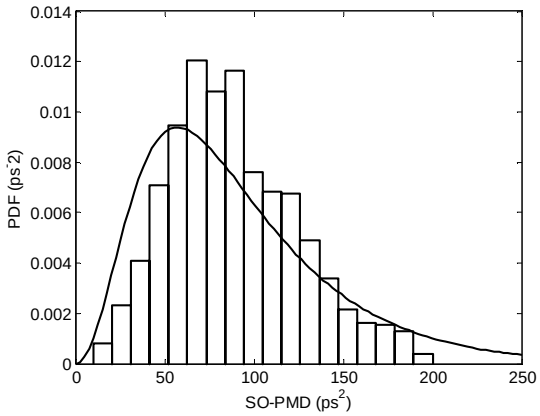

Fig. 2.7: The statistical distribution of SO-PMD for a 42 km deployed buried fibre in Port Elizabeth owned by Telkom South Africa. The solid line is the theoretical PDF fit proposed by Foschini et al. (1999).

The SO-PMD statistics in this study have been compared to the theoretical distribution by Foschini *et al.* (1999). Fig. 2.7 illustrates how the SO-PMD statistics of a 42 km deployed fibre link is close to the SO-PMD theoretical fit. The SO-PMD statistics of the fibre is evidence of the presence of numerous mode coupling sites, random mode coupled, along the fibre length.

2.1.5 The autocorrelation function

In order to quantify PMD measurements acquired from deployed fibres and PMD emulators in this study, the autocorrelation function (ACF) is a useful tool. ACF describes how correlated the PMD is to neighbouring channels in the frequency domain and how correlated PMD is at a single channel in the time domain (Waddy *et al.* 2005). There are four properties that ACFs should satisfy (Damask 2005):

i. The ACF connects ensemble averages with frequency averages
ii. The PMD-vector correlation bandwidth depends only on the mean DGD
iii. The variance of an estimated mean DGD derived from measurements depends inversely on the total measurement bandwidth
iv. All moments of the PMD vector depend only on the mean DGD and the moment order.

FO-PMD statistics acquired using PMD frequency domain measurement techniques need to be quantified using the frequency ACF and those acquired using time domain measurement

techniques should be quantified using the time ACF. For more information regarding PMD measurement techniques the reader is referred to Chapter 4.

I. The frequency ACF

The ACF gives an indication of how large a frequency separation should be for two FO-PMD vectors to be statistically independent (Damask 2005). This means the ACF gives the bandwidth over which a FO-PMD vector is applicable. The frequency ACF is more applicable to buried fibres and PMD emulators than aerial fibres. Since the research work is centred on PMD emulation, this subsection is focused towards the ACF for emulators and buried fibres.

Since $\vec{\tau}(\omega) = |\vec{\tau}| \cdot \vec{q}$ (Eq. (2.1)), the ACF is generally expressed as (Gupta *et al.* 2007):

$$g_{\vec{\tau}}(\omega,\omega_0) = \left| \left\langle \vec{\tau}(\omega).\vec{\tau}(\omega_0) \right\rangle / \left\langle \vec{\tau}(\omega_0).\vec{\tau}(\omega_0) \right\rangle \right| \tag{2.20}$$

where ω is the angular frequency and ω_0 is the carrier frequency. The former and latter also apply to Eq. (2.23). Eq. (2.20) is applicable to emulators with random mode coupling and varying birefringence. In the presence of limited numbers of birefringent segments, the ACF exhibits a significant background autocorrelation (BAC) outside the central bandwidth. The BACF level should be close to zero in the presence of many fibre segments. To characterise this property, the normalised BACF is used (Lima *et al.* 2001):

$$\text{BAC} = \frac{1}{N_f} \sum_{|\omega_i - \omega_0| > \pi/\langle\tau\rangle}^{N_f} \left| \frac{\left\langle \vec{\tau}(\omega_i).\vec{\tau}(\omega_0) \right\rangle}{\left\langle \vec{\tau}(\omega_0).\vec{\tau}(\omega_0) \right\rangle} \right| \tag{2.21}$$

where ω_i are N_f angular frequencies equally spaced outside the bandwidth of high correlation centered at ω_0. Karlsson and Brentel (1999), derived an analytical expression of the ACF for practical transmission fibres:

$$g_{\vec{\tau}}(\omega,\omega_0) = \frac{3}{\Delta\omega^2}\left[1-\exp\left(\frac{-\langle\tau\rangle\Delta\omega}{3}\right)\right] \tag{2.22}$$

The above equation is also applicable in PMD emulators where polarization scramblers connect fibre sections. Marks *et al.* (2002) also derived ACF equations that are more or less similar to that derived by Karlsson and Brentel (1999). By using the two equations below, one can observe the polarization ACF (Marks *et al.* 2002):

$$\begin{aligned}\left\langle \vec{\tau}^{n}(\omega).\vec{\tau}^{n}(\omega_0)\right\rangle = \tau_n^2 &+0.5\left[\cos(\tau_n\Delta\omega)+1\right]\left\langle \vec{\tau}^{n-1}(\omega).\vec{\tau}^{n-1}(\omega_0)\right\rangle \\ &+0.5\left[\cos(\tau_n\Delta\omega)-1\right]\left\langle \vec{\tau}_z^{n-1}(\omega)\vec{\tau}_z^{n-1}(\omega_0)\right\rangle\end{aligned} \tag{2.23a}$$

$$\begin{aligned}\left\langle \vec{\tau}_z^{n}(\omega)\vec{\tau}_z^{n}(\omega_0)\right\rangle = 0.25&\left[\cos(\tau_n\Delta\omega)-\cos(\tau_n\omega)\right]\left\langle \vec{\tau}^{n-1}(\omega).\vec{\tau}^{n-1}(\omega_0)\right\rangle \\ &+0.25\left[\cos(\tau_n\Delta\omega)+3\cos(\tau_n\omega)\right]\left\langle \vec{\tau}_z^{n-1}(\omega)\vec{\tau}_z^{n-1}(\omega_0)\right\rangle\end{aligned} \tag{2.23b}$$

where τ_n is the FO-PMD in the *n*-th section, $\Delta\omega = \omega - \omega_0$ and $\vec{\tau}_z$ corresponds to the z component of the FO-PMD $\vec{\tau}$ vector in Stokes space.

II. The time ACF

Time drift ACF is of more interest in aerial fibres. Aerial fibres are known to decorrelate faster than buried fibres (Waddy *et al.* 2001). The directional time drift is expressed empirically as (Waddy *et al.* 2001, Karlsson *et al.* 2000):

$$E\left(\vec{S}(t).\vec{S}(t+\Delta t)\right) = \exp\left(\left|-\Delta t\right|/t_d\right) \tag{2.24}$$

where $\vec{S}(t)$ is the output unitary Stokes vector as a function of time t and t_d is a fitting parameter. The experimental directional drift ACF can also be calculated as (Waddy *et al.* 2001):

$$R(\Delta t) = \frac{1}{N}\sum_{t=0}^{N-1}\vec{S}(t)\bullet\vec{S}(t+\Delta t) \tag{2.25}$$

where $\vec{S}(t)$ is the output normalized Stokes vector as a function of time, and N is the total number of data points over the measurement period. In order to measure how fast an ACF decorrelates, use (Waddy *et. al.* 2001):

$$D_{decorelate} = 1 - \frac{t_{0.5}}{t_{max} - t_{min}} \quad (2.26)$$

where $t_{0.5}$ is defined when the ACF drops below 0.5 and $t_{max} - t_{min}$ is the length of time over which the ACF is performed.

2.1.6 PMD compensation and mitigation

Several solutions have been developed to mitigate for the PMD effects on transmission links. These are: transmission over short distances, transmission at lower bit rates per wavelength, improved cabling, using low chirp lasers, using dispersion-managed return to zero optical soliton transmission, or forward error correction (FER) transmission, specialised manufacturing, intentional introduction of mode coupling and/or incorporating PMD compensators into the fibre network. Specialised manufacturing involves minimising asymmetry in the index profile and stress profile of the fibre, and spinning the fibre during the manufacturing process (Barlow *et al.* 1981). Other researchers (Huttner *et al.* 1999, Rogers 1981, Galtarossa and Palmieri 2004) including the NMMU Fibre Optics Research Unit (Sibaya 2004, Conibear *et al.* 2005) identified dominant high birefringent (HiBi) sections using a P-OTDR and replaced them with low PMD fibres.

There are several compensation techniques used to reduce PMD effects, which employ either optical domain (passive) structures of automatic compensation (Brinkmeyer 2002, Sunnerud *et al.* 2000) or electronic signal processing (active) techniques (Winters and Santoro 1990). As highlighted in Section 2.1.2 II due to extrinsic variations, such as temperature changes, vibrations, wind, and movements along the fibre, the FO-PMD and the PSPs also drift randomly with time. This makes PMD compensation challenging since compensation schemes then have to dynamically adapt to these random variations. Active compensation techniques have limitations in response time due to the limitation of the speed of electronic devices, giving the passive techniques the upper hand.

Optical PMD compensation can be broadly classified either as pre-transmission or post-transmission. In pre-transmission compensation, the transmitted light is exclusively launched into either of the PSPs. Any change in the orientation of the PSPs monitored at the receiver end is fed into the polarization controller at the transmitter end to adjust to changes in input

PSPs (Ono *et al.* 1994). Post-transmission compensation confines the compensation process entirely to the fibre output end/receiver. Thus light exiting the fibre enters a PMD compensation device which is used to cancel the PMD, eliminating the need to feedback information to the transmitter end during each compensation step. The compensation device either has the magnitude of PMD equal but opposite in direction to that of the link. This is the concept Winters and Santoro (1990) used to develop an active analogue delay line equaliser.

First-order PMD compensation is less of a challenge than second-order and higher-order PMD. That is why most experimental optical PMD compensation techniques under investigation are based on first-order approximation (Merker *et al.* 2001) and most of high-order PMD compensation are still theoretical in nature (Yu *et. al.* 2000, Shtaif *et al.* 2000). However, Merker *et al.* (2001) built an experimental compensator up to second-order by tracking the PSPs using a two-section compensator. Zheng *et al.* (2002) proposed a three-stage compensator comprising of two fixed delays and one variable delay line that is capable of compensating PSP-depolarization and PCD, as well as FO-PMD. Gibbon (2007), a member of our group, used the degree of polarization (DOP) as a PMD monitoring and control technique for FO- and SO-PMD compensation. It should be noted that FO-PMD compensators can induce detrimental levels of depolarization (Foschini *et al.* 2001). For more information on compensation schemes and their performace refer to Sunnerud *et al.* (2002).

2.1.7 Systems impairment due to PMD

As highlighted in Chapter 1, the PMD phenomenon has drawn considerable attention due to its limitation on optical multigigabit long-haul lightwave systems. This section focuses on the complications PMD (FO- and SO-PMD) introduces on propagating light pulses. Some of the signal impairments reported in this section will be used in Chapter 7 to give a detailed analysis of how a high FO-PMD section (HiFO-PMD) affects optical system performance.

I. First order PMD

a. Pulse broadening and signal degradation

The two orthogonal modes that propagate along the fibre PSPs are subject to pulse broadening due to dispersion. The amount of broadening depends on the FO-PMD and the relationship between the SOP of the signal and fibre PSPs. Karlsson (1998) derived an analytical expression for FO-PMD induced pulse broadening. Neglecting input chirp, nonlinearity and chromatic dispersion, the FO-PMD induced broadening is (Karlsson 1998):

$$B_{PMD} = \left(\vec{\tau}^2 - \left(\vec{s}.\vec{\tau}\right)^2\right)\Big/4 \qquad (2.27)$$

where $\vec{\tau}$ is the input FO-PMD vector and $\vec{s}$ is the pulse input Stokes vector which is taken to be constant across the pulse. Galtarossa and Palmieri (1998) showed pulse broadening increases with increasing FO-PMD in long single mode fibres.

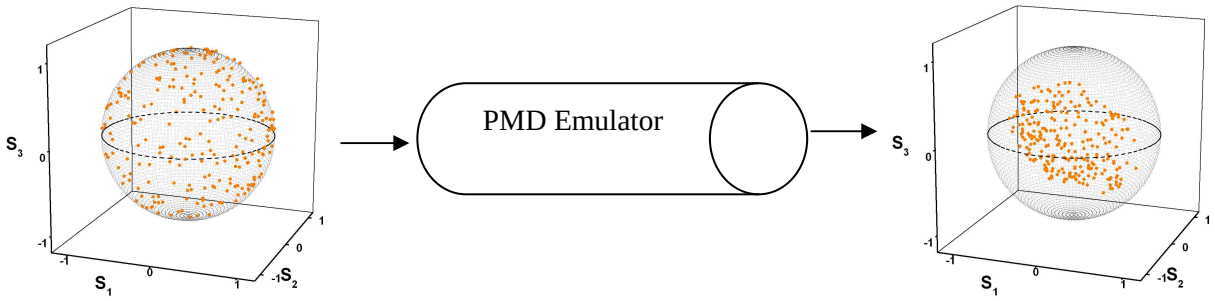

Fig 2.8: Signal depolarization of a scrambled polarization input due to FO-PMD. The PMD emulator had a FO-PMD = 8 ps. The emulator comprises of 10 coupled PMF sections.

If the polarized signal has components along both PSPs, it means impulse broadening will occur in the time domain, and the signal becomes depolarized in the frequency domain (Noé *et al.* 1999). According to Chou *et al.* (2001), FO-PMD depolarizes a scrambled polarization input so as to form an ellipsoid in Stokes space (Fig. 2.8). This results in changes in the SOP, DOP and pulse broadening, which become stochastic due to FO-PMD being environmentally dependent. The light signal gets depolarized with increasing propagation distances, thereby limiting the total distance over which light can travel.

b. Intersymbol interference

Intersymbol interference (ISI) is caused by FO-PMD, chromatic dispersion and multiple-path propagation. Intersymbol interference is when the input polarization of the signal does not match the PSPs of the fibre (Nelson and Jopson 2004). Besides the pulse splitting into two orthogonal modes, each of the modes broadens as it propagates. When pulses are sent close to each other, there is a high probability of an overlap thus making it difficult to distinguish the 1s and 0s (Fig. 2.9), resulting in data loss. Zhang *et al.* (2005), through an experiment showed that although chromatic dispersion and initial chirp do not affect the spectrum of each PSP component, they change the overlap between two PSP components compared to the case

when FO-PMD occurs alone. The broadening of the signal is complicated over the fibre length due to intrinsic and extrinsic factors, causing the signal to become distorted.

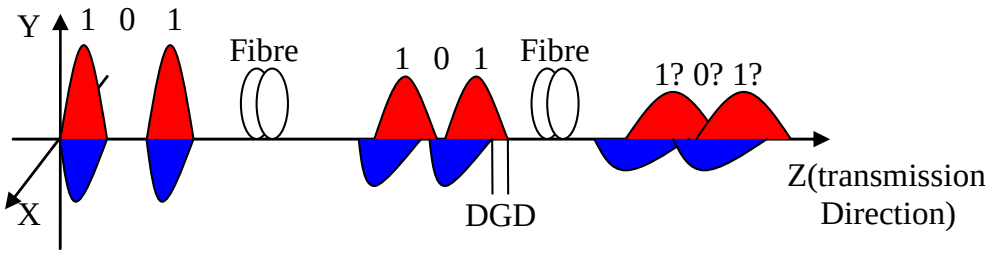

Fig. 2.9: PMD within fibres degrade the signal making it difficult to distinguish between 0s and 1s.

c. Power penalty

The impairments caused by the splitting of the pulse into two modes and being delayed by an arrival time can be expressed as a power penalty (Poole and Nagel, 1997):

$$\varepsilon(\mathrm{dB}) \cong \mathrm{A}\frac{\tau^2\gamma(1-\gamma)}{\mathrm{T}^2} \qquad (2.28)$$

where, ε is the power penalty in dB, τ is the FO-PMD, γ is the power splitting ratio between the two components $(0 \le \gamma \le 1)$ and T is the full-width at half-maximum (FWHM) of the lightwave pulse. The factor A is a dimensionless parameter obtained by the pulse shape and receiver characteristics. Simulation and experiments are used to determine A. The power penalty changes with FO-PMD and with the launch power factor g, given by (Nelson and Jopson, 2004):

$$\mathrm{g} = \left[1-(\vec{\mathrm{p}}.\vec{\mathrm{s}})^2\right] = (\vec{\mathrm{p}}\times\vec{\mathrm{s}})^2 \qquad (2.29)$$

This factor depends on the alignment between the Stokes vectors $\vec{\mathrm{s}}$ of the input polarization and the instantaneous PSP $\vec{\mathrm{p}}$. γ and g in equations (2.28) and (2.29) describe the same thing. As an example, if we have 14 ps FO-PMD for a 10-Gb/s transmission, the power penalty is 3-dB.

d. Bit error rate and Q-factor

The bit error rate (BER) is the ratio of the number of bit errors to the total number of bits transmitted in an optical system. A figure of merit related to the BER is derived from computed noise and signal power at the receiver level (Bruyère and Audouin 1994). Determining the BER facilitates the analysis of an optical communication system to predict its performance. Huttner *et al.* (2000) refers to the BER as the most important parameter characterising the network, making it the preferred parameter for measuring system performance in Chapter 7. The quality (Q)-factor simplifies the calculation of the BER due to random noise.

The Q-factor represents the optical signal-to-noise ratio (OSNR) for binary communication systems. The Q-factor can be determined from the eye diagram. An eye diagram is an oscilloscope display of a digital signal that is repetitively sampled to offer insight into the nature of channel imperfections. The system performance can be estimated in terms of the quantity Q which is directly related to the BER (Olson 1989) by:

$$\mathrm{BER} = \frac{1}{2}\mathrm{erfc}\left(\frac{\mathrm{Q}}{\sqrt{2}}\right) \tag{2.30}$$

where erfc is the complementary error function. Huttner *et al.* (2000) investigated the BER induced in a 600 km long fibre as a function of the FO-PMD and clearly found that distortions are higher (larger BER) for higher FO-PMD. Pelaelo (2008) found out that the BER increases further without changes in the amount of FO-PMD when polarization dependent loss (PDL) is present. Bruyère and Audouin (1994) discovered that fluctuations in the BER result mainly from the subtle interplay of PDL and FO-PMD with polarization dependent gain (PDG) acting as a dramatic enhancer of BER fluctuations.

e. Bit rate and span limitation

As stated before, FO-PMD results in increased errors, particularly a higher bit error rate (BER) in long-haul systems. The ITU G.691 Standard (1997), recommends that in the absence of modal and chromatic dispersion, a maximum FO-PMD delay of 10% of the bit period is permissible. A relationship that gives an estimation of the FO-PMD induced limitation on the bit rate and the span of the digital fibre-optics system is (Poole and Nagel 1997):

$$B^2L \approx \frac{0.02}{(\text{FO-PMD})^2} \qquad (2.31)$$

where, B and L are the bit-rate (Gb/s) and the link length (km) respectively, and FO-PMD has the units ps/km$^{1/2}$. The relation in Eq. (2.31) was arrived at by considering that FO-PMD induced delay is less than 14% of the bit-period in order to avoid incurring a FO-PMD induced penalty of 1 dB or greater for a period of 30 min per year. Using Eq. (2.31), Fig. 2.10 illustrates the maximum permissible value for PMD in a fibre of given length, for specific transmission bit rates.

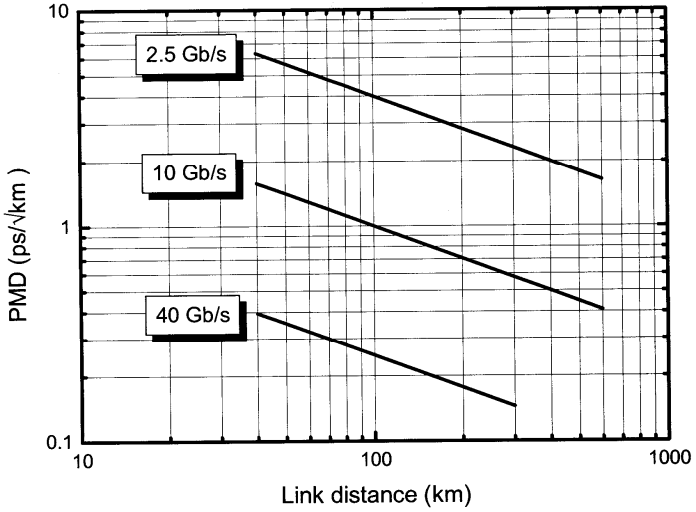

Fig. 2.10: The limit set by PMD on a maximum link length, for three different transmission rates (Leitch et al. 2001).

f. Outage probability

Signal quality may be intolerable due to the occurrences of high instantaneous FO-PMD, resulting in FO-PMD induced outage. These are the rare probability events (with a probability of 10^{-6} or less, as illustrated in Fig. 2.6) that usually lie on the tail of the Maxwellian distribution and usually occur less than a minute per year (Kaminow 2002). Outage specifications depend on the application. Outage probability P_{out} can be defined as the probability for the penalty to exceed N dB (Nelson and Jopson 2004),

$$P_{out} = \exp -\left(\frac{N}{\overline{\zeta}}\right), \qquad \overline{\zeta} = N/\text{In}\left(1/P_{out}\right) \qquad (2.32)$$

where the penalty limit N is usually expressed as 1 or 2 dB, and $\overline{\zeta}$ is the mean penalty associated with the specification of an outage probability P_{out}.

II. Second-order PMD

From the standard well known SO-PMD expression in Eq. (2.3), it suggests that its effects on system performance increases with the reduction in frequency (channel) spacing. System impacts of SO-PMD have been studied. These are mainly PCD which is a minor component of SO-PMD and PSP-depolarization which is a major contributor to SO-PMD. Bülow (1998) and Gleeson *et al.* (1997) experimentally proved that second-order PMD penalties are negligible as long as the first-order PMD outage specification is met. This led to an investigation into the impacts of SO-PMD on propagating light signals with comparison to FO-PMD in this study.

With increasing demand for high transmission speeds, SO-PMD and other higher-order PMD are seen to possess major deleterious complications (i.e. such as high system penalty, BER and signal distortions) as compared to FO-PMD (Kaminow 2002). However Francia *et al.* (1998) proved that FO-PMD turns out to have the most important contribution in the statistical analysis of PMD-induced system penalties. Nelson *et al.* (2000) showed that SO-PMD impairments due to PSP depolarization can lead to significant penalties in parts of the spectrum where FO-PMD of the fibre is low.

Experimental and theoretical work found that second-order PMD induced power overshoots on long sequences of “1’s” and “0’s” (Francia *et al.* 1998). They also gave an expression to allow a fast estimation of the time pulse deformation on long bit sequences through understanding different impacts of frequency dependencies of the FO-PMD and those of the PSP’s. Furthermore, SO-PMD is known to affect the performance of FO-PMD emulators by making the central ACF peak asymmetric (Gupta 2007) and to distort the depolarization ellipsoid formed only in the presence of FO-PMD (Gibbon 2007).

2.2 Polarization dependent loss

PMD cannot exist in isolation in an optical network system, polarization dependent loss (PDL) is also present. This section is aimed to bring an insight into understanding PDL, its behaviour and its implications on propagating light signals.

2.2.1 Definition of PDL and its origins

PDL is found in linear optical components and optical fibres. PDL is defined as the maximum peak to peak difference in transmitted power to all SOPs. This occurs as a result of energy loss from one of the PSPs in the optical material. PDL can be defined either using transmission intensity (TIA/EIA-455-157 1995) or output power (Derickson 1998) as:

$$PDL = 10Log_{10}\left(\frac{T_{max}}{T_{min}}\right) = 10Log_{10}\left(\frac{P_{max}}{P_{min}}\right) \quad (2.33)$$

where T_{max} and T_{min} are the maximum and minimum transmission intensities through the system and P_{max} and P_{min} are the maximum and minimum output powers, respectively. PDL is defined in decibels (dB) and is a positive quantity. As in the case with PMD, PDL also evolves along the network since network systems constitute several optical components. The cumulative PDL vector $\vec{\Gamma}$ evolution equation describes how the PDL evolves through the optical network system as (Damask 2005):

$$\frac{\partial\vec{\Gamma}}{\partial z} = \vec{\alpha} - \left(\vec{\alpha}.\vec{\Gamma}\right)\vec{\Gamma} \quad (2.34)$$

where $\vec{\alpha}$ is the PDL vector.

Most of the optical devices are known to be PDL elements due the difference in the attenuated polarization modes of transmitted signals (see Fig. 2.12). This means that linear optical components have one input polarization state that produces the maximum transmission loss relative to the other orthogonal input polarization state which gives minimum transmission. Factors causing PDL include angle interfaces, oblique reflections, dichroism of molecules like in polymer waveguides, macro and micro optical fibre bends (see Fig. 2.11). Such optical devices include optical filters, splitters, fused couplers, polarization controllers etc.

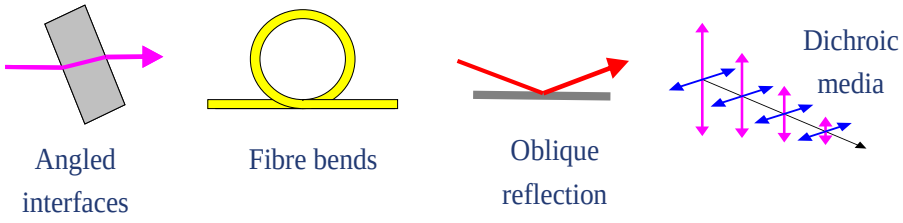

Fig 2.11: Factors known to cause PDL.

2.2.2 Implications of PDL and its mitigation

Yamamoto *et al.* (1989) stated that the primary effect of PDL in an amplified system is to cause slow fluctuating changes in signal-to-noise (SNR) levels at the receiver and increase the bit error rate (BER). Such fluctuations occur in transoceanic systems and minimise control of the PDL in system components. PDL results in the local signal power to fluctuate in response to slowly varying changes in the incident polarization state. This deteriorates system performance complicates power management. Besides the demerits mentioned above, optical components with high PDL values tend to polarize a partially or unpolarized signal. A partial PDL element is known to continuously change the polarization state of the input light and reduce the overall intensity (Pelaelo 2008). In order to reduce PDL impacts, Yan *et al.* (2002) proposed a PDL compensation scheme which reduced the power penalty tail to less than 2 %. Improving the quality of optical components during manufacturing also reduces the PDL of an optical network system.

2.3 PMD and PDL interaction

PMD and PDL coexist within an optical network system. This section gives an overview of the combined effects of PMD and PDL, and their evolution along the fibre length. The impact of PDL on PMD emulators will be investigated in Chapter 6.

2.3.1 Combined effects of PMD and PDL

A combination of birefringent elements and partial polarizers along an optical network yields deleterious polarization effects that are more complex than PDL or PMD in isolation. In such a case the FO-PMD can be greater than the sum of individual delays (Huttner and Gisin 1997) and a propagating pulse can suffer distortion even with negligible FO-PMD (Huttner *et al.* 1999). There are abrupt interchanges of the PSPs in the presence of PDL (Steinkamp and

Voges 2007), thus complicating SO-PMD. Therefore, the coexistence of PDL and PMD proves to be a major challenge for their joint compensation.

The principal results from combined PMD and PDL are summarised as (Damask 2005, Willner *et al.* 2004, Gisin and Huttner 1997, Yang *et al.* 2005):

i. The PSPs are not orthogonal to one another (see Fig. 2.12); this is due to the complex PMD vector operator.
ii. Abrupt interchange of the PSPs occurs with wavelength (Steinlamp and Voges 2007).
iii. The output polarization state does not follow simple processional motion as a function of frequency.
iv. The FO-PMD probability distribution degenerates from its Maxwellian shape.
v. The PDL becomes wavelength dependent in the presence of PMD. In optical network systems forward PDL statistics follows the Maxwellian distribution when expressed in decibels (Mecozzi and Shtaif 2002). The round-trip PDL statistics follows the Rayleigh distribution (Galtarossa and Palmieri 2003).

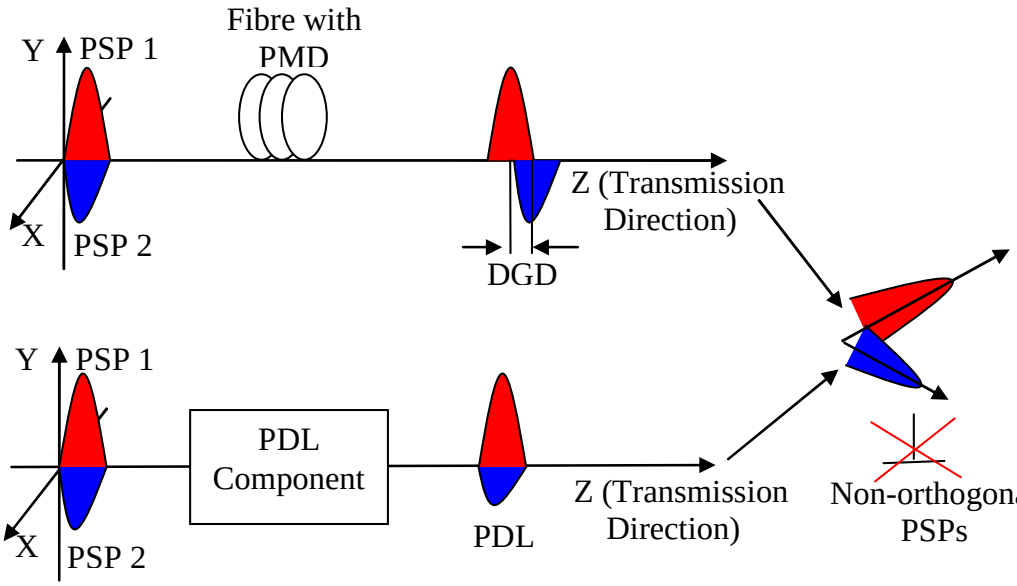

Fig. 2.12: Interaction of PMD and PDL results in the non-orthogonality of the two PSPs.

2.3.2 PMD and PDL interaction evolution equations

In the presence of PDL, the resultant equation of motion for FO-PMD is (Damask 2005):

$$\frac{\partial\vec{\tau}}{\partial z} = \vec{\beta}_{\omega} + \left(\vec{\beta} + j\vec{\alpha}(z)\right)\times\vec{\tau} \qquad (2.35)$$

Comparing equation (2.35) with the pure FO-PMD evolution equation Eq. (2.14), PDL adds to the curl of $\vec{\tau}$ and makes the vector a complex quantity. $\vec{\alpha}(z)$ is the PDL per-length. The equation of motion for the cumulative PDL vector $\vec{\Gamma}$ is (Damask 2005):

$$\frac{\partial\vec{\Gamma}}{\partial z} = \vec{\beta}\times\vec{\Gamma} + \vec{\alpha} - \left(\vec{\alpha}.\vec{\Gamma}\right)\vec{\Gamma} \qquad (2.36)$$

The cumulative PDL equation when compared to Eq. (2.34) has the term $\vec{\beta}\times\vec{\Gamma}$ which generates a rotation for $\vec{\Gamma}$ about the local birefringence vector $\vec{\beta}$.

The background on PMD characteristics and its equations are vital in the design of PMD emulators to be presented in Chapters 3 and 6. The PDL of these PMD emulators was maintained as low as possible because PDL influences the PMD statistics.

CHAPTER 3

ASPECTS OF POLARIZATION MODE DISPERSION EMULATION

This chapter will focus on the need for polarization mode dispersion (PMD) emulation and define the conditions PMD emulators should satisfy in order for them to accurately mimick deployed fibres. Furthermore, descriptions of some of the tools and devices commonly used to construct PMD emulators are presented. Emulator types are classified into various categories with each type having at least two literature reviewed emulator designs. Lastly, the limitations of PMD emulators will be highlighted.

3.1 The need for PMD emulation

PMD emulation is the first vital step to undertake in order to analytically understand the complex behaviour of PMD under the laboratory environment over a short time frame. Emulation is also known to be the key to the effective design of adaptive PMD compensators. PMD emulators can be further used in testing for system tolerance, diagnosing system impairments, as calibrators in instruments used for accurate characterisation and measurement of PMD, and as models for deployed fibre links. Therefore, PMD emulation is a novel approach essential in the move towards a cost-effective optical network upgrade through system analysis within the laboratory before field testing. Some of the merits of PMD emulation will be highlighted in the sections and chapters that follow.

3.2 Requirements for a PMD emulator

There are certain conditions emulators should meet in order to accurately reproduce PMD in deployed networks. Below is an overview of these conditions. These vary depending on the expected outcome and properties of the emulator design.

3.2.1 Autocorrelation function (ACF)

When the ACF is averaged over an ensemble of fibre realisations, the background autocorrelation (BAC) should tend towards zero outside the limited frequency range. The presence of SO-PMD has been seen to affect the symmetry of the FO-PMD ACF central peak

(Gupta *et al.* 2007). For a good PMD emulator the ACF peak should be centred at zero, however, in a combined FO- and higher-order PMD emulator this might not be achievable.

3.2.2 FO-PMD statistics

The FO-PMD should be Maxwellian-distributed over an ensemble of fibre realisations at any fixed optical wavelength and over a wide wavelength spectrum (Willner and Hauer 2004). However, some fibre links do not approach the Maxwellian-distribution (Musara *et al.* 2009). Emulators constructed to mimic the PMD behaviour in these fibres do not need to have FO-PMD distributions which are Maxwellian. Therefore, a PMD emulator should accurately reproduce the FO-PMD statistics of a particular or given deployed fibre link or fibre plant.

3.2.3 Higher-order PMD statistics

The emulator should be able to produce accurate higher-order PMD (i.e. SO-PMD and above) statistics and should be able to reach any combination of first and higher-order PMD values (Willner and Hauer 2004). Just as for FO-PMD, SO-PMD emulators should accurately mimic the SO-PMD statistics of the fibre link under investigation. Some researchers have maintained either FO-PMD fixed and varied SO-PMD or vice versa (Zeng 2003, Musara *et al.* 2009a). Other emulators can have either FO- or SO-PMD null as one parameter is investigated (Phua and Haus 2002).

3.2.4 Stability

Stability should be achievable over a measurement period, which may last from minutes to hours (Willner and Hauer 2004). This solely depends on how the properties of the emulator components behave under certain laboratory environments i.e. stable temperature, high tolerance to vibrations or movements during experimental measurements. Stability ensures emulator repeatability or reproducibility (Yan *et al.* 2003), which ensures the emulator is applicable for important sampling (IS).

3.2.5 Low loss

The emulator should have low insertion loss and exhibit negligible polarization dependent loss. The presence of PDL distorts PMD statistics away from theoretical distributions even in the presence of infinite random mode coupling (Willner *et al.* 2004).

3.2.6 Simplicity

Implementation of the emulator should be easily controllable from one emulator state to the other (Willner and Hauer 2004). This can be achieved either through programming or manual control. Simplicity makes the emulator user friendly and marketable.

3.3 PMD emulator components and tools

A PMD emulator is designed from a combination of different components. These components are configured to ensure a desired PMD statistical outcome is achieved. This section covers some of the components used to design PMD emulators, with more emphasis on components used for this study. These components are grouped into two groups namely: optical delay and polarization orientation control components. Lastly, simulation will be addressed as it is a vital design tool for this study (Chapter 7).

3.3.1 Optical delay components

I. Polarization maintaining fibres (PMFs)

There are high and low birefringent polarization maintaining fibres available (Okoshi and Kikuchi 1986). Of interest to this study is the high-birefringent (HiBi) fibre, which is what will be focused on. A polarization maintaining fibre (PMF) maintains the launched linearly-polarized light wave with little or no cross-coupling of optical power between the polarization modes when light is launched along one of its birefringent axes. The polarization state of light will still be maintained even if the fibre is bent. This makes it more stable than the single mode fibre. If the input light is aligned at 45^{o} to the fast or slow axes, the output will vary between linear and circular polarization otherwise the output is elliptically polarized.

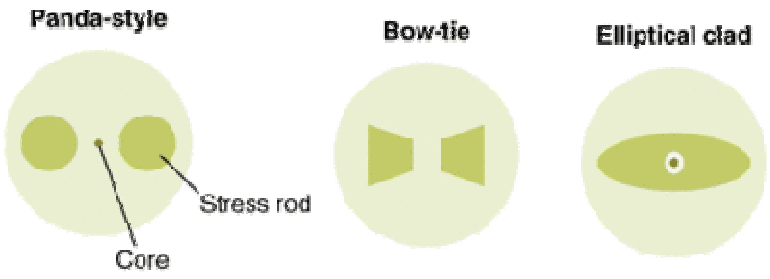

Fig. 3.1: The cross-Sections of Panda, Bow-tie and Elliptical clad PMFs.

PMFs are designed by deliberately inducing high stress in the fibre core or cladding. This is achieved either by having an asymmetry on the core or cladding or using rods (Noda *et al.* 1986). These rods are made of modified glass composition e.g. consists of boron oxide

(B_2O_3)-doped silica (Rashleigh 1983), which can be shaped into different PMF types such as panda (stands for polarization-maintaining and absorption reducing), bow-tie or elliptical clad, as shown in Fig. 3.1. The FO-PMD (or DGD) of the PMF is proportional to the fibre length in the absence of mode coupling.

PMFs are commonly used for telecommunication application, fibre-optic sensing and interferometry (Noda *et al.* 1986). However they are rarely used for long-distance transmission because they are expensive and have higher attenuation than the single mode fibre. PMFs were used to build PMD emulators in this research and to study the impacts of a high FO-PMD (or HiBi) section on PMD statistics (Chapter 6). The PMFs used for this research have PMD coefficients of ~ 1.5 ps/m and 1.3 ps/m. For more details on PMFs the reader is referred to Noda *et al.* (1986).

II. Birefringent crystals

A birefringent crystal (BC) constitutes a material structure that is anisotropic and directionally dependent (Kasap 2001). These materials for example are calcite ($CaCO_3$) crystals, rutile (TiO_2), boron nitride, silicon carbide, yttrium ortho-vanadate (YVO_4) and liquid crystals. Most of these birefringent materials are used to develop waveplates, polarization prisms, Lyot filters and birefringent crystals. Among these materials, undoped YVO_4 is the best birefringent optical crystal implemented for opto-electronic research due to its properties: a very high transmission in a wide wavelength range from visible to infrared, large refractive index and birefringence difference. A birefringent crystal decomposes an input ray of light into two polarized rays orthogonal to each other like a PMF. This is because the birefringent crystal has two different refractive indices corresponding to two orthogonal polarization states. This is known as birefringence and its magnitude is expressed as (Kasap 2001):

$$\Delta n = n_e - n_o \qquad (3.1)$$

where n_e and n_o are refractive indices for polarizations parallel (extraordinary) and perpendicular (ordinary) to the axis of anisotropy, respectively. As discussed in Section 2.1.2 I manufacturing imperfections in optical fibres cause birefringence, which can cause distortions with fibre length in fibre optics systems due to PMD. To mimic PMD accurately, stable PMD emulators and compensators have been built from birefringent crystals. PMD

emulators built using birefringent crystals have also been used for importance sampling (IS) due to their stability (Yan *et al.* 2004).

III. Delay Line

Delay lines are modules that are meant to induce a delay time in one of the two orthogonal polarization modes of light. This results in the disparity in arrival times of the two orthogonal modes at the receiver end. These two orthogonal modes belong to the same pulse. The delay represents the FO-PMD in optical networks, which means a delay line is a PMD emulator module. There are different types of delay lines with different control mechanisms which are all designed to induce an adjustable FO-PMD. Some of these variable delay lines are manufactured by Oz Optics Limited, ThorLabs and General Photonics Corp. This section gives emphasis to the delay line manufactured by Oz Optics Limited (Fig. 3.2) since it was used in this study. This delay line is referred to as the variable polarization differential delay line (DDL).

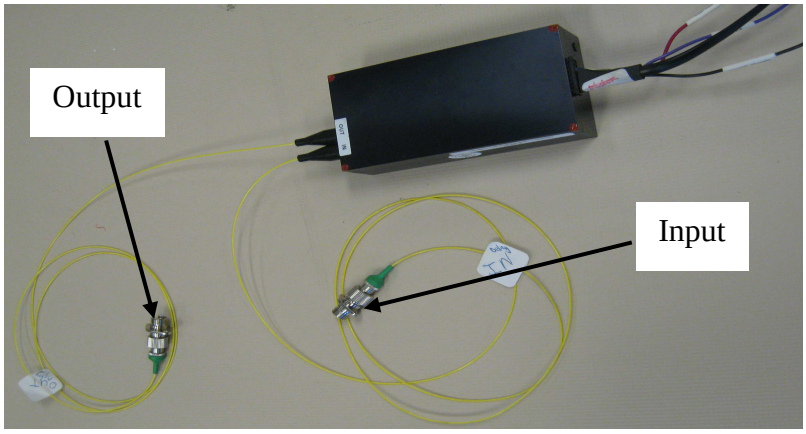

Fig. 3.2: Photograph of the DDL from OZ Optics in the NMMU Fibre Optics laboratory.

The DDL by Oz Optics is an electrically controlled, reflector-style, variable device. It consists of an input fibre collimator, output fibre coupler and polarization beam splitting optics. The optics are mounted and aligned to produce a fixed gap between collimators for one orthogonal polarization and a variable gap for the other orthogonal polarization. The collimator projects light into free space and the coupler collects it into the output fibre. The difference in path travelled by the two orthogonal polarizations is the FO-PMD. The difference in the optical paths is precisely controlled by reflecting the light off a moveable reflector. Most if not all delay lines are equipped with a microprocessor to enable remote communication through an electrical device or personal computer. The DDL used in this study covers over ± 65 ps delay

range with a resolution of 0.0017 ps. For more specifications on this DDL refer to Appendix III.

3.3.2 Polarization orientation control components

I. Acrobat^{TM} polarization rotator (Boston Applied Technologies 2008)

This polarization rotator rotates up to 180^{o} any input SOP by the application of voltage to the rotation plate. For any arbitrary input SOP the polarization rotator, a half waveplate (HWP), covers the full Poincaré sphere. The PRM utilises the OptoCeramic^{TM} electro-optic materials developed by Boston Applied Technologies Incl. (BATi). When the HWP has no applied voltage, they are isotropic, resulting in null device PMD. Application of voltage to the plate induces birefringence whose magnitude increases with the square of the voltage, thus making the retardation angle in each plate a quadratic function of the applied voltage. The voltage supply range is from 0 to 4 V under an operating temperature between 0 - 70 ^{o}C. The HWP is connected to a PCB430 board powered by a 5 V power supply that enables a step response time of < 10 ms (Fig. 3.3). The HWP has a pair of single mode fibres at either ends (input and output). In the construction of the adjustable PMD emulator in Section 6.3, this type of HWP was used. This type of HWP has applications for polarization switching, polarization management, instrumentation and variable digital group delay. For a detailed specification of the PCB430 and HWP, refer to Appendix III.

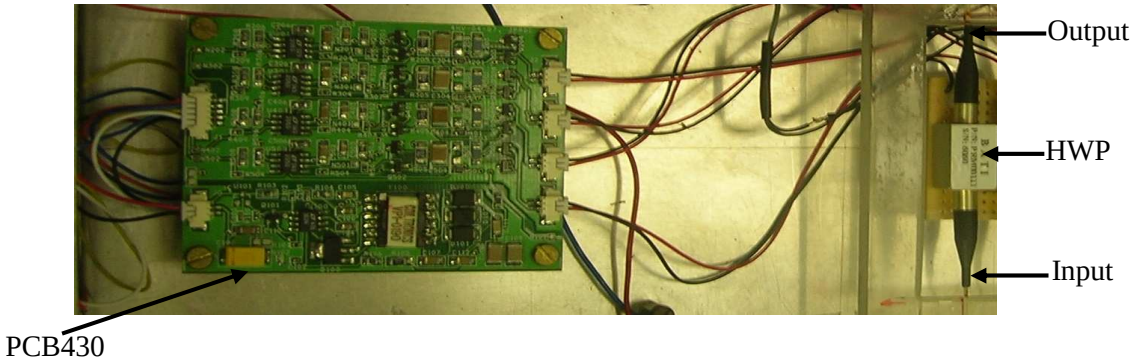

Fig 3.3: Photograph of the HWP and PCB430 board.

II. Faraday Rotator (FR)

A Faraday rotator (FR) is an optical device that rotates the polarization of light due to the Faraday effect, discovered by Michael Faraday in 1845. The Faraday effect is a magneto-optic effect. The FR has one polarization of the input light in ferromagnetic resonance with the material, causing its phase velocity to be higher than the other. To rotate the plane of

polarization of polarized light, a magnetic field is applied parallel to the propagation direction. The empirical angle for rotation is given by:

$$\phi = VBd \qquad (3.2)$$

where ϕ is the angle of rotation, B is the magnetic flux density in the direction of the propagation, V is the Verdect constant for the material which is wavelength and temperature dependent (e. g. terbium gallium garnet ~ - 40 rad $T^{-1}m^{-1}$) and d is the length of the path where the light and magnetic field interact. Alexandra and Thomas (2007) showed that the FR can be enhanced by the Zeeman Effect. Faraday rotators are suitable for most applications such as optical isolators, variable PMD emulation (Mimura 2003, Mimura *et al.* 2003) and compensation (Mimura *et al.* 2003).

III. Lithium Niobate ($LiNbO_3$) polarization controller (Adaptif Photonics 2004)

The $LiNbO_3$ polarization controller (PC), integrated with the Adaptif Photonics A3200 family, will be discussed in this subsection because it is used extensively in this study. This PC is comparable to a cascade of five endless rotatable waveplates, comprising four quarter waveplates and a single half waveplate (see Fig. 3.4). The state of the PC is given by the position of the waveplates which is expressed in terms of five angles ranging from 0 to 360^o. The angle of each $LiNbO_3$ waveplate is proportional to the supplied voltage. Retardation may slightly differ from nominal values depending on the operating wavelength and temperature. Due to the adaptive nature of the PC, these deviations are not much of an issue in most applications. The angles can either be statistically or dynamically set by means of a look-up-table stored in the memory of the instrument or manually adjusted using the polarizationNAVIGATOR software settings. By rotating the waveplates at different speeds, the PC can act as a mode scrambler which can populate the whole or a greater part of the Poincaré sphere. A many-segment PMD emulator using a combination of polarization scramblers has been constructed (Phua and Ippen 2005).

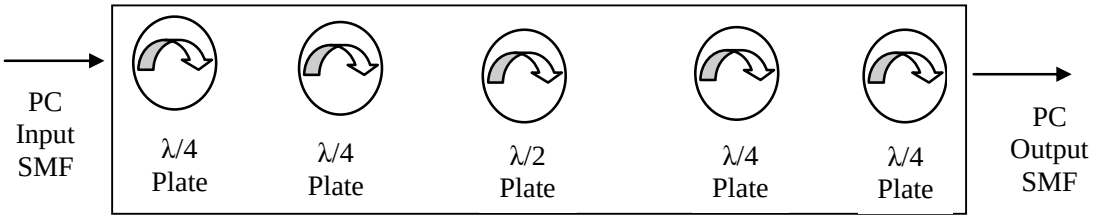

Fig. 3.4: The Lithium Niobate ($LiNbO_3$) Adaptif Photonics polarization controller.

IV. Fibre-squeezer polarization controller

This polarization controller comprises at least one stack of nematic liquid crystal cells arranged such that radiation incident on the stack will pass through each cell in the stack in sequence. Phase retardation of the transmitted radiation is changed by applying a synchronised electric or magnetic field through each cell. The optical axes of the cells are oriented relative to each other such that the polarization of incident radiation on the controller changes from first to second state onwards. This type of polarization controller, a fibre squeezer, was used by Yan *et al.* (2006) to emulate slow polarization state change in an investigation on the Hinge model in PMD statistics through a variable DGD based emulation design.

V. Polarization switch

Polarization switching enables the quick conversion of an incoming linear SOP aligned to the input PMF axis to be switched between the two orthogonal output axes. Switches usually have low losses and virtually zero back reflection. This device is easy to operate and flexible by requiring only a controlled current source, for example switches from companies like Phoenix Photonics and General Photonics. Some polarization switches are made from solid state materials; for example the magneto-optic (MO) polarization switch that can generate controlled FO-PMD (Yan *et al.* 2003a). Polarization switches are applicable for PMD monitoring, polarization modulation, polarization detection and polarization metrology. They have also been used for PMD emulation and importance sampling (Yan *et al.* 2004). In 1994, Yao and Maleki proposed a photonic true time delay based on polarization switching that generated precise controlled FO-PMD.

3.3.3 Simulation

Emphasis will be given to computer simulation since it is of application in this research to assist in investigating the implications of polarization effects in optical networks (Chapter 7). The commonly available simulation programs include Matlab Simulink, Monte Carlo simulations and the VPItransmission marker software. In this study, PMD emulators were virtually built using VPItransmission marker (Version 8). Fig. 3.5 shows a simple simulation diagram used to mimic birefringence or FO-PMD. The polarizarion beam splitter (PBS) and polarization beam combiner (PBC) are used to split the light into two orthogonal modes and recombine it later. The delay element applies a delay in the pico-second (ps) range.

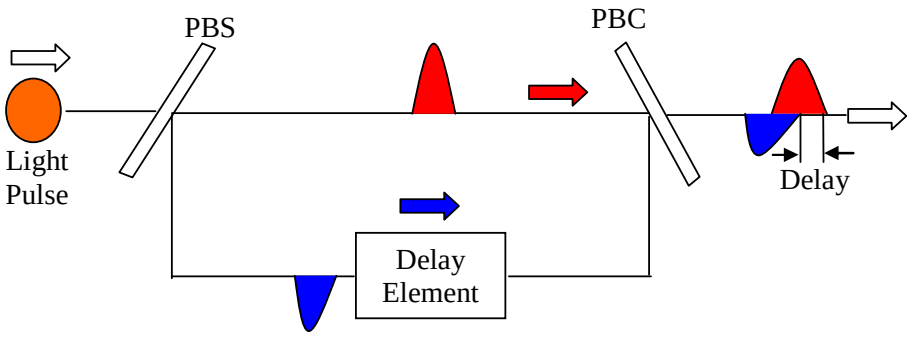

Fig. 3.5: Simulation diagram for generating a delay.

3.4 Types of PMD emulators available

This section will consider first-order and second-order PMD emulators only, although there are also other higher-order PMD emulators available. The emulators discussed in this section (shown in Fig. 3.6) are classified into six categories. Emulator designs presented in Chapter 6 will fall into any of these categories.

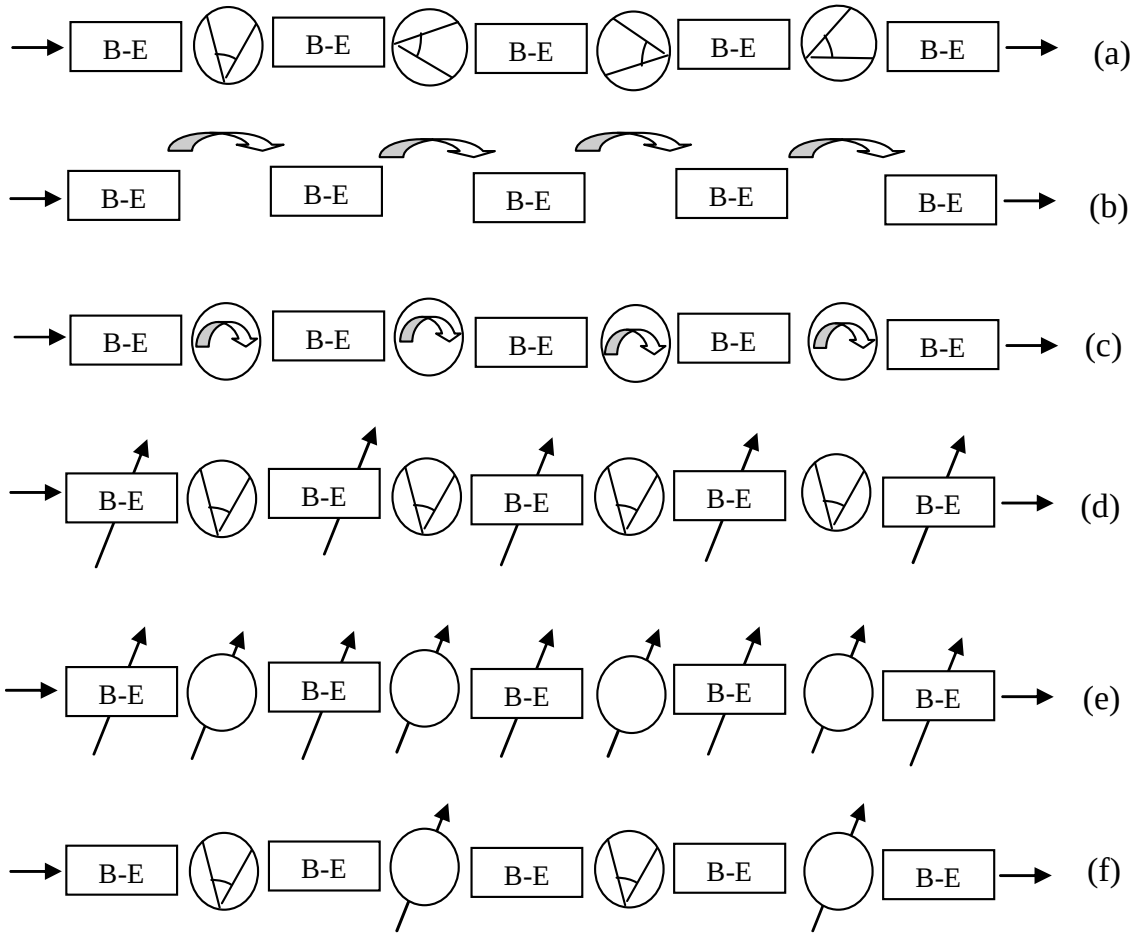

Fig 3.6: Schematic representation of the six types of emulators. Emulators with (a) fixed orientations, (b) uniform rotatable sections or polarization states, (c) uniform scattering of polarization states, (d) tuneable birefringence, (e) all elements tuneable and (f) both fixed and rotatable orientations. B-E stands for birefringent element or section.

3.4.1 Fixed birefringent sections and polarization orientations

These types of emulators are constructed from cascading two or more PMF sections (Fig 3.6 (a)). The equal or unequal PMF sections are joined together through fusion splicing. The mode coupling angles are fixed. Some of the emulator designs in this study, Chapter 6, fall within this class. Highlights of some of the available emulators falling into this category are presented below.

Gupta *et al.* (2007) analysed the performance of a multi-section fibre FO-PMD emulator based on random fibre sections and ordered sections, with the inclusion of SO-PMD in individual sections. The authors found that the presence of SO-PMD affects the accuracy of the FO-PMD emulator by causing an asymmetry in its ACF but has negligible influence on the background autocorrelation (BAC). The presence of SO-PMD also causes the probability distribution function (PDF) of the FO-PMD to shift to the right, hence giving undesirable mean FO-PMD values. Of interest is the discovery that ordered sections lower the BAC considerably as compared to the randomly distributed fibre sections, despite the recommendation by most researchers that good emulators have random varying elements.

Dal Forno *et al.* (2000) came up with an experimental and theoretical model for PMD in a 8.7 km-long single mode fibre. The emulator model was built out of 20 sections of HiBi fibre with random lengths varying within 20% standard deviation of the mean length, similar to their simulation. The author showed that a single set of randomly coupled fibre lengths, coupling angles and phases account for the Maxwellian statistics and non-periodical FO-PMD spectral dependence. A comparison between the experimental and numerical results showed that the random coupled lengths mathematical simulation model and the emulator device are powerful tools for either FO- or SO-PMD statistical emulation of a deployed fibre. Results show that different PMD values converge within 4% to the desired PMD depending on the number of fibre sections, distribution of coupling lengths and mode coupling angles.

Lizé *et al.* (2004) used a low-cost easy to control customised single polarization controller as part of a PMD emulator design instead of multiple polarization scrambling stages. The emulator consists of a number of HiBi PMFs spliced to segments of single mode fibres (SMF) spooled independently on three paddles of a custom motorised Lefèvre polarization controller (PC). The diameter of the paddles is such that a relative phase retardation of $\pi/6$, is induced per turn at 1550 nm. There is no correlation in polarization rotation between successive fibre

sections. This is achieved by changing the number of times the fibre is spooled on a paddle, which changes the transfer function of the controller, from one section to the next even though the coupling angles are the same. Monte Carlo simulations were also performed to confirm the validity of the emulator design. PMD statistics from simulation and experimental results were in good agreement with the known FO- and SO-PMD theoretical distributions for an emulator with 25 PMF sections which are Gaussian distributed in length.

Williams (1999) proposed an alternative design to the spliced PMF emulator. The PMD emulator consisted of a stack of quartz plates with single mode fibre pigtails at its extreme ends. Each plate is ~ 2 mm thick and possesses a delay ~ 63 fs (with a birefringence of 0.009403). Since the target range of the emulator was ~ 0.5 ps, thirty-five randomly oriented quartz plates yield a PMD of ~ 0.37 ps, close to the target PMD value. It would have been difficult to achieve such compactness with PMF sections and get such an overall low PMD value. For the emulator to achieve random mode coupling similar to a 25-km deployed fibre, the 35 quartz plates were cemented to each other whilst they were randomly oriented enabling a stochastic FO-PMD versus wavelength spectrum. All the quartz plates had matching refractive indices in order to reduce reflections from within the stack. Continuous increase in the number of wave plates (or quartz plates) increases the insertion loss and makes the emulator costly. Computer simulations were therefore performed to determine the required number of quartz plates.

3.4.2 Rotatable birefringent sections or polarization orientations

The birefringence sections are randomly rotated relative to one another to obtain different FO-PMD states. Such emulators consist of either birefringence elements mounted on rotatable stages, PMFs interlinked via rotatable connectors or a long PMF strand with fibre-twisters placed along its length to vary the polarization coupling between sections. Fig. 3.6 (b) illustrates this example schematically. Below are descriptions of some of the PMD emulator designs within this classification.

Khosravani *et al.* (2001) came up with a technique, experimentally and theoretically, for real PMD emulation. The emulator constitutes of 15 unequal length PMF sections with an average length of ~ 7 m and a 20% Gaussian deviation, and rotatable connectors between the PMFs. Randomly rotating the connectors enables the emulator to generate an ensemble of high PMD fibre realisations. These 15 unequal sections produced FO- and SO-PMD statistics close to the

ideal theoretical distributions whilst the ACF had an average level of 10% correlation between well spaced wavelengths. This investigation also showed that the use of polarization controllers instead of rotators slightly reduces the residual correlation. Monte Carlo simulation based on the coarse step method gave FO-PMD density functions converging to a Maxwellian pdf for PMD emulators with more than ten PMF sections.

Yan *et al.* (2003a) designed and fabricated a novel programmable delay module using six birefringence crystals (a six bit module) that generated tuneable FO-PMD values between -45 to +45 ps with a resolution of 1.4 ps. The emulator device comprised of multiple switch/delay sections. Each switch/delay section consisted of a birefringent crystal to generate a fixed amount of delay and a magneo-optic (MO) polarization switch to generate different delays at a speed < 1 ms. The lengths of the birefringent crystals were arranged in a binary power series, increasing by a factor of two in each section. This particular emulator emulated pure or statistical all-order PMD distributions, which prove powerful in evaluating the dynamic performance of PMD emulators. The delay range and delay resolutions of this device was designed for 10 Gb/s networks but is easily modified to suit 40 Gb/s networks. This emulator is known to be of high speed, stable and repeatable thus yielding tuneable PMD statistics. Due to its reproducibility, it is also applicable to importance sampling in order to independently investigate high PMD values lying on the tail of the Maxwellian PDF.

Bogoni *et al.* (2002) proposed a multisection deterministic emulator (five- and eight-sections) for statistical reproduction of a deployed fibre with accurate statistics up to third-order PMD through simulations. This emulator consisted of fixed delay sections coupled by rotators. The rotators were exhaustively scanned in steps of ~ 10^{o} to create a map of rotational angles and PMD emulator parameters. For each order of PMD, 10 000 different combinations of angles were deterministically imposed on the emulator. From the map, any combination of parameters is chosen to give desired “deterministic” PMD realisations. The proper selection of rotational angles resulted in the emulator accurately reproducing the statistics of PMD parameters up to third order with reduced number of sections, although the best PDF results were obtained for the eight section PMD emulator. The third-order PMD parameter was calculated in the eight-section case in correspondence of each fibre realisation satisfied by the emulator.

Palmer *et al.* (2005) designed a standard concatenated section emulator in which a finite number of fixed uniform length birefringent sections are cascaded. The birefringence length of each section imparts on the FO-PMD between the two polarization modes and the mode coupling in between the sections is dynamically varied by independently rotating each section. The 15-section emulator (with a mean FO-PMD = 37 ps) comprised of uniform random fibre section orientations and arbitrary chosen section lengths. This resulted in a BAC of approximately 10% outside the ACF peak, as well as some periodicity. Contrary to known findings that the BAC gradually decreases with increased number of birefringent fibre sections, these findings show that the order of distributing birefringent sections is important for minimising the emulator BAC even when there are a few number of fibre sections. Through geometrical explanations and derivations of an algebraic model the authors accurately predicted the BAC. Interestingly, the model shows that those emulators with low BAC can be designed by minimising the FO-PMD of the end sections.

Mimura (2003) developed a programmable emulator device based on variable Faraday rotators (VFRs) that are capable of emulating FO-PMD and the two components of SO-PMD. The emulator consisted of four delay sections concatenated by three VFRs, each with a response time less than 60 ms for a 90^{o} rotation. The VFRs were used as polarization controllers, in front of them were polarizers to control the input SOP. All the delay sections had the same delay value of about 7.5 ps to give a full spectrum range (FSR) of 133.3 GHz. The FSR of a device was determined by the length of each delay section. Due to the correlation among FO-PMD, PCD, PSP-depolarization and SO-PMD, they cannot be individually set to any arbitrary value. Therefore by simultaneous non-linear fitting of numerous target profiles, rotational angles can be calculated and assigned to the VFRs on the emulator. The emulator FO-PMD is tuneable from 0 to 30 ps and the variable SO-PMD range is from 0 to 260 ps^2, although it has an insertion loss of 1.7 dB. The emulator also demonstrates that for a fixed SO-PMD value, different PCD and PSP-depolarization profiles can be achieved by changing the number of delay sections on the emulator. By setting the VFR angles to zero the number of delay sections can be reduced. The programmable VFR enables the emulator to be stable hence exhibiting repeatability. Results observed for this emulator agreed with theoretical calculations obtained using the concatenation rules.

3.4.3 Uniform scattering of polarization orientations

These PMD emulators have polarization scramblers placed between PMF sections to uniformly scatter the polarization state over the Poincaré sphere (Fig. 3.6 (c)). Below are highlights of some of the designs falling within this class.

Phua and Ippen (2005) invented a PMD emulator with "combinatorial" polarization scramblers for many fibre segments. The combinatorial approach significantly reduced the number of phase plates without reducing the number of birefringent segments in a many segment PMD emulator. These phase plates, in this case six, effectively scramble light into hundreds of different polarization states thus making the emulator achieve the various key properties of a good emulator as highlighted in Section 3.2. The retardation angles of the six phase plates were randomly tuned for the different realisations of the fibres, resulting in FO-PMD (with mean value ~ 5 ps) and SO-PMD (with mean value ~ 10 ps^2) behaviour that is close to theoretical distributions. The combinatorial approach can also be adopted for emulators using thermal tuning, waveplates and polarization controllers. The emulator is built from unequal birefringence length segments which are Gaussian distributed with a mean value of 1.2 ps and standard deviation of 20% about this mean value. Numerical simulations were performed and the outcome was in good agreement with experimental results.

Lima *et al.* (2001) investigated and attempted optimising a variety of emulators. These emulators were made up of PMF sections interconnected via polarization scramblers. The uniform scattering is easy to model in a computer but hard to realise in practise where polarization scramblers are used. The authors concluded through simulation that ten or more PMF sections are required for the PDF of the FO-PMD to approach the Maxwellian distribution. It was also found that the 15 section emulator with rotatable sections represented a good design compromise compared to emulators with fixed PMF sections and those emulators compromising of three sections were found to be clearly inadequate. Since the polarization states of communication fibres are constantly changing in the real world, controlling mode coupling (uniform scattering) in emulators is vital to enable emulation of the whole ensemble of the fibre.

3.4.4 Tuneable birefringence and fixed polarization orientations

For this type of emulator the birefringence in the birefringent fibre sections is varied whilst the polarization controllers are fixed (Fig. 3.6 (d)). In this study, a tuneable delay line was implemented (Chapter 6). Descriptions of some of the emulator models within this class are given below.

In 2004, Hauer *et al.* constructed a 30 section all-fibre PMD emulator that used an integrated series of 2.5-cm-long micro-heaters to thermally tune the birefringence of each PMF section and accurately reproduce FO- and SO-PMD statistics (Fig. 3.7). The micro-heaters consisted of a 15 nm titanium layer for good adhesion to the fibre and a 120 nm gold layer for good conductivity; these layers of metal were applied through deposition. The 30-sections of FibreCore HiBi PMF (PANDA fibre) were fusion spliced together at fixed 45^{o} angles. The micro-heaters were mounted close to the centre of each PMF. The emulator accurately reproduced the FO-PMD statistics, with the SO-PMD differing slightly only in the low probability tail from theoretical distributions. The autocorrelation function (ACF) had a high residual correlation value of 20%. By increasing the number of fibre sections, the difference in the low probability events tail and residual correlation value can be reduced. This emulator has advantages over other emulators in that it has a low loss, electrically controllable, static parts, negligible PDL and no internal reflections.

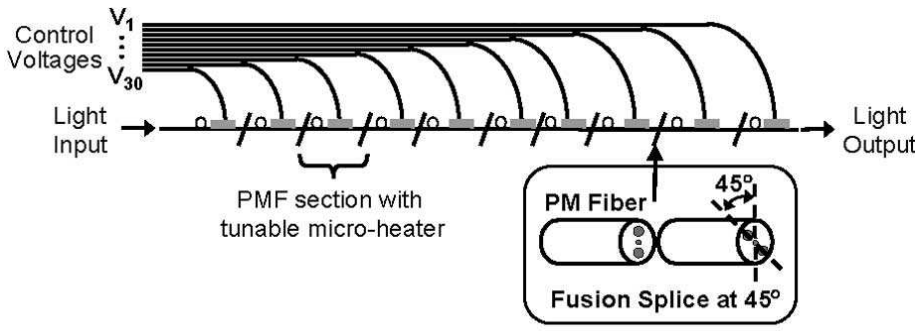

Fig. 3.7: Schematic diagram of the PMD emulator using evaporated micro-heaters on PMF section spliced at 45^{o} (Hauer et al. 2004).

Lee *et al.* (2003) reported a PMD emulator which can generate FO-PMD with exact Maxwellian statistics and SO-PMD approximating the theoretical distribution proposed by Foschini *et al.* (1999). In addition to the former, the emulator shows that reasonable autocorrelation characteristics less than 30% can be achieved with at least four variable delay

elements. This emulator was built using only five variable delay elements, polarization controllers in between delay elements produced arbitrary polarization states and the microprocessor controlled the variable delay elements. Thus this technique generates various PMD statistics through the change in control signals to delay elements without changing its physical configuration. One delay element can even emulate FO-PMD with an exact Maxwellian distribution; however, for the generation of higher-order PMD five elements were used.

Raja and Arabasi (2003) built a virtual FO-PMD emulator (Fig 3.8) used in system simulation. To simulate the behaviour of PMD in a deployed fibre they ensured the polarization controller had ellipticity $\varepsilon = 0$ and the azimuth angle $\theta = 45^{o}$. These settings were introduced in order to rotate the polarization of income light by 45^{o}. The polarization beam splitter divided the two polarization components equally. A delay was introduced in one of the polarization components using the delay tool, thus creating a disparity in arrival time (delay) between the two components. In order to get random delays, several emulators such as the one shown in Fig. 3.8 have to be coupled together. This coupling also results in the emulation of SO-PMD. Raja and Arabasi (2003) used this type of PMD emulator to also design an effective virtual PMD compensator.

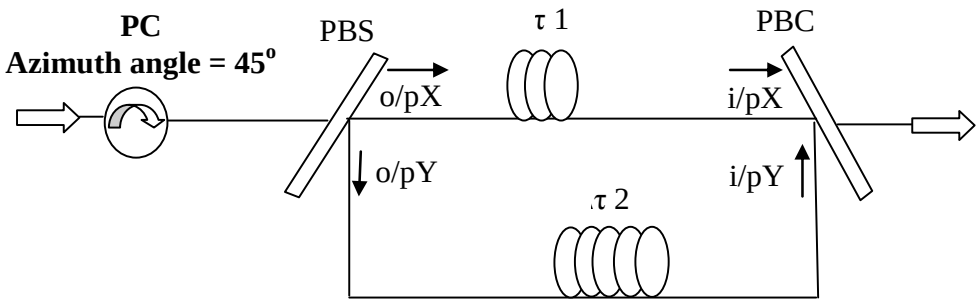

Fig. 3.8: FO-PMD emulator used for system simulation, where o/p and i/p stand for output and input respectively (after Raja and Arabasi 2003). PBC and PBS stand for polarization beam combiner and polarization beam splitter, respectively.

3.4.5 All elements tuneable

These are emulators in which there can be simultaneous adjustments of the birefringence and polarization orientations as illustrated by Fig. 3.6 (e). Insights into some of the already existing PMD emulators falling within this class are provided below.

Yan *et al.* (2006) constructed a PMD emulator to emulate the PMD statistics based on the Hinge model. The emulator consisted of three variable delay elements and three fibre-squeezer-based polarization controllers. Each variable delay element generated FO-PMD statistics approaching the Maxwellian distribution. The polarization controllers varied slowly through a sinusoidal drive of the different fibre-squeezers. Thus polarization coverage of the whole Poincaré sphere was not sacrificed. The overall generated FO-PMD also followed the Maxwellian distribution with an average value of 29 ps, while the dynamics of the FO-PMD statistics was slow, thus meeting the requirements of the Hinge model. The SO-PMD also varies slowly although its statistics was limited by the number of delay elements and coupling angles. The SO-PMD statistics of the emulator followed the theoretical distribution with a mean value of 255 ps^2.

In 2003, Zeng reported the first PMD emulator with tunable SO-PMD and a constant mean FO-PMD. The emulator was based on a variable delay line (variable from $\tau_{variable/max}$ and $\tau_{variable/min}$), a polarization controller, and a HiBi fibre segment with a fixed FO-PMD value of τ_{fixed}. The equations by Gisin and Pellaux (1992) in Section 2.1.3 Ib were used to theoretically predict the PMD of the emulator, the SO-PMD value ranged from Φ to $0.5(\tau_{fixed})^2 + \Phi$ (where $\Phi \sim 10.0\ ps^2$ is the constant residual SO-PMD in the HiBi segment) and the mean FO-PMD was kept constant at a value $\sim \tau_{fixed}$. Experimentally the mean SO-PMD value was varied from 37.0 to 522.0 ps^2 when the variable DGD line was tuned from 0.68 to 45.18 ps and the mean FO-PMD was maintained constant at 32.5 ± 1.0 ps. The PMD statistics of the emulator however did not follow expected theoretical distributions as that of an infinitely mode coupled fibre. An application suggested for such an emulator in high bit rate (> 10 Gb/s) systems is to test for the SO-PMD induced fluctuations around the mean penalties caused by FO-PMD and to evaluate the performance of FO- and SO-PMD compensators.

3.4.6 Both fixed birefringent sections and rotatable polarization orientations

These are types of emulators that contain both fusion spliced birefringence elements and coupled sections via rotatable polarization controllers (Fig. 3.6 (f)). An overview of some of the existing PMD emulators of this class are provided below.

Phua and Haus (2002) proposed a module that generated SO-PMD without producing any FO-PMD. The emulator constituted of two fixed delay segments and one variable DGD element concatenated via two tuneable polarization controllers (PCs) (Fig. 3.9). The concatenation of the two fixed delay segments generated the required SO-PMD, and the variable delay segment cancelled the unwanted FO-PMD generated by these two fixed delay segments. Due to the two sets of concatenated segments generating SO-PMD, a smaller amount of third-order PMD was observed. A mathematical proof of the behaviour of this emulator was derived using the concatenation equation in Section 2.1.3 IIIa. A Monte Carlo simulation of over 100 000 independent repetitions showed that this module can be controlled to produce any desired PDF of the SO-PMD statistics similar to that of real transmission fibres. The same module was used for deterministic controlled PMD emulation.

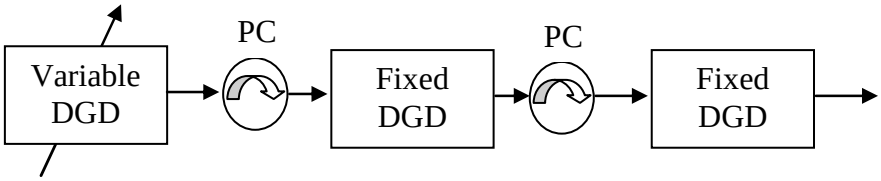

Fig. 3.9: Schematic of the variable SO-PMD module without FO-PMD.

Wegmuller *et al.* (2002) simulated a PMD emulator using two delay elements, with a coupling angle in between their birefringent axes. Each of these delay elements was represented by a delay block, polarization beam splitter (PBS), polarization beam combiner (PBC). The FO-PMD adjustments were achieved by varying the delay blocks, in this case from 0 – 300 ps. Contrary to most approaches, the invention of this emulator (like Zeng's (2003) emulator) was not to mimic a deployed fibre. The authors maintained the FO-PMD and SO-PMD wavelength independent. In one case the FO-PMD was varied whilst the coupling ratio remained fixed i.e. at 0.3 and in the other case the coupling ratio was varied while the FO-PMD remained fixed i.e. at 15.75 ps. The simulation values for the FO-PMD and instantaneous SO-PMD agreed to expectation values. Equation 2.7 and its frequency derivative were used to theoretically calculate the PMD expectation values. The unique

properties of this emulator enable investigations into the low-probability events of large FO-PMD and SO-PMD, which are crucial causes for system outage.

Yan *et al.* (2008) developed a low cost all-fibre PMD emulator with limited number of electrically driven polarization controllers (PCs). The emulator consisted of six fibre squeezer based PCs which generate uniform SOP scattering between seven PMF sections, each consisting of four sub-sections with unequal lengths and fusion spliced at 45^{o} relative to each other. The lengths of the PMFs were Gaussian distributed and the correct choice of the FO-PMD values of the four sub-sections was done through optimisation. The FO-PMD (with mean ~ 25 ps) and SO-PMD (with mean ~ 372 ps^2) statistical distributions generated using only six polarization controllers were close to the theoretical distributions. This emulator design resulted in a low BAC.

3.5 Limitations of PMD emulators

Emulators based on rotating coupling angles of birefringence crystals, rotating or heating sections of PMFs and those that split input light and delay one component by free space optics suffer from a slow response time (in the order of seconds) and poor repeatability. This makes them less effective in evaluating PMD compensators (Yan *et al.* 2003a). Emulators also have a threshold minimum and maximum PMD value depending on the configuration and number of fibre sections whilst in the real situation, the number of sections extends to hundreds if not thousands. Thus the statistics is limited by the number of birefringent sections in some emulators; an increase in the number of PMF sections makes the emulator more costly depending on the length and type of PMF used.

The other drawback with some emulators is that the statistics are fixed at a point in time to mimic a particular manufactured fibre and are not easily reconfigurable to emulate different fibre plants and fibres as they age. However, a few emulators overcome some of these above mentioned limitations. For example Yan *et al.* (2003) developed a delay module capable of generating repeatable FO-PMD variations as fast as 200 μs, which was used to evaluate the impulse response of a PMD compensator with a speed of the order 1 ms. This emulator also enables tuneable PMD statistics which can suit different deployed fibres or fibre plants.

The different classes of emulators used in this chapter will be used to categorise the emulators designed in this study (see Chapter 6). The PMD of the emulators can be measured using any of the measurement techniques mentioned in Chapter 4.

CHAPTER 4

MEASUREMENT TECHNIQUES

This Chapter aims to highlight only those specific experimental techniques used to measure PMD in this research, although there are many more techniques available. PMD measurement methods are classified as either in the time domain or frequency domain. The frequency domain techniques: namely Jones matrix eigenanalysis (Heffner 1992, Forestieri and Vincetti 2001), Fixed analyser (Poole and Favin 1994), Poincaré sphere arc (Poole *et al.* 1988, Galtarossa *et al.* 1996, Cyr *et al.* 1999), Attractor-Precessor (Eyal and Tur 1997) and Müller matrix (Jopson *et al.* 1999), measure PMD by detecting output SOP changes as a function of frequency. The time domain methods: namely interferometric method (Gisin *et al.* 1991, TIA/EIA 455-124-A 2004), time-of-flight (Williams 2004), polarization-optical time domain reflectometry (Rogers 1981, Galtarossa and Palmieri 2004b) and modulation phase shift method (Williams 1999a), determine PMD by measuring the time delay between the fast and slow orthogonal polarization modes of the transmitted light pulse. The polarization-optical time domain reflectometry (P-OTDR) technique measures PMD with fibre distance based on back-reflected light. More information on the P-OTDR technique can be found in Appendix II.

4.1 The Frequency Domain Technique

In this domain, the Jones matrix eigenanalysis (JME) technique for PMD and PDL measurement will be considered. The JME was found suitable for this study although there are several other frequency domain techniques available as listed above. The transmission of fully polarized coherent light through a linear medium such as an optical fibre can be described in Jones space. This method needs a sophisticated algorithm for computative derivatives and stable measurement conditions due to its sensitivity to vibrations. In order to determine the Jones matrix of an optical medium, polarizers are oriented at 0^o, 45^o and 90^o from a tuneable narrowband source to give three input SOPs (Fig 4.1 (a)). The PMD and PDL vectors are then obtained by differentiating the Jones matrix (Gisin and Pellaux 1992). Forestieri and Vincetti (2001) showed how the Jones matrix of a fibre can be exactly evaluated in the presence of PMD of any order through rigorous derivations.

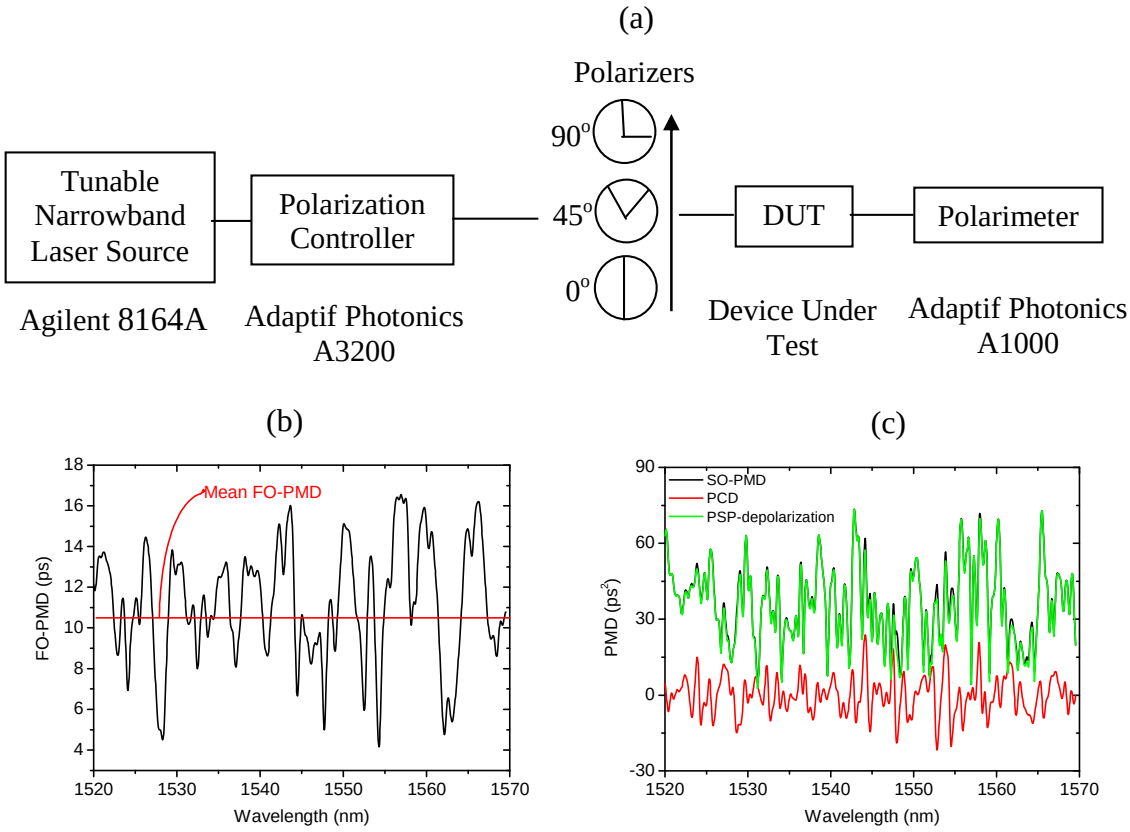

Fig . 4.1(a) The experimental setup to measure PMD and/or PDL using the JME method as three linear input polarization states 0^o, 45^o and 90^o are set. The variation of (b) FO-PMD with wavelength and (c) SO-PMD and its components with wavelength. The PMD measurements in (b) and (c) were obtained from a 28.4 km buried fibre link (FUT) in Port Elizabeth South Africa, owned by Telkom South Africa.

The setup shown in Fig. 4.1 (a) was used during laboratory and field measurements of PMD (Fig. 4.1 (b – c)). The same setup was used for all the PDL measurements obtained in this study.

4.1.1 JME for PMD measurement

The three input SOPs, as referred above, generate a 2 x 2 matrix at each wavelength or frequency. In the absence of PDL, the Jones matrix of the n'th birefringent section of a fibre link or emulator can be expressed as (Gupta 2007):

$$T_n = \begin{pmatrix} \cos\theta_n & -\sin\theta_n \\ \sin\theta_n & \cos\theta_n \end{pmatrix} \times \begin{bmatrix} \exp\left(i\frac{\Delta\omega\tau_n}{2}\right) & 0 \\ 0 & \exp\left(-i\frac{\Delta\omega\tau_n}{2}\right) \end{bmatrix} \times \begin{pmatrix} \cos\theta_n & \sin\theta_n \\ -\sin\theta_n & \cos\theta_n \end{pmatrix} \qquad (4.1)$$

where θ_n is the orientation of the fast axis of the n'th section with respect to a fixed axis (say, x axis), $\Delta\omega = \omega - \omega_o$ is the angular frequency difference with respect to the central frequency ω_o and τ_n is the FO-PMD (or DGD) of the n'th section. The angle θ_n lies between 0^o and 360^o, and for random mode coupling, θ_n is assumed to be uniformly random distributed between this range.

The frequency dependent Jones transfer matrix for the entire fibre link or emulator $T(\omega)$ is a product over T_n for all the N fibre sections:

$$T(\omega) = \prod_{n=1}^{N} \left(\begin{pmatrix} \cos\theta_n & -\sin\theta_n \\ \sin\theta_n & \cos\theta_n \end{pmatrix} \times \begin{bmatrix} \exp\left(i\frac{\Delta\omega\tau_n}{2}\right) & 0 \\ 0 & \exp\left(-i\frac{\Delta\omega\tau_n}{2}\right) \end{bmatrix} \times \begin{pmatrix} \cos\theta_n & \sin\theta_n \\ -\sin\theta_n & \cos\theta_n \end{pmatrix} \right) \tag{4.2}$$

By measuring the transfer matrix $T(\omega)$ of an entire optical medium, it is possible to determine the total FO-PMD and the PSPs using the standard JME. Heffner (1992) and Derickson (1998) showed that the FO-PMD at the angular frequency midway between two closely spaced angular frequencies, ω_1 and ω_2, is given by:

$$\tau_{tot} = \left| \frac{\arg(\rho_1/\rho_2)}{\Delta\omega} \right| = \left| \frac{\arg(\rho_1/\rho_2)}{\omega_2 - \omega_1} \right| \tag{4.3}$$

where ρ_1 and ρ_2 are the eigenvalues of the matrix product $T(\omega_2)T^{-1}(\omega_1)$ and $\arg(\ )$ is the argument function. The fast and slow PSPs of the fibre are given by the two eigenvectors of $T(\omega_2)T^{-1}(\omega_1)$ (Heffner 1992). Poole and Wagner (1986) obtained an expression for the corresponding output PSP for each random concatenated section. When the PSPs are converted to their corresponding Stokes representation, the PMD vector in Stokes space is as given in Eq. 2.1.

When there is presence of PDL in the network system or PMD emulator, Eq. 4.1 modifies to:

$$T_n = \begin{pmatrix} \cos\theta_n & -\sin\theta_n \\ \sin\theta_n & \cos\theta_n \end{pmatrix} \times \begin{bmatrix} \exp\left(i\frac{\Delta\omega\tau_n}{2} + \frac{\alpha_n}{2} \right) & 0 \\ 0 & \exp\left(-i\frac{\Delta\omega\tau_n}{2} - \frac{\alpha_n}{2} \right) \end{bmatrix} \times \begin{pmatrix} \cos\theta_n & \sin\theta_n \\ -\sin\theta_n & \cos\theta_n \end{pmatrix} \quad (4.4)$$

where α_n is the PDL present in the n'th fibre section. As discussed in Section 2.3 the two PSPs then become non-orthogonal. The application of Eq. 4.1 in this case compromises the accuracy of PMD measurements.

4.1.2 JME for PDL measurement

As mentioned in the previous subsection, the transmission properties of an optical medium or component are represented by the complex transfer matrix $T(\omega)$. PDL can be determined from (Huttner *et al.* 2000, Chen *et al.* 2005):

$$T^{*\dagger}(\omega)T(\omega) = A^2 \geq 0 \quad (4.5)$$

where $T^{*\dagger}(\omega)$ denotes the complex transpose conjugate matrix and A is the Hermitian matrix representing the effective PDL. Finding the maximum and minimum intensity transmission coefficients is equivalent to finding the highest and lowest values (extrema values) of $T^{*\dagger}(\omega)T(\omega)$. Therefore, using the eigenvalues, λ_1 and λ_2, of $T^{*\dagger}(\omega)T(\omega)$ in Eq. (4.5), PDL is expressed as (Yang *et al.* 2005):

$$\mathrm{PDL} = 10\log\frac{\lambda_2\left(T(\omega)^{*\dagger}T(\omega)\right)}{\lambda_1\left(T(\omega)^{*\dagger}T(\omega)\right)} \quad (4.6)$$

Equation 4.6 compares well with Eq. 2.33, therefore PDL can also be represented as:

$$PDL = 10\log\frac{\lambda_2\left(T(\omega)^{*\dagger}T(\omega)\right)}{\lambda_1\left(T(\omega)^{*\dagger}T(\omega)\right)} = 10\log\frac{T_{max}}{T_{min}} = 10\log\frac{P_{max}}{P_{min}} \quad (4.7)$$

Thus using the same configurations in Fig. 4.1, the JME method can be used to measure the PDL resulting from polarization sensitive components.

4.2 The time domain interferometry method

The commercially available time domain interferometry techniques include EXFO's FTB-5500B generalized interferometry technique (GINTY) and FTB-5500 traditional interferometry techniques (TINTY). These interferometry PMD measurement techniques are very popular for field work since they facilitate rapid and accurate determination of FO-PMD even in the presence of fibre movement and vibrations, making them conducive for aerial fibre FO-PMD measurements. The two were compared by the NMMU Optical Fibre Research Unit (Musara 2006, Wu 2006) and by others (Cyr 2004). GINTY was found to be more accurate than TINTY making it our preferred measurement technique in this study. For more insight into TINTY, refer to TIA/EIA 455-124-A (2004). Both interferometric techniques, TINTY and GINTY, are based on the Michelson interferometer (MI). The other time domain technique to be considered is the polarization - optical time domain reflectometry (P-OTDR) and is addressed in Appendix II.

4.2.1 Michelson interferometer (MI)

This subsection introduces the Michelson interferometer, related to light interference with respect to the nature of the light source. The broadband LED light source entering the interferometer passes through a 50/50 polarization beam splitter (PBS), with one beam directed to the fixed mirror and the other to the moveable mirror (Fig. 4.2). Each of the mirrors reflects the light beam back to the PBS where they interfere before travelling to the detector where an interference pattern is detected.

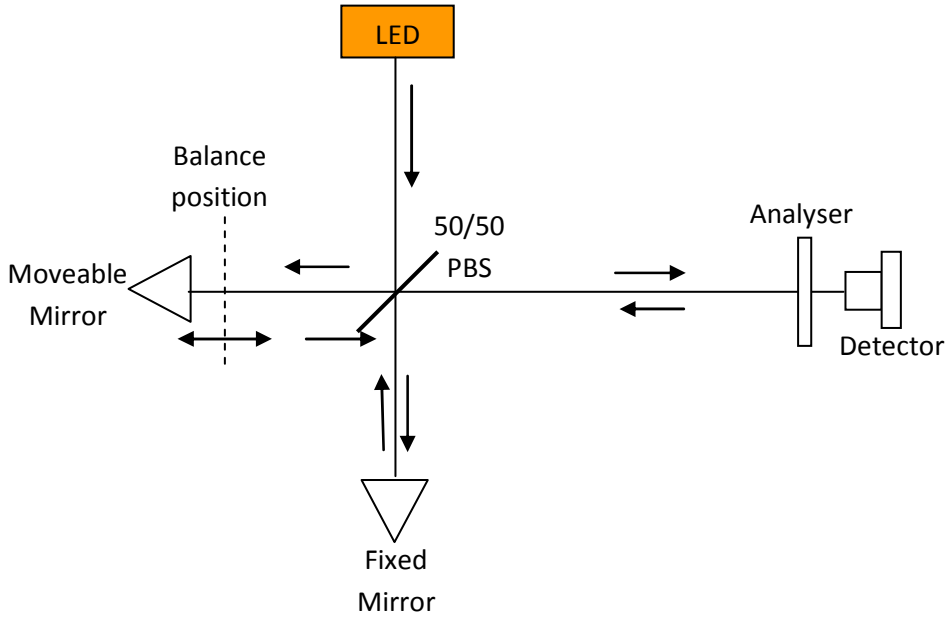

Fig 4.2: The Michelson interferometer setup located in the interferometry techniques, used for PMD measurements.

The degree of interference depends on the optical delay time relative to the coherence time (time interval over which the phase of the source remains constant). The coherence time σ_c is expressed as (TIA/EIA 455-124-A 2004):

$$\sigma_c = \lambda_o^2 / (\Delta\lambda . c) \qquad (4.8)$$

where λ_o is the source central wavelength, c is the velocity of light in free space and $\Delta\lambda$ is the full-width at half-maximum (FWHM) of the source. Interference occurs for optical delay times that are less than the coherence time. Constructive interference occurs when the moveable mirror is at the balance mirror position. Destructive interference is observed when the moveable mirror moves away from the balance point. When the delay times and coherence times become increasingly similar, the intensity of the interference diminishes. The observed central peak, for example on the TINTY interferogram, arises from the interference of light from different arms of the MI that follow the same path through the fibre. The peak will be at zero position since light follows the same path through the fibre with a zero time delay.

Interference peaks result when the path difference in the two arms of the MI compensates the difference in the propagation speeds of the fibre modes. The interference of light from the same source may be dealt with using the Fourier transform theory. The Fourier transform of the narrow spectral source in the frequency domain gives a broad interference envelope in the time domain and *vice versa* for a broad spectrum source.

4.2.2 The General interferometry technique (GINTY: FTB-5500B)

The generalized interferometric technique (GINTY) developed by EXFO has a modified setup and incorporates different analysis of the interferograms from the one used by TINTY. The main key modification is that GINTY, unlike TINTY, is designed with an algorithm meant to remove the effect of the central auto correlation peak (ACP), leaving only the cross correlation peaks (CCP) used to calculate the FO-PMD value. The ACP contains no FO-PMD information and is known to affect the accuracy of the FO-PMD measurement in TINTY. GINTY removes all the assumptions made when using TINTY for determining FO-PMD (Cyr 2004). For a detailed comparison between TINTY and GINTY, the reader is referred to Cyr (2004) and Musara (2006). In this section, we highlight how GINTY operates with the support of mathematical equations.

Fig. 4.3 (a) shows a FO-PMD measurement setup, comprising of GINTY. The setup consists of a polarized broadband source, fibre under test (FUT), the Michelson interferometer, polarization beam splitters (PBS), analysers and the two detectors. The additional polarization beam splitter (PBS) splits the beam and directs it to two detectors for analysis. This setup is used to measure the FO-PMD of a mode coupled fibre resulting in an interferogram with interference fringes, as shown in Fig. 4.3 (c). The root mean square (rms)-FO-PMD value is then determined from the Gaussian curve fit to the interferogram. The interferogram for a PMF or PMD emulator with negligible mode coupling has limited peaks (Fig. 4.3 (b)); the FO-PMD is then the distance from the centre of the central peak to the centre of the satellite peak.

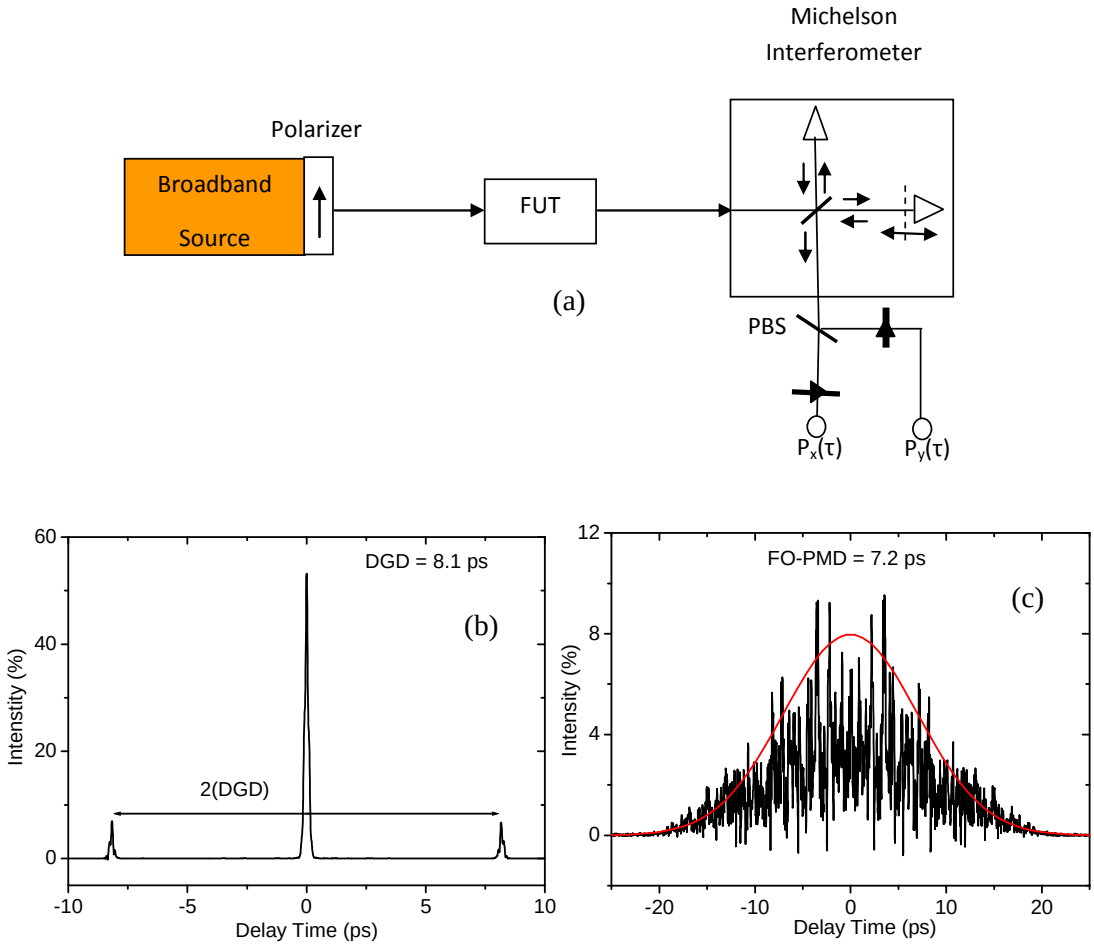

Fig. 4.3 (a) Schematic setup of GINTY, (b) interferogram from a weak mode coupled fibre and (c) interferogram from strong mode coupled fibre. FUT stands for fibre under test, this

Considering the general mathematics and referring to Fig. 4.3 (a), it can be seen that (TIA/EIA 455-124-A 2004):

$$\text{Detector 1: Intensity} = I_1^2 + I_2^2 + 2I_1I_2\cos\theta \qquad (4.9a)$$

$$\text{Detector 2: Intensity} = I_1^2 + I_2^2 - 2I_1I_2\cos\theta \qquad (4.9b)$$

where I_1^2 is the auto correlation (AC) from the first arm of the interferometer, I_2^2 is the AC from the second arm of the interferometer and I_1I_2 is the cross correlation (CC). GINTY utilises only the CC for accurate FO-PMD measurements.

The auto correlation and cross correlation envelopes for a single input/output (I/O) SOP pair are:

$$\text{AC: } E_o(\tau) = \left|\tilde{P}_x(\tau)+\tilde{P}_y(\tau)\right| \equiv \text{Detector 1 + Detector 2} = 2\left(I_1^2 - I_2^2\right) \quad (4.10a)$$

$$\text{CC: } E_x(\tau) = \left|\tilde{P}_x(\tau) - \tilde{P}_y(\tau)\right| \equiv \text{Detector 1 - Detector 2} = 2\left(2I_1I_2\cos\theta\right) \quad (4.10b)$$

where $\tilde{P}_x(\tau)$ and $\tilde{P}_y(\tau)$ represent the respective raw interferograms observed along the two orthogonal analyser axes.

The exact mathematical analysis gives measured FO-PMD as (Cyr 2004):

$$\text{Measured FO-PMD} = \sqrt{3/2\left(\sigma_x^2 - \sigma_o^2\right)} \quad (4.11)$$

where σ_x is the root mean square (rms) width of the mean square (MS) CC envelope and σ_o is the rms width of the MS AC envelope. Both MS envelopes are obtained simultaneously but separately without interfering as shown by equations 4.10a and 4.10b.

GINTY is not sensitive to the source shape spectrum and interferogram shape. The only condition to be satisfied for Eq. 4.11 to apply is that the FUT should exhibit linearity, be stable (although difficult to attain during experiments) and should have zero polarization dependent loss (PDL). GINTY has an averaging window and remains mathematically exact. Subtraction of the offset, as in Eq. 4.11, eliminates the systematic bias induced by a narrow or ill shaped spectrum, thereby allowing measurements through a network with EDFAs and optical components. In principle, FO-PMD = 0 can be measured when $\sigma_x = \sigma_o$ (Eq. 4.11).

These techniques will be used in Chapters 5-7 where the experimental results for this study will be presented.

CHAPTER 5

CHARACTERISING DEPLOYED FIBRES FOR PMD

Polarization mode dispersion (PMD) has already been highlighted as a major impediment towards high speed data transmission in optical network systems (Chapter 2). Therefore, accurate PMD measurement techniques can provide reliable data for statistical analysis. This chapter focuses on the measurement of PMD in deployed fibres and its analysis. In order to understand the PMD phenomenon in depth, novel PMD emulation is critical. In this study, Chapter 6, PMD emulators falling in different categories have been designed. The JME and GINTY methods referred to in Chapter 4, will be used to measure PMD. The SOPs will be used to monitor the behaviour of light as it propagates through deployed fibres.

5.1 PMD measurements

First-order PMD, second-order PMD and SOP measurements presented in this section were obtained from ITU-T G.652 28.4 km buried fibres and 14.2 km aerial fibres. These fibres are deployed in South Africa in the city of Port Elizabeth, and are owned by Telkom South Africa. All the buried fibre links, each made from looping two 14.2 km fibre links using a single mode patchchord to allow end to end access, are secured in a single cable. Buried fibre PMD measurements carried out using the JME method were conducted over the 1520 to 1570 nm wavelength range at an optimal resolution of 0.3 nm to avoid noisy spectra. Aerial fibre PMD measurements were carried out using GINTY since it is not sensitive to fibre movement compared to JME which will introduce measurement errors. The reader should take note that GINTY can also be used for buried fibre measurements. The output SOP of light from an Agilent 8164A laser source was monitored using the A1000 polarization analyser. Single mode fibre (SMF) patchcords with negligible PMD were used to connect the fibre links under test and measurement devices. In this section, firstly, FO-PMD measurements obtained using the JME will be used to determine whether the buried fibre links under test can accommodate high transmission bit rates ($\geq$ 2.5 Gb/s). Secondly, PMD measurements acquired over wavelength and time will be statistically analysed. In the following section, the focus will be on SOP monitoring with time.

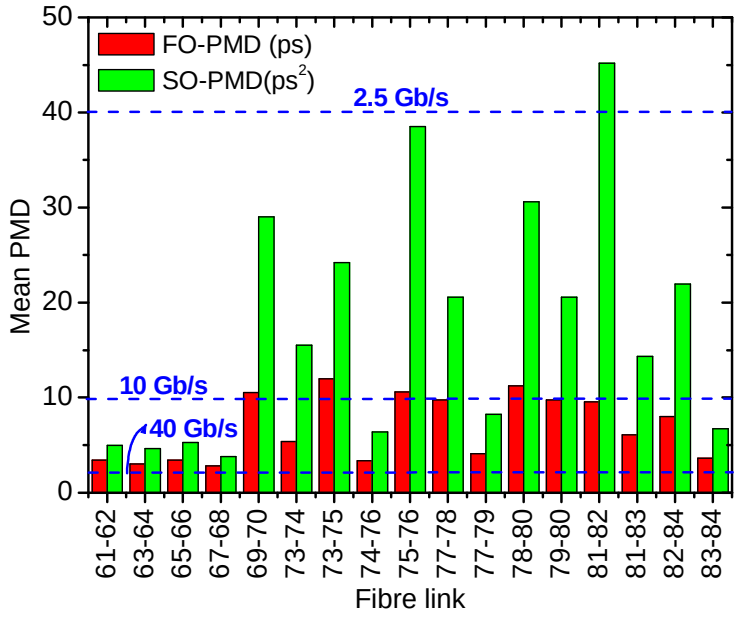

Fig. 5.1: FO- and SO-PMD measurements from 28.4 km ITU-T G.652 buried fibre links. At each transmission bit-rate (2.5 Gb/s, 10Gb/s and 40 Gb/s), the maximum tolerable amount of FO-PMD corresponds to 10% of the bit period.

The histogram in Fig 5.1 shows the mean PMD values obtained when two 14.2 km buried fibre links were looped. The maximum tolerable amount of FO-PMD when transmitting at 2.5 Gb/s is 40 ps, 10 Gb/s is 10 ps and 40 Gb/s is 2.5 ps. This therefore means Telkom South Africa can transmit at 2.5 Gb/s over all the tested fibres without major impediments from PMD. However, an increase in the transmission speed to 10 Gb/s makes fibre links 69-70, 73-75, 75-76 and 78-80 inappropriate for data transmission due to signal impairments (Section 2.1.7). A further increase in transmission speed to 40 Gb/s is not practically feasible for all the fibre links due to all the fibre links having FO-PMD values above 2.5 ps, the maximum tolerable value. Thus to transmit at high speeds (≥ 10 Gb/s), Telkom South Africa should replace these fibre links or high birefringent (HiBi) sections along the fibre length with those having low PMD. PMD can also be mitigated by the application of PMD compensators; for more information refer to Section 2.1.6. To better understand how HiBi or high FO-PMD (HIFO-PMD) sections affect the PMD statistics and output SOPs of a fibre link, PMD emulators designed and implemented in this study will be applied (see Sections 6.1.3, 6.4 and Chapter 7). In the following subsection focus will be on the statistics of PMD with wavelength and time in buried and aerial fibres.

5.1.1 PMD variation with wavelength and time in buried fibres

In this subsection we characterise deployed buried fibre links for both FO- and SO-PMD using the JME. The PMD emulators designed in this study will have similar statistical PMD distributions as those of the tested deployed fibres. The experimental setup is similar to that in Fig. 4. 1 (a). The reader should take note that buried fibres are secured in ducts and installed underground. Firstly, PMD variations with wavelength will be analysed and followed by an analysis into their variation with time. The results shown in this subsection are from only some of the buried fibre links, though all fibre links given in Fig. 5.1 were analysed.

FO- and SO-PMD spectra similar to those in figures 4.1 (b - c) were obtained for each fibre link. The results were found to be stochastic in nature and so were their SO-PMD components, namely PCD and PSP-depolarization. Figure 5.2 shows the statistical distribution of FO- and SO-PMD obtained from fibre Link 61-62 and Link 81-82. These two highlighted links in general represent the PMD statistical behaviour obtained from all the tested fibre links. Figures 5.2 (a') and (b') provide information (not shown) showing that PSP-depolarization is the dominant SO-PMD contributor compared to PCD. This agrees with findings by Foschini *et al.* (1999), where 8/9 is the expected ratio of PSP-depolarization to SO-PMD. The PSP-depolarization to SO-PMD ratio obtained from Link 61-62 deviates slightly by 3.4% from the expected value and that of Link 81-82 deviates by 9.7% (Fig. 5.2). The SO-PMD statistics generated by PMD emulators designed in this study will also be used to verify this finding.

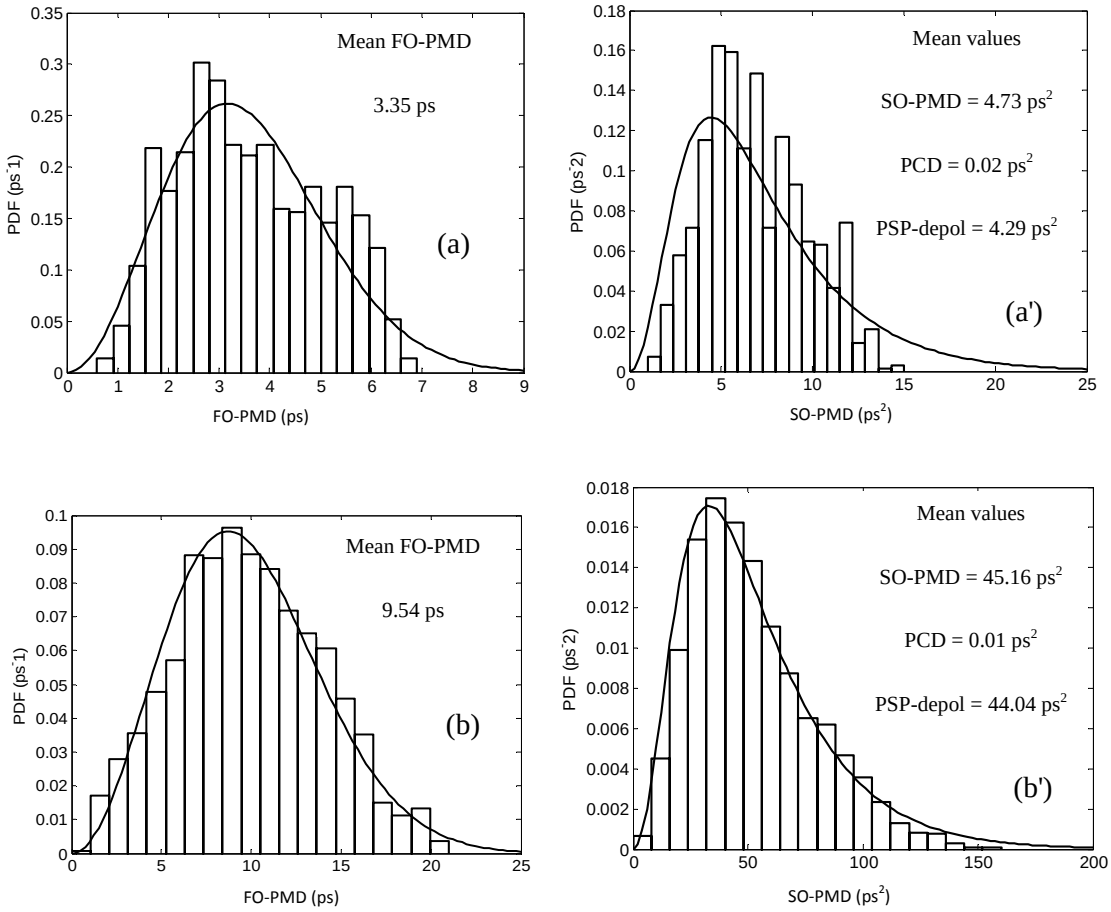

Fig. 5.2: The FO-PMD statistical distribution for (a) Link 61-62 and (b) Link 81-82, and the accompanying SO-PMD statistical distribution for (a') Link 61-62 and (b') Link 81-82. The solid line mapped to the FO-PMD histogram is the theoretical Maxwellian distribution and that mapped to the SO-PMD histogram is the theoretical distribution proposed by Foschini et al. (1999).

Figures 5.2 (b - b') show that the FO-PMD or DGD statistical distribution of Link 81-82 approaches the theoretical Maxwellian distribution and that of the SO-PMD approaches the theoretical distribution proposed by Foschini *et al.* (1999). The PMD distribution from Link 61-62 (see figure 5.2 (a - a')) does not approach the theoretical distributions to the same extent. This is likely due to limited random mode coupling that does not promote the significant variation of the FO-PMD and PSPs with wavelength. The former comes from the assumption used by Foschini and Poole (1991) to relate FO-PMD statistics to the Maxwellian distribution. The assumption states that, FO-PMD follows a Maxwellian distribution when there is infinite random mode couple. By comparing the histograms of FO-PMD data obtained from all the fibre links, it can be deduced that the magnitude of the FO-PMD is independent of whether the FO-PMD statistics approach the Maxwellian distribution or not. This means

the key factor is sufficient random mode coupling. To justify this, PMD emulators in Chapter 6 will be implemented.

SO-PMD measurements show that links with high SO-PMD (i.e. see Fig 5.2 (b')) approach the theoretical distribution. This is due to the presence of high random mode coupling which promotes the increased variation of the FO-PMD and PSPs with wavelength. The FO-PMD variation with wavelength is equivalent to PCD and that of PSPs with wavelength is equivalent to PSP-depolarization. Limited mode coupling results in low SO-PMD, for example see Fig. 5.2 (a'). A detailed look into SO-PMD behaviour will be addressed through PMD emulation in Chapter 6 where mode coupling will be altered. Take note that there is not always a linear relationship between FO- and SO-PMD as was observed with the tested fibres. The PMD emulator designs in Chapter 6 will show that in some cases; FO-PMD and SO-PMD are inversely proportional, FO-PMD is fixed but SO-PMD varies and vice versa, and negligible SO-PMD can yield varying FO-PMD.

In order to monitor PMD (both FO- and SO-PMD) with time over a fibre link, the computer was programmed to continuously sample PMD versus wavelength statistics similar to those in Fig. 4.1 (b – c) at 1 minute intervals over a 98-hour period. Measurements were taken from fibre Link 63-64, the results of which are presented in Fig. 5.3. It can be deduced from Fig. 5.3 that the PMD changes with time at a fixed wavelength were gradual and had limited variations. These gradual and limited PMD variations are probably due to limited temperature changes on the fibre links. This results in limited changes in fibre birefringence and mode coupling. These findings agree with the work by Kogelnik *et al.* (2005) who found limited PMD changes with time. However, slight temperature changes or movement that may occur on the looped SMF patchcord can affect the SOP of light and the coupling angle between the two 14.2 km fibre links. This coupling angle can affect the total PMD of the link per wavelength. This SMF patchcord can be referred to as a Hinge with respect to studies by Galtarossa *et al.* (2008) and Antonelli and Mecozzi (2006). To monitor the behaviour of the Hinge with time, a Hinge model has been developed (Antonelli *et al.* 2008). A Hinge site is a discrete location along a fibre link which is exposed to environmental pertubations usually where buried fibres lead to optical devices along the network sytem. The variation of PMD with wavelength at a fixed time in this study was stochastic. This is due to the presence of random mode coupled along the length of the fibre link.

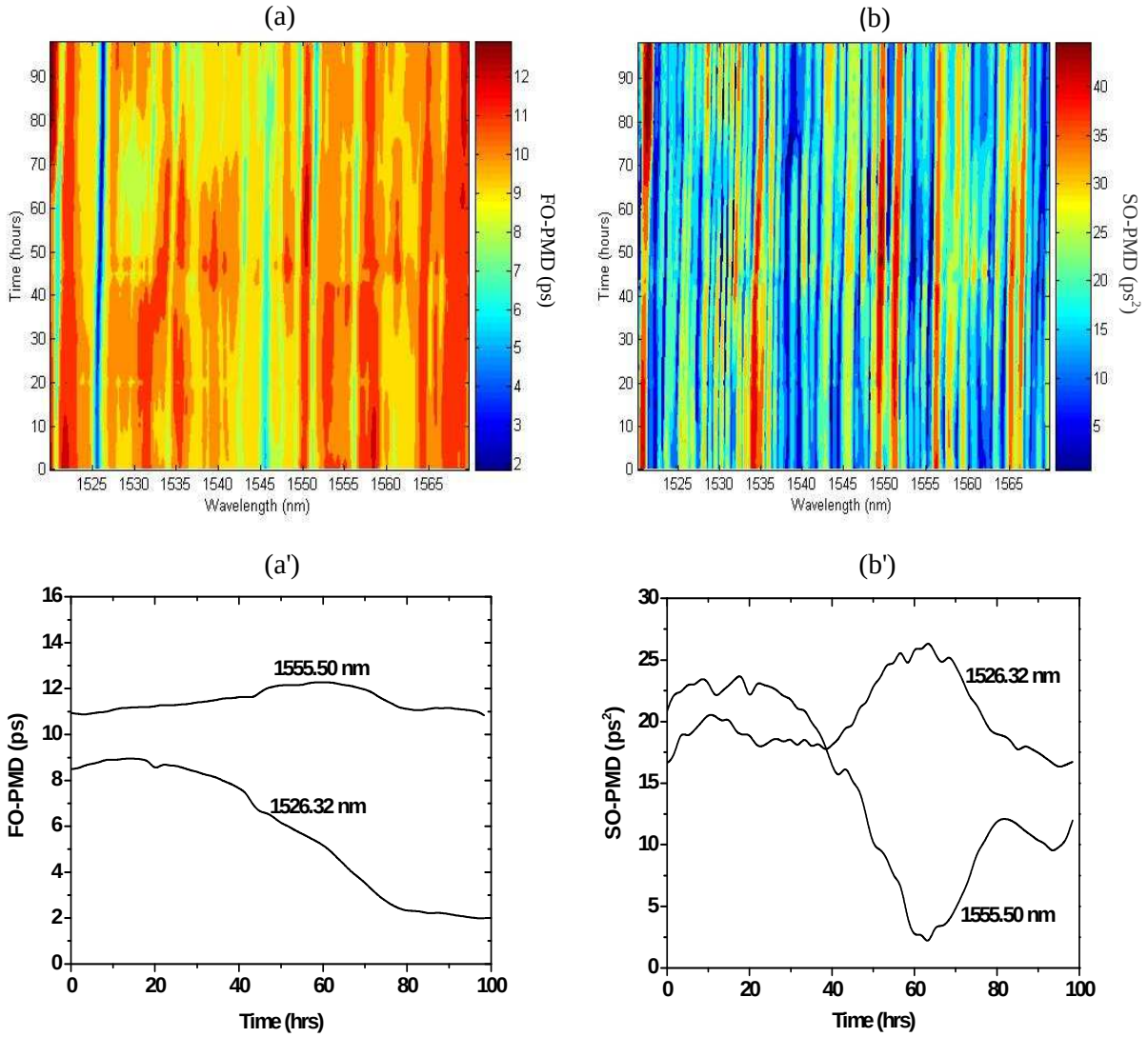

Fig. 5.3: (a) FO-PMD and (b) SO-PMD versus wavelength and time density maps for a coupled fibre link. This coupled link is a result of coupling Links 63 and 64. An illustration of (a') FO-PMD and (b') SO-PMD behaviour with time at the 1526.32 and 1555.50 nm wavelengths.

Each wavelength has independent PMD vectors (FO- and SO-PMD vectors) as illustrated in Fig. 4.1 (b – c). Therefore, regions where the SO-PMD magnitude increases (Fig. 5.3 (b')), e.g. between 40 - 63 hrs at 1526.32 nm and 63 – 80 hrs at 1555.50 nm, indicates a reduction in the angle separating these two vectors (one of link 63 and the other of link 64). In this case the SMF patchcord region which can be referred to as the Hinge, determines the angle between the two vectors. When there is a decreasing trend in the SO-PMD (e.g. between 63 - 83 hrs at 1526.32 nm and 40 – 63 hrs at 1555.50 nm), the reverse is true. A large separation angle ($\approx 180^{o}$) between two SO-PMD vectors of almost similar magnitude will give a

decreasing resultant SO-PMD approaching zero. A smaller vector separation angle ($\approx 0^o$) will give a resultant SO-PMD vector which is almost equivalent to the sum of the two vectors. A similar argument as above could be used to describe the trend observed in the FO-PMD with time in Fig 5.3 (a'). If one of the vectors dominates the other, the resultant vector will be close to the dominant vector even if the separation angle between these vectors ranges from 0 to 180^o (Musara *et al.* 2009a). The former will be verified experimentally in Chapters 6 and 7 through PMD emulation.

Fig. 5.3 (a' - b') shows a distinctive behaviour of the two PMD phenomena (FO- and SO-PMD), they do not necessarily follow the same trend or direction at particular wavelengths with time. This difference likely emanates from their definitions, by definition FO-PMD is considered wavelength-independent and SO-PMD is considered frequency-dependent (Section 2.1.3 Ia). The unevenness in SO-PMD changes with time as in Fig. 5.3 (b') is most likely due to the measurement error of the JME. The SO-PMD vector at any particular wavelength is also affected by rotating vectors at adjacent neighbouring wavelengths. The gradual and limited FO- and SO-PMD between the 1 minute time over the 98-hour period results in non-stochastic FO- and SO-PMD distributions, which do not approach the PMD theoretical distributions. A non-stochastic PMD distribution will still be maintained over a long period of time if these external perturbations remain limited or vary gradually.

5.1.2 PMD variation with time in aerial fibres

In this study, the amount of FO-PMD in an aerial fibre was measured using GINTY only since it is less sensitive to movements. Polarization scrambling of the signal at the input and output of the fibre during measurement is known to reduce the measurement error of GINTY (Wu *et al.* 2006, Musara 2006 and Mudau 2008). Polarization scrambling enables all possible polarization states to be sampled thus giving a more accurate FO-PMD value. Input/output scrambling was performed using the Adaptif A3200 polarization controllers (Section 3.3.2 III) whilst FO-PMD measurements were sampled over a 14 day period (from 06/08/2007 to 21/08/2007) at 5 minute intervals. Wind speed and temperature were also monitored. The FO-PMD statistical changes of the aerial fibre will be mimicked in Section 6.3 using an adjustable PMD emulator.

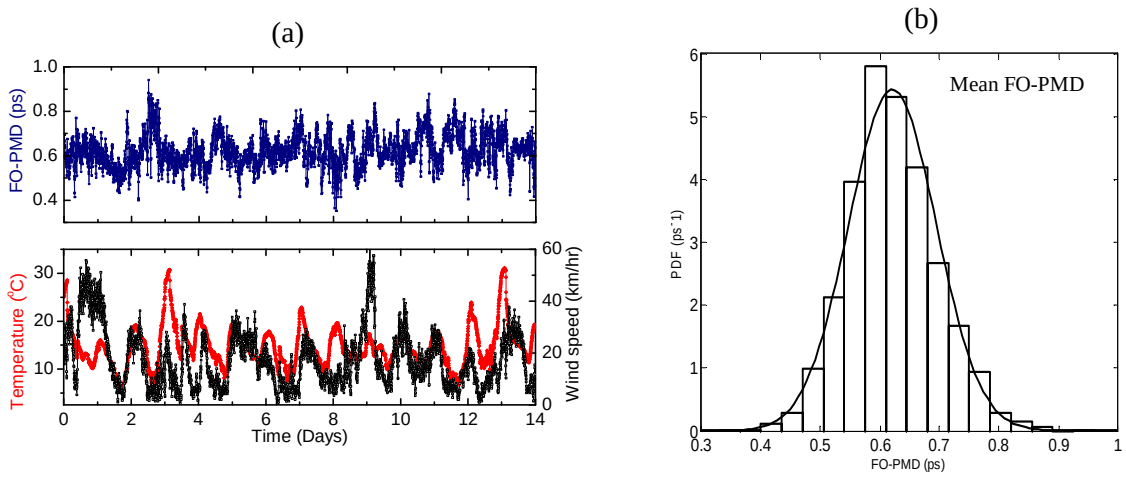

Fig. 5.4: (a) FO-PMD variation with time[1] *and (b) Statistical distribution of FO-PMD. The solid line in (b) is the Gaussian distribution fit.*

The FO-PMD behaviour in Fig. 5.4 and the prevailing environmental changes seemed correlated to each other. This suggests that the FO-PMD changes are due to external perturbation changes (wind speed, wind direction and temperature). However, intentional input/output scrambling also results in the FO-PMD stochastic changes, as was experimentally found by Wu *et al.* (2006) and Musara (2006). Input/out polarization scrambling changes the input and output polarization state of light while the wind speed, wind direction and temperature change affect the fibre birefringence, SOP of propagating light and possibly fibre mode coupling. The emulator in Section 6.3 will be used to change the FO-PMD by randomly altering mode coupling using seven half waveplates (HWPs). The stochastic FO-PMD changes of the aerial fibre with time resulted in a statistical distribution that approaches the Gaussian distribution (Fig. 5.4 (b)). This distribution will be compared to that generated by the PMD emulator in Section 6.3.

5.2 Monitoring the state of polarization of light in optical fibres

In this section, the Adaptif A1000 polarization analyser was used to monitor the SOPs of propagating light over a buried and aerial fibre link. The SOP measurements were collected over a 24 hour period at 30 ms intervals. Aerial fibre measurements were from 6 pm (10 June 2009) to 6 pm (11 June 2009). SOP measurements will assist in monitoring polarization changes that light experiences mainly due to extrinsic perturbations. The polarization analyser

[1] The author would like to thank Eric Mudau, a 2008 Masters graduate at the Nelson Mandela Metropolitan University, for providing the measurements presented in Fig. 5.4 (a).

is used to collect the output SOPs. The variations of these SOPs are mapped to the Poincaré sphere for polarization analysis and also for statistical analysis.

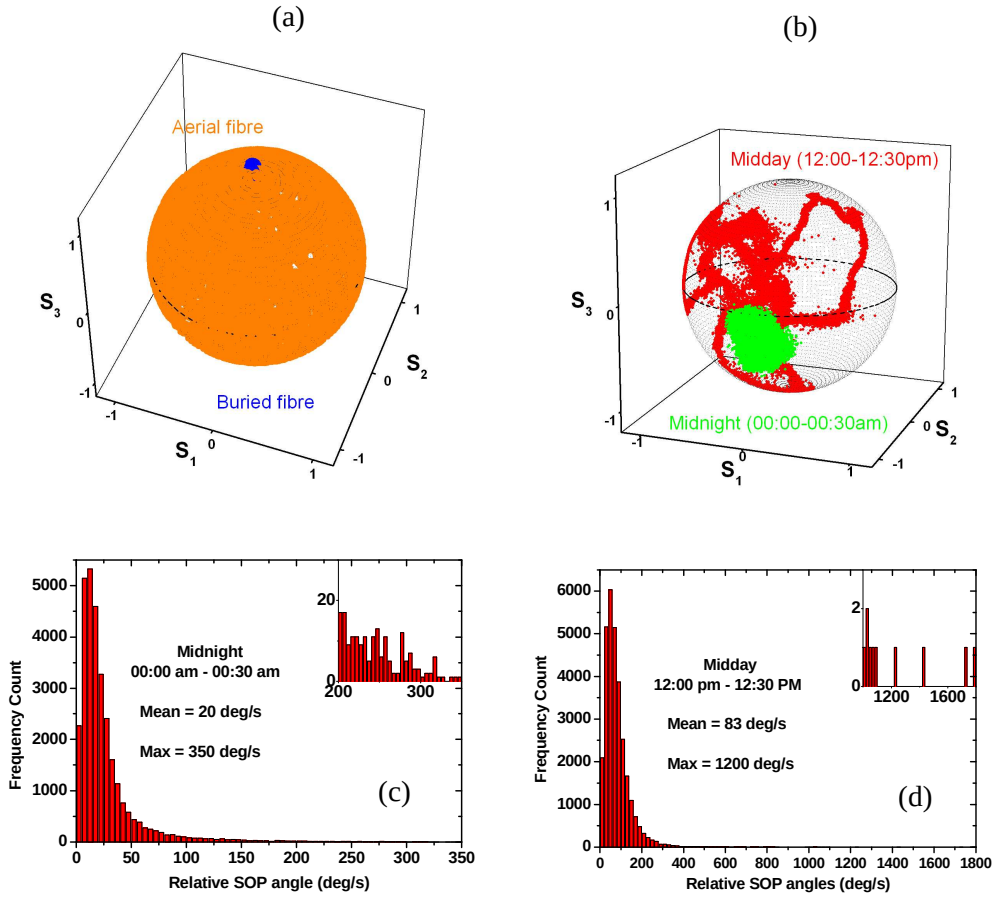

Fig. 5.5: (a) Variation of SOPs over a 24-hour period in an aerial and buried fibre, (b) SOP variation during midday and midnight on an aerial fibre, (c) Statistical distribution over an aerial fibre during the night and (d) Statistical distribution over an aerial fibre during the day.[2]

Fig. 5.5 (a) shows the evolution of the SOPs on an aerial fibre and a buried fibre. The SOPs of the buried fibre evolves over only a few polarization states; this is likely due to limited temperature variations. Since buried fibres are secured in ducts and buried underground, they are not exposed directly to external perturbation variations i.e. wind. However, the SOPs of aerial fibres cover many polarization states due to their exposure to varying environmental changes. The emulator in Section 6.3 will be used to mimic the SOP behaviour of aerial fibres

[2] The author extends his thanks to Winston Ireeta, a PhD candidate at Nelson Mandela Metropolitan University, for assisting with aerial fibre SOP measurements.

by varying the half waveplates (HWPs) in order to cover as many polarization states as possible. Fixing the HWPs and keeping the emulator under a stable laboratory environment as in Section 6.3, results in SOPs remaining fairly fixed at the same polarization state. This is how a buried fibre would behave when it is not subject to extrinsic perturbation changes.

Fig. 5.5 (b) shows that there are only slight changes in SOPs for the aerial fibre during the night (00:00 am – 00:30 am) as compared to during the day (12:00 pm – 12:30 pm). During midnight, the temperature was 21.7±0.2 ^{o}C, wind speed was 2.9±0.3 m/s and wind direction was 346.4±0 deg. Midday had a temperature of 25.3±0.5^{o}C, wind speed of 3.7±0.5m/s and wind direction of 19±16.4 deg. The slight changes of SOP around midnight are evidenced by a low relative average rate of SOP change (20 deg/s) compared to around midday (83 deg/s) (Fig. 5.5 (c - d)). Therefore, there is more SOP coverage over a short time span around midday. Drastic changes in the polarization angles experienced per second are evidenced by a relative maximum SOP change of as high as 1200 deg/s during midday (Fig. 5.5 (d)). At night a maximum relative rate of SOP change equal to 350 deg/s is experienced (Fig. 5.5 (c)), which is far less than that experienced during midday due to the difference in environmental conditions highlighted above. The relative rate of SOP changes obtained in this study, fall within ranges found by Waddy *et al.* (2001), Gibbon (2007), and Mudau (2008). The ACF (Section 2.1.5 II) is a vital tool to measure the degree of SOP change with time.

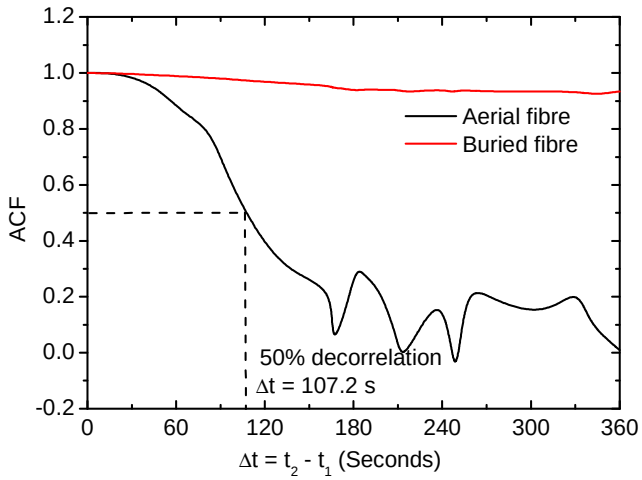

Fig. 5.6: The ACF for an aerial and buried fibre. SOP measurements that were used to come up with this ACF were collected from 12:00 pm – 12:06 pm. Equation 2.24 was used to calculate the ACF.

Fig. 5.6 shows that the SOP decorrelates faster in an aerial fibre compared to a buried fibre over 360 seconds time span. The SOP data used in Fig. 5.6 were collected during midday. The ACF of the buried fibre changes insignificantly; decorrelation is likely to occur over a very long time span (of the order of days). The decorrelation time is an important parameter showing how rapidly SOPs change with time. Fig. 5.6 shows that the aerial fibre had a decorrelation time of 107.2 s which is in agreement with results by Waddy *et al.* (2001). Waddy *et al.* (2001) found decorrelation times for aerial fibres between 13.62 s and 600 s. Within our research study group using the same aerial fibre on different days, Gibbon (2007) obtained a decorrelation time of 218.6 s and Mudau (2008) obtained 597 s. The ACF can change in direction with time, depending on the degree of impact the prevailing extrinsic perturbations have on the SOPs of propagating light. The ACF of the emulator used to mimic the behaviour of the aerial fibre was 126.3 s (Section 6.3). Waddy *et al.* (2001) referred to the ACF as a parameter that shows whether propagating light returns to a similar phase space after a certain time interval.

CHAPTER 6

PMD EMULATOR DESIGN AND IMPLEMENTATION

This Chapter focuses on the design and implementation of different types of PMD emulators in order to further understand the PMD phenomenon. These PMD emulators are grouped into four classes as highlighted in Section 3.4. An emulator is considered optimal only when it reproduces the same statistical output as that of a given fibre link or plant. The emulators presented in this chapter generate stochastic PMD distributions that are similar in behaviour to what is observed in deployed fibres (e.g. see Chapter 5) though some do not necessarily follow the known PMD theoretical distributions due to their desired mechanism. The PDL of the PMD emulators was maintained as low as possible, < 0.08 dB, so that it does not have any influence on the PMD statistics. The insertion loss of the emulators designed in this study ranged from 0.7 to 12.85 dB. The JME was used to measure the FO- and SO-PMD of the emulators. GINTY was used to measure FO-PMD only. PMD measurements carried out using JME were conducted over the 1520 – 1569 nm wavelength range at an optimal 0.3 nm wavelength resolution.

6.1 PMD emulators with fixed birefringent sections and polarization orientations

As highlighted in Section 3.4.1, these types of emulators are built from cascading polarization maintaining fibres (PMFs). These PMFs are joined together through fusion splicing or through the use of midcouplers to create fixed polarization orientations or mode coupling. Fusion splicing was done using the Sumitomo 36 fusion splicing machine, which gave low losses (< 0.01 dB) after splicing. The insertion losses for the emualtors designed in this section range from 0.7 to 2.1 dB. All the PMFs used in this study have uniform birefringence; the induced time delay is proportional to the length of the PMF. Birefringence is the difference between the refractive indices of the fast and slow orthogonal axes of a fibre. In this study, this class of emulators was characterised using the JME method.

This section firstly focuses on an emulator with varying FO- and SO-PMD, and then followed by an emulator with inverse trend in FO- and SO-PMD. Lastly, an emulator with constant FO-PMD and varying SO-PMD is considered.

6.1.1. Emulator with an increase in both FO- and SO-PMD

The emulator comprises up to 30 concatenated PMF sections (Fig. 6.1). This was made possible by concatenating smaller fusion-spliced emulators together using midcouplers. The PMF used has a PMD coefficient of 1.3 ps/m. The emulator was designed to ensure that, at any point in time, the length of the fibre segments lie within 20% standard deviation of the mean emulator length (Dal Forno *et al.* 2000, Khosravani et al. 2001, Phua and Ippen 2005). The lengths of the PMFs were Gaussian distributed.

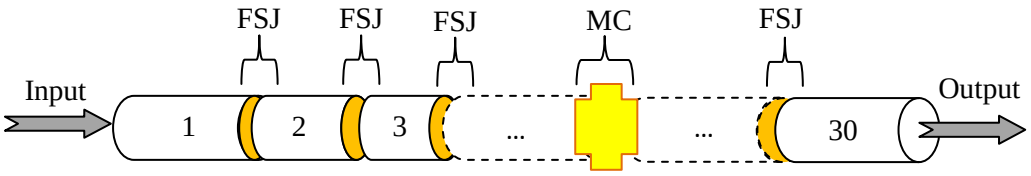

Fig. 6.1: Schematic PMD emulator design made by increasing the number of concatenated PMF sections. Mode coupling and fibre length are randomly distributed. FSJ stands for fusion splice joint and MC for midcoupler. The emulator had insertion losses from 0.7 -1.1dB.

The FO-PMD of the emulator increased linearly with increasing number of PMF sections from 1 to 30. This is depicted in Fig. 6.2 where the root mean square (RMS) FO-PMD values of the emulator increases from 4 to 13.2 ps. However, the increase in the RMS FO-PMD is not a direct sum of the FO-PMD contributions from each PMF section. This is due to random mode coupling enhancing FO-PMD vector cancellations; hence the overall RMS FO-PMD is less than the direct sum of all FO-PMD contributions. This therefore means the effective FO-PMD of the emulator is the root-mean-square-sum of the FO-PMD values provided by the individual PMF sections. It should be noted that the RMS FO-PMD is equivalent to 1.085 times the mean FO-PMD (Poole and Favin 1994).

The accompanying SO-PMD also increased linearly from 0.5 to 42.3 ps^2 with an increase in the number of PMF sections and mode coupling sites, along with its two components, namely PCD and PSP-depolarization. The increase in SO-PMD was mainly due to increased random mode coupling since each PMF section possessed a minute amount of residual SO-PMD of around 0.31 ps^2. Mode coupling enhances PSP rotations and FO-PMD (DGD) variations with wavelength, which correspond to PSP-depolarization and PCD respectively. PSP-depolarization unlike PCD was the major SO-PMD contributor. The former is in agreement with findings in the field (Section 5.1.1).

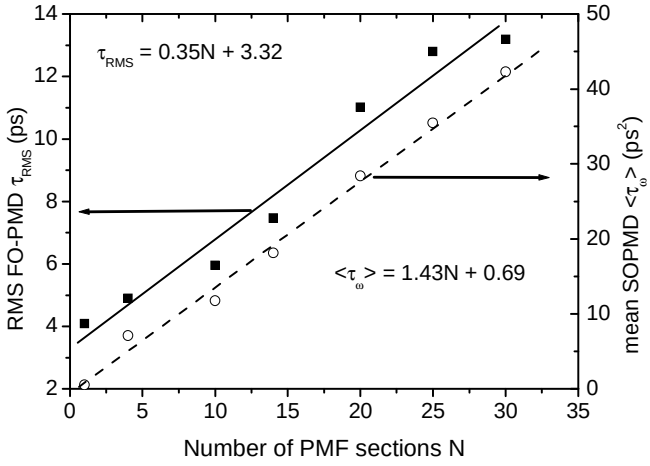

Fig. 6.2: The RMS FO-PMD and mean SO-PMD variation of the emulator for increasing of PMF sections (1 to 30).

Besides measuring the mean PMD values (FO- and SO-PMD), the PMD statistics were also investigated. Results show that when there are limited number of randomly concatenated PMF sections, PMD statistics fall short of the PMD theoretical distributions (see Fig. 6.3 (a - a') when the emulator has 4 PMF sections). Figures 6.3 (b) and (b') show that when the number of PMFs are 30 the FO-PMD approaches the Maxwellian distribution and the SO-PMD follows the theoretical distribution described by Foschini *et al.* (1999). This is due to the increase in random mode coupling sites which promoted the PMD spectra to become more stochastic in nature. An increase in the number of randomly distributed PMF sections made the PMD statistics of the emulator approach theoretical distributions. The former helps support the findings in Section 5.1.1, that fibre links with PMD approaching theoretical distributions have a large number of fibre sections and random mode coupling as opposed to those which do not approach theoretical distributions. Therefore the optimal configurations for an emulator that mimics fibre links approaching theoretical distributions are large random mode coupling and birefringent distribution. Further increases in the number of PMF sections above 30 will result in PMD distributions that approximate theoretical distributions.

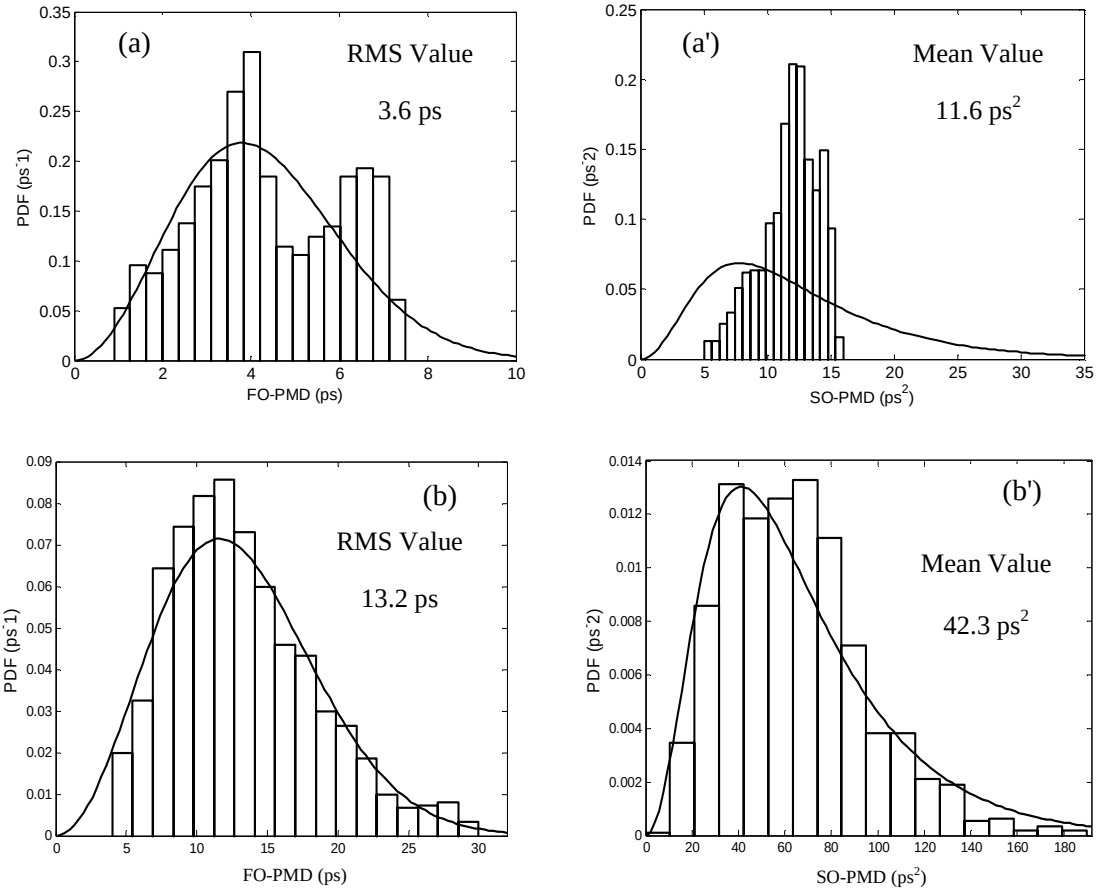

Fig. 6.3: The histograms for FO- and SO-PMD for 4 section ((a) and (a')) and 30 section ((b) and (b')) emulators. The solid fitted lines on the FO-PMD histograms are the Maxwellian distribution fits and that on the SO-PMD histograms are the SO-PMD theoretical distributions proposed by Foschini et al. (1999). The number of bins used for each histogram is 18.

In order to quantify the FO-PMD statistics of the emulator acquired using the JME, the frequency ACF given in Section 2.1.5 I is applied. The ACFs for the 4 and 30 section emulators are depicted in Fig. 6.4 (a). The region outside the central bandwidth of the ACF is known as the background autocorrelation function (BACF) and has been previously discussed in Section 2.1.5 I. Fig. 6.4 (b) shows that the BACF of the ACF decreases towards 0.13 (close to null) with increasing number of PMF sections. This agrees with the BACF provided by Eq. 2.21 and findings by Yan *et al.* (2008). This is in contrast to theoretical findings by Gupta *et al.* (2007), in which it was found that a low BACF (0.18) is obtained when the length of the PMFs are distributed in sequential order (from high to low lengths). Lack of symmetry (see Fig. 6.4 (a)) of the ACF is likely due to the presence of SO-PMD as suggested by Gupta *et al.* (2007). SO-PMD has no effect on the BACF.

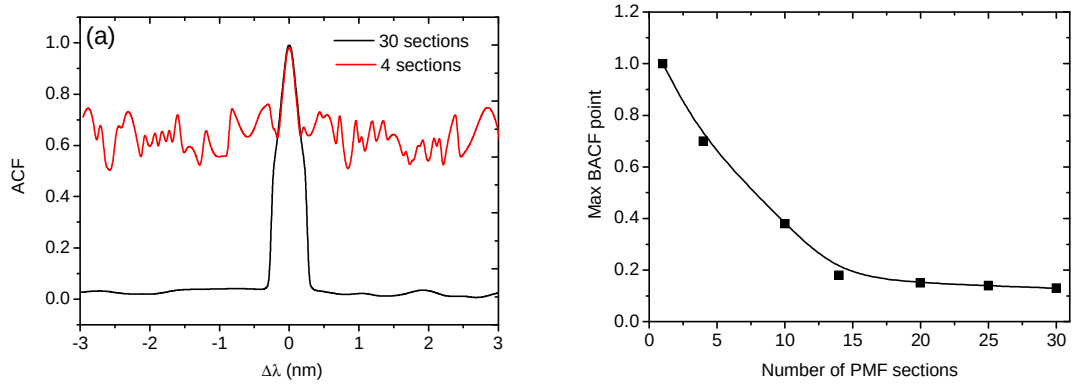

Fig. 6.4: (a) The ACF for the 4 and 30 section PMD emulators and (b) The relationship between the BACF and the number of PMFs on the PMD emulator. The centre wavelength is 1550 nm.

The emulator shows that increased random mode coupling and PMF sections gives FO-PMD statistics approaching the Maxwellian distribution and SO-PMD statistics approaching the theoretical distribution. These are only valid when the length of each of the PMF segments lie within 20% standard deviation of the mean sub-emulator length. Increased number of random mode coupled PMF sections reduces the BACF towards null, with the introduced SO-PMD making the ACF asymmetric.

6.1.2. Emulator with inverse trend in FO- and SO-PMD

Some emulator designs and buried fibre measurements in Section 5.1.1 show an increase in SO-PMD as FO-PMD is increased (Yan *et al.* 2003, Lizé *et al.* 2004, Younsi *et al.* 2007). It is found that this is not always true. This subsection presents an emulator design exhibiting decreasing FO-PMD but increasing SO-PMD. This emulator was built from polarization maintaining fibres (PMFs), of which a 22 metre PMF was subdivided from 2 to 31 random lengths. The 31 random PMF lengths are Gaussian distributed. All the fibre lengths fall within 20% standard deviation of the mean emulator length (~ 0. 7 m). The PMF sections were concatenated through fusion splicing. The emulator had insertion losses from 0.7 -1.2dB.

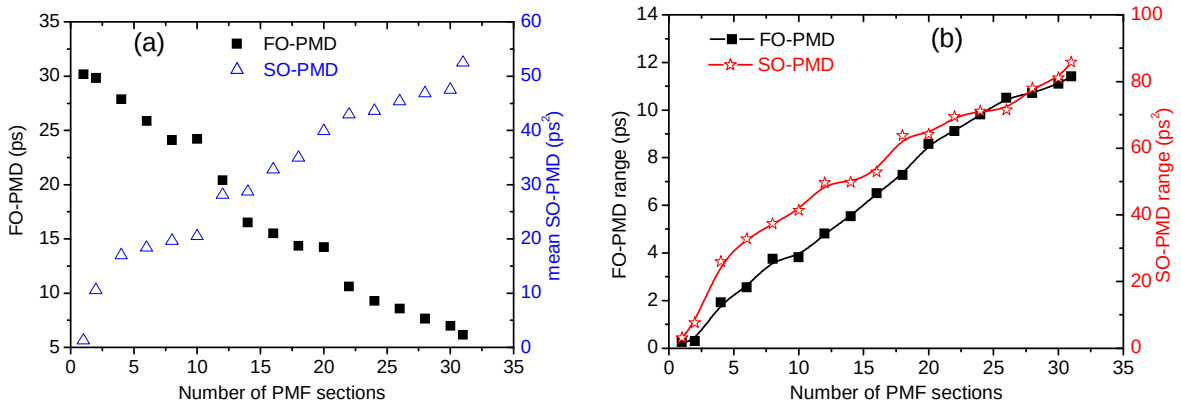

Fig. 6.5: (a) Mean FO- and SO-PMD with increasing number of subdivisions on the 22 metre long PMF and (b) the variation of the PMD range with number of sections or subdivisions. The lines in (b) act as guides to the eye.

The emulator FO-PMD was decreased from 31 ps to 1.26 ps (Fig. 6.5 (a)) by maintaining a constant fibre length (22 m) whilst subdividing the fibre into different random distributed lengths and having random mode coupling. This is in contrast to the FO-PMD trend in Section 6.1.1 above. The decrease in FO-PMD was due to continuous FO-PMD vector cancellation, this agrees with our previous experimental findings (Younsi *et al.* 2007). However, the continuous increase in random mode coupling increased SO-PMD since mode coupling promotes FO-PMD variation and PSP rotation with wavelength as found in Section 6.1.1. This therefore means SO-PMD is mainly due to mode coupling and FO-PMD is due to birefringence, although these fibre properties affect both FO- and SO-PMD. The emulator design justifies the argument that FO-PMD is not always proportional to SO-PMD.

Besides the increase in the mean SO-PMD, Fig. 6.5 (b) shows that the FO- and SO-PMD range also increased. The PMD range is the difference between the maximum and minimum PMD values on the PMD statistics. The minimum and maximum PMD values are as depicted in Fig. 6.6. This means simultaneous increases in both the number of PMF sections and mode coupling widens the spread of the PMD statistics as illustrated in Fig. 6.6.

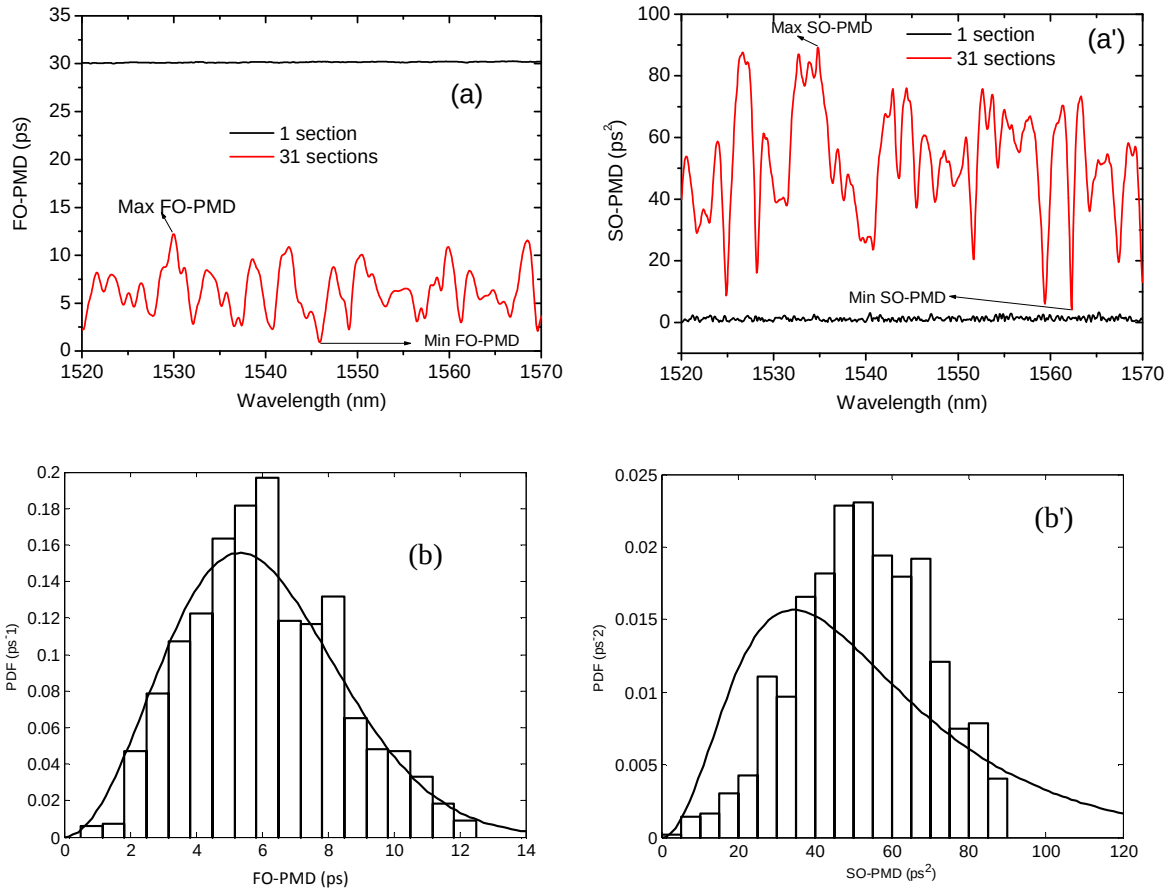

Fig. 6.6: ((a) and (a')) The PMD variation with wavelength as mode coupling and the number of PMF sections increase. ((b) and (b')) The PMD statistical distributions when there are 31 coupled PMF sections. The solid line in (b) is the Maxwellian PDF fit and that in (b') is the PDF fit of the SO-PMD theoretical distribution first proposed by Foschini et al. (1999).

An investigation into the PMD (FO- and SO-PMD) statistics shows an increase in the stochastic nature of the PMD spectra as the number of PMF sections increase (Fig 6.6 (a - a')). These distributions resemble the PMD behaviour in deployed fibres. Higher number of randomly mode coupled PMF sections (i.e. 31 sections in this case) result in PMD distributions approaching theoretical distributions which agrees to findings in Section 6.1.1. However, some regions of the SO-PMD distribution are not populated. This emulator design agrees with findings in Section 5.1.1, that the value of mean FO-PMD does not determine whether a FO-PMD distribution approaches the Maxwellian distribution or not. The absence of (or negligible) mode coupling gave a wavelength-independent FO-PMD distribution at 31 ps whilst generating a very low SO-PMD of 1.26 ps^2.

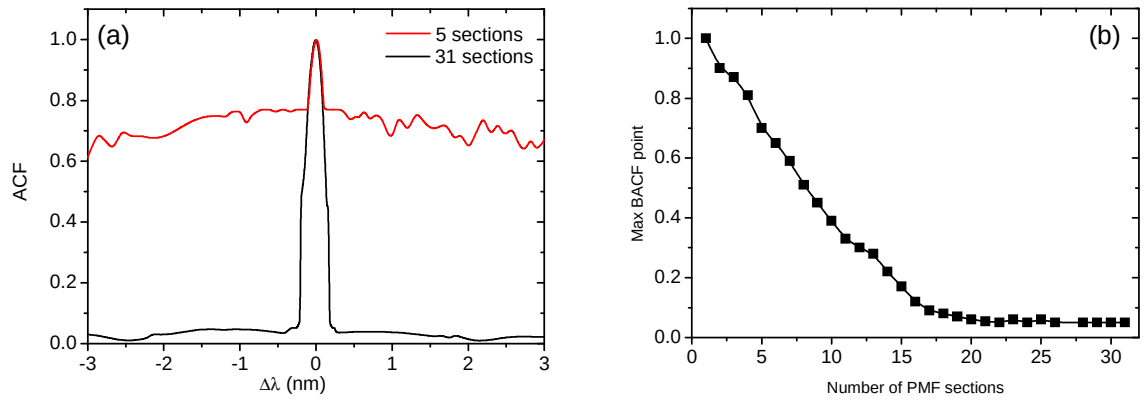

Fig 6.7: (a) The ACF when the emulator has 5 and 31 PMF sections. (b) The behaviour of the BACF with increasing numbers of PMF sections. The centre wavelength is 1550 nm.

A similar BACF trend to Fig. 6.4 is observed in Fig. 6.7 when the number of fibre sections increase (in this case the miximum BACF value reached is 0.06). This trend again complies with equation 2.21. Thus this emulator clearly shows that for high number of PMF sections the BACF is independent of the FO-PMD value but solely depends on the nature of the fibre link. The ACF is asymmetric due to the presence of SO-PMD as was also observed in Section 6.1.1.

6.1.3. Emulator with fixed FO-PMD but varying SO-PMD

It has been observed that SO-PMD introduces fluctuations around the mean penalty induced by FO-PMD (Bruyére 1996, Nelson *et al.* 2000). To emulate this, Zeng (2003) designed an emulator of fixed mean FO-PMD and varying SO-PMD from an optical delay line, a polarization controller (PC) and a single high FO-PMD (HiFO-PMD) fibre segment (refer to Section 3.4.5). Presented in this subsection is a low-cost emulator with similar behaviour designed from combining a variable sub-emulator (consisting of PMF Sections), a PC and a high FO-PMD (HiFO-PMD) PMF segment. Other designers (Wegmuller *et al.* 2002, Zeng 2003) have paid particular attention only to altering the mean FO-PMD and SO-PMD values but our design has been extended to allow for control of the extreme FO- and SO-PMD values (maximum and minimum values) of its PMD statistics. This is because our design allows us to alter the number of mode coupling sites, unlike designs by Wegmuller *et al.* (2002) and Zeng (2003), which have only a single mode coupling site. However, it should be noted that the PMD control mechanism of the emulator is not completely in real time. Firstly, the

operation principle of the emulator is addressed, thereafter the PMD characteristics of the emulator and lastly the impact of the HiFO-PMD segment on PMD statistics.

I. Operational principle of the PMD emulator

The emulator comprises a variable sub-emulator (made up from cascading PMF sections), a PC and a 23 m long PMF segment (fixed length) as shown in Fig. 6.8. The 23 m long PMF segment possesses high FO-PMD (HiFO-PMD) approximately equal to 31 ps; from here onwards it will be referred to as the HiFO-PMD PMF segment. The sub-emulator is the emulator previously described in Section 6.1.1, in which 1 to 30 PMF sections were joined together. The variable sub-emulator is tuned by joining or removing PMF fibre sections. The sub-emulator is assumed to be random mode coupled since the exact coupling angles could not be determined during fusion splicing of the PMF sections and through the use of mid couplers. The PC provides a coupling angle θ (arbitrary set at 45^{o}) between the sub-emulator and the HiFO-PMD PMF segment, which we assume is not correlated to any other mode coupling angle on the sub-emulator. The length of the HiBi fibre segment was chosen in such a way that it lies outside the 20% standard deviation of the mean length of the sub-emulator, unlike conditions used to construct the emulators in Sections 6.1.1 and 6.1.2. Since different coupling angles result in different amounts of SO-PMD, the exact amount of SO-PMD the emulator possesses at each configuration could theoretically be calculated from the modulus of Eq. (2.6) if the mode coupling angles were known (Zeng 2003). The same is possible for FO-PMD by simply using Eq. (2.6).

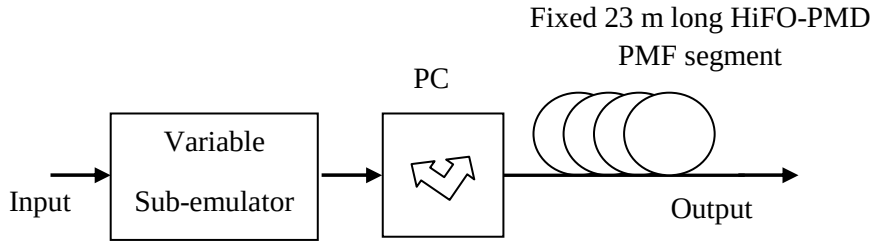

Fig. 6.8: Schematic for a fixed RMS FO-PMD and varying mean SO-PMD emulator. The PC is set at a fixed angle. The emulator had insertion losses from 1.5-2.1 dB.

The 23 m HiFO-PMD PMF segment alone has a FO-PMD vector independent of wavelength. The residual SO-PMD in the HiFO-PMD segment is ~ 0.31 ps^2; although low, this contributes slightly (by an amount ~ 0.31 ps^2) to the SO-PMD of the emulator. The stochastic wavelength-dependent FO- and SO-PMD changes of this emulator is more comparable with

deployed fibres than designs by Wegmuller *et al.* (2002) and Zeng (2003) in which only two birefringent elements were used. Firstly, the properties of the emulator comprising the sub-emulator coupled to the HiFO-PMD segment (Fig. 6.8) are investigated. The properties of the sub-emulator were discussed in Section 6.1.1. Lastly, the impact of the HiFO-PMD (or high birefringent (HiBi)) segment on FO- and SO-PMD statistical distributions are investigated.

II. PMD emulator characteristics

This section will look at the vertical (PMD range) and horizontal (PMD changes with wavelength) characteristics of the PMD emulator. The horizontal characteristics will assist in the analysis of PMD statistics when the HiFO-PMD segment is absent or present.

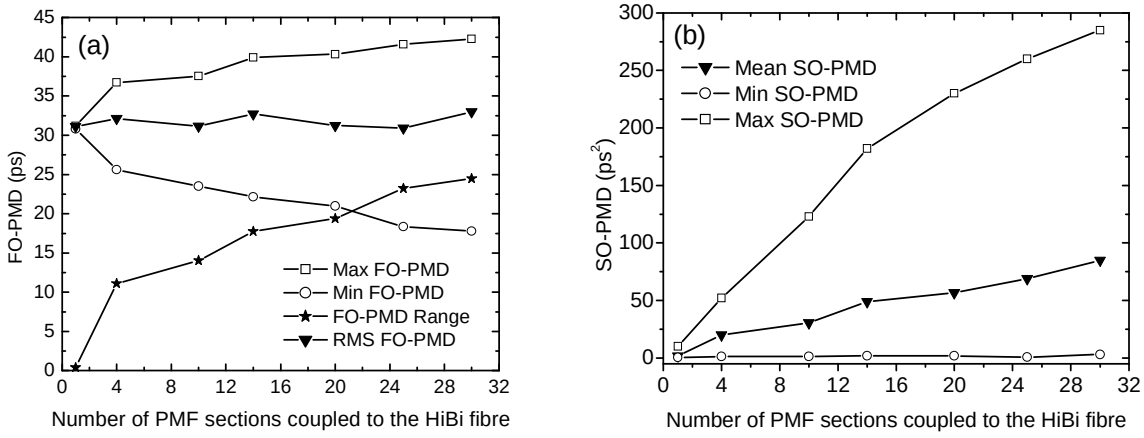

Fig. 6.9: (a) The FO-PMD and (b) SO-PMD vertical behaviour of the emulator as the number of PMF sections on the sub-emulator were varied. The 23 m long HiFO-PMD PMF segment was connected to the sub-emulator via a polarization controller (PC).

The vertical PMD characteristics of the emulator are illustrated in Fig. 6.9. A dominant HiFO-PMD segment was coupled to the sub-emulator so that the RMS FO-PMD remained fairly fixed at ~ 31 ps, as shown in Fig. 6.9 (a), despite there being both mode coupling and birefringent increase similar to that of Fig. 6.2. Unlike the sub-emulator conditions where each PMF section is expected to contribute to the overall RMS FO-PMD of the emulator, the HiFO-PMD PMF segment on the emulator provided a dominant FO-PMD vector which biased the emulator RMS FO-PMD towards its RMS FO-PMD value. The RMS FO-PMD of the HiFO-PMD segment lies between 2.35 to 7.75 times higher than that of the sub-emulator. The mean SO-PMD of the emulator increased as the number of coupled PMF sections increased, although the RMS FO-PMD was uniform at ~ 31 ps (Fig. 6.9). This is because SO-PMD is strongly mode coupling dependent.

Figures 6.9 and 6.10 show the emulator FO-PMD and SO-PMD statistical information as well as its wavelength dependence, respectively. Fig. 6.9 shows the FO- and SO-PMD vertical behaviour (range) of the emulator as the number of PMF sections on the sub-emulator increased from 1 to 30. The FO- and SO-PMD range was increased by simultaneously adding birefringence (PMF sections) and mode coupling on the sub-emulator. The FO-PMD range extended from close to null for a single PMF segment to 24.5 ps for 30 PMF segments. The simultaneous changes in the maximum and minimum FO-PMD are opposite in trend. A further increase in the number of random PMF sections will likely result in a FO-PMD range from zero to the maximum FO-PMD. The corresponding SO-PMD range, from close to null for a single PMF section to 286 ps^2 for 30 sections, was always approximately equal to the max SO-PMD value since the minimum SO-PMD was always close to null.

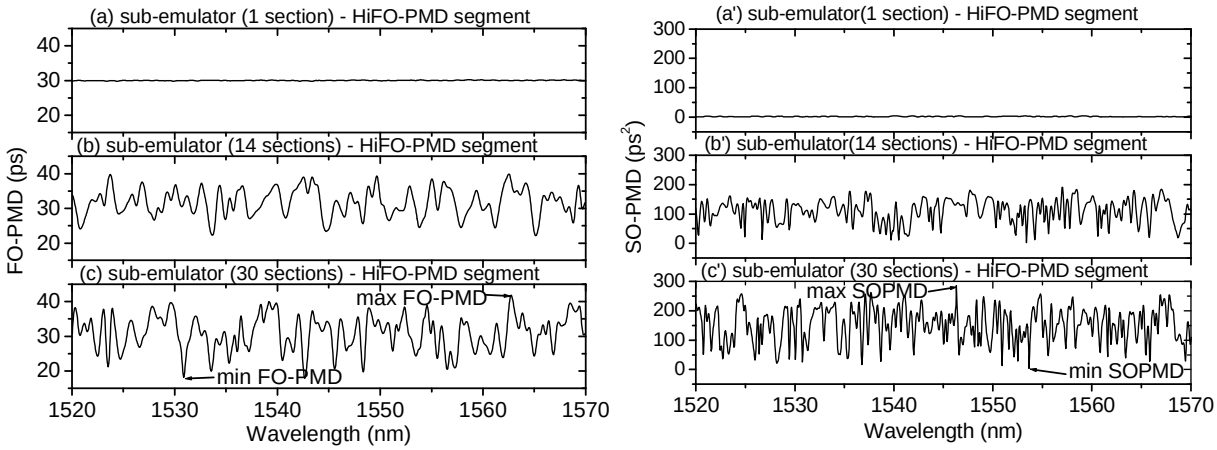

Fig. 6.10: The FO-PMD spectra for the emulator for (a) 1 section (b) 14 sections and (c) 30 sections on the sub-emulator. The corresponding SO-PMD behaviour for (a') 1 section (b') 14 sections and (c') 30 sections on the sub-emulator. The arrows indicate the max and min values on the PMD spectra.

Fig. 6.10 also shows that besides controlling the emulator vertically (FO- and SO-PMD range), it was also controlled horizontally (FO- and SO-PMD changes with wavelength). Fig 6.10 (a) shows the FO-PMD spectrum of a single PMF section coupled to the HiFO-PMD PMF segment. The accompanying SO-PMD spectrum (Fig. 6.10 (a')) is close to null. This was due to the limited PSP rotations that did not enhance significant PSP-depolarization and FO-PMD variations with wavelength (PCD). The addition of random mode coupled PMF sections to the sub-emulator resulted in random fluctuations of the FO-PMD (Fig. 6.10 (b - c)) about a fixed RMS value (~ 31 ps), with SO-PMD changes becoming more stochastic (Fig 6.10 (b' - c')). This is the equivalent of irregular wavelength-dependent PMD changes in deployed fibres. Thus the irregular fluctuations about the RMS FO-PMD were likely due to

SO-PMD and or other higher-order PMD. In order to significantly influence the shape of the FO-PMD spectra but have minimal effect on the RMS FO-PMD value, the sub-emulator mode coupling angles should be adjusted. The accompanying SO-PMD would change both its spectrum and mean value due to its sensitivity to mode coupling changes.

III. The impact of the high first-order PMD segment on PMD statistics

This subsection seeks to investigate the impact generated by high first-order PMD (HiFO-PMD) segments on the nature of the FO- and SO-PMD statistics through the use of a PMD emulator. Further investigations on the impact of HiFO-PMD segments on PMD and the output state of polarization (SOP) of light in buried fibres will be presented in Chapter 7. In this subsection, the FO- and SO-PMD statistics of the sub-emulator (presented in Section 6.1.1) alone are first looked into and thereafter the PMD statistics of the emulator is considered (Fig. 6.8).

As the number of random PMF lengths and mode coupling sites were increased, the sub-emulator generated more stochastic FO- and SO-PMD changes. This resulted in the FO-PMD statistical behaviour approaching the theoretical Maxwellian distribution and the generated SO-PMD approaching the SO-PMD theoretical distribution (Fig. 6.11 (a – b)). Thus a closer agreement to the theoretical distributions was achieved in this case when there were 30 PMF sections, as discussed in Section 6.1.1.

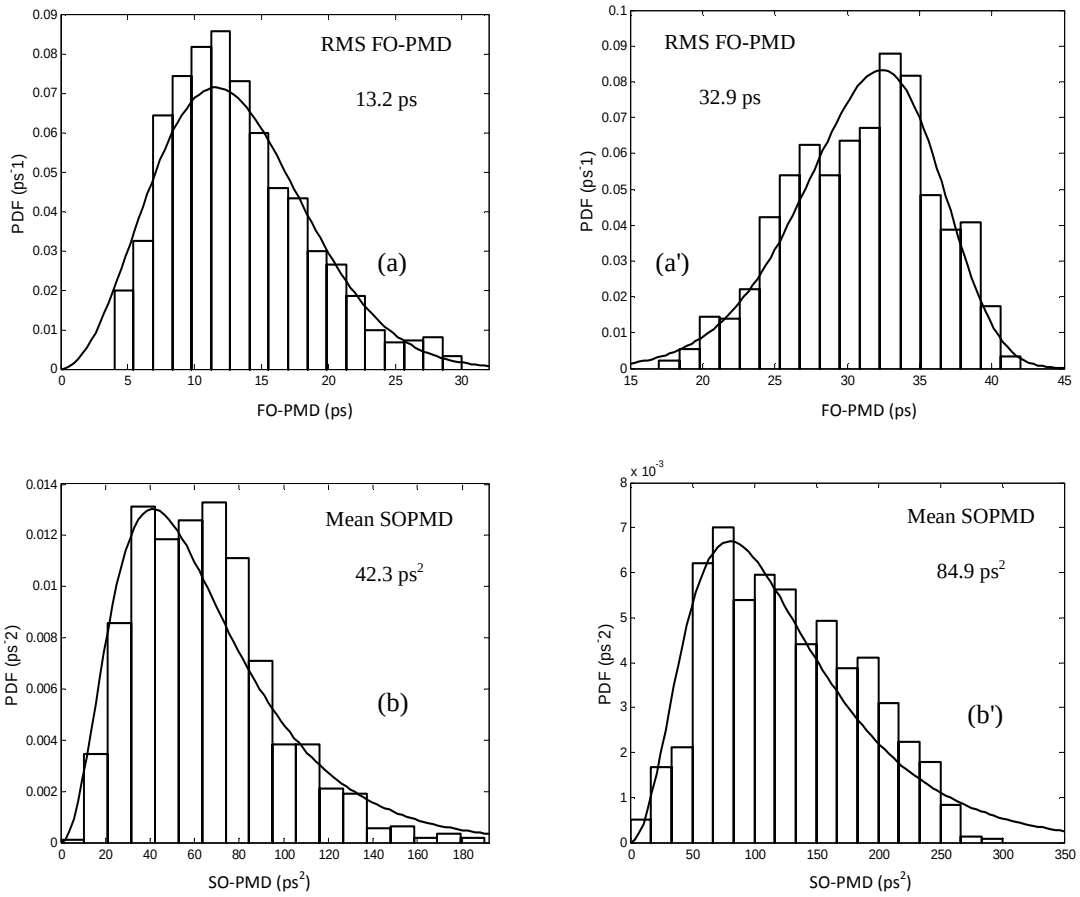

Fig. 6.11: The histograms for (a) the FO-PMD and (b) SO-PMD of a 30 section sub-emulator. The histogram for (a') the FO-PMD and (b') SO-PMD of the emulator comprising a 30 section sub-emulator. The solid line indicates (a) the Maxwellian distribution, (a') Weibull distribution, and for (b) and (b') a SO-PMD theoretical distribution described by Foschini et al. (1999).

Fig. 6.11 (a') shows the FO-PMD statistical distribution of the emulator when there were 30 PMF sections coupled to each other on the sub-emulator. The FO-PMD distribution in this instance approaches a Weibull distribution instead of the Maxwellian distribution, having the appearance of a reversed Maxwellian distribution, with a low probability events tail lying to the left (with low FO-PMD). However, Karlsson (2001) found out that the PMD distribution becomes Gaussian. The minimum FO-PMD value in Fig. 6.11 (a) is greater than that in Fig. 6.11 (a'), indicating that a shift in the FO-PMD statistics occurs towards the dominant wavelength-independent FO-PMD vector when a HiFO-PMD segment is added. This interpretation is supported by Fig. 6.9 (a) which shows a constant RMS FO-PMD equal to 31.9±1.0 ps regardless of the number of PMF sections in the sub-emulator. For PMF sections numbering less than 30 on the sub-emulator, the emulator results in various (different unpredictable) statistical distributions which possess high FO-PMD values. This means that

there are more possibilities of high system impairments due to the higher likelihood of high FO-PMD values occurring, e.g. see the right hand tail of Fig. 6.11 (a'). This also shows that the presence of such a HiFO-PMD segment in a deployed fibre link would bias the FO-PMD outcome closer to the RMS FO-PMD value of the HiFO-PMD segment. Such a RMS FO-PMD does not give an accurate representation of the entire FO-PMD in an optical fibre link.

The SO-PMD statistical distribution of the emulator with the 30 section sub-emulator (Fig. 6.11 (b')), retains a similar shape to that of the sub-emulator alone (Fig. 6.11 (b)) and approaches the ideal theoretical distribution. The addition of a mode coupling site concatenating the sub-emulator and the HiFO-PMD PMF segment together, and the low residual SO-PMD of 0.31 ps^2 in the HiFO-PMD PMF segment results in negligible changes in the SO-PMD statistical distribution. The major changes occur on the mean SO-PMD (from 42.3 ps^2 to 84.9 ps^2) and max SO-PMD (from 182 ps^2 to 286 ps^2) values. Due to the shift in the FO-PMD variation with wavelength towards the RMS FO-PMD of the HiFO-PMD segment as discussed before, there is likely to be an impact on the PCD, a component of SO-PMD. This PCD change has little effect (~ 1/9) on the SO-PMD distribution compared to contributions by PSP-depolarization (~ 8/9). Overall, the presence of a HiFO-PMD segment thus has little impact on the nature of the SO-PMD statistics but has significant impact on FO-PMD statistics.

6.2 Tuneable delay element

This type of emulator adjusts the PMD without changing the number of fibre sections. This is achieved by changing the birefringence of the material, i.e. a fibre can be subjected to temperature changes which change the birefringence hence changing the PMD (Hauer *et al.* 2004). In this section a digital delay line (DDL) from the company Oz Optics is used. Unlike the delay induction used by Hauer *et al.* (2004), the DDL introduces a delay in optical paths between the fast and slow orthogonal polarizations by adjusting the relative travel distance of the two orthogonal modes. The insertion loss of the DDL is 1.5 dB. For more information on the internal mechanism, function and specifications of the DDL the reader is referred to Section 3.3.1 III and Appendix III.

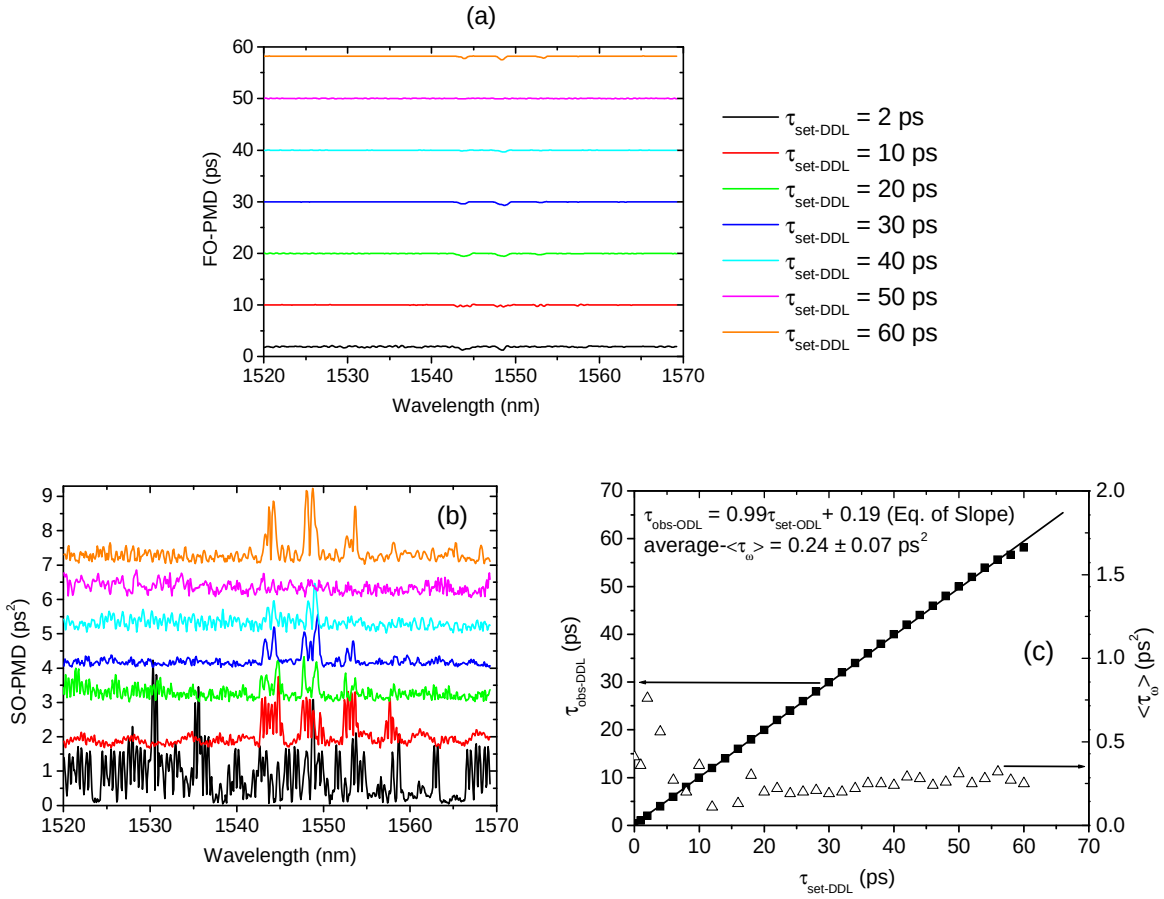

Fig. 6.12: ((a) and (b)) FO- and SO-PMD at different DDL FO-PMD settings ($\tau_{set\text{-}DDL}$). (c) DDL characteristics in terms of the observed FO-PMD ($\tau_{obs\text{-}DDL}$) and the mean SO-PMD ($\langle\tau_\omega\rangle$) when $\tau_{set\text{-}DDL}$ is adjusted. The average-$\langle\tau_\omega\rangle$ ($\langle\tau_\omega\rangle_{avg}$) over 20 ps ≤ $\tau_{set\text{-}DDL}$ ≤ 60 ps is 0.24 ± 0.07 ps^2. The JME was used to measure both FO- and SO-PMD. The SO-PMD spectra in (b) were offset for clarity.

A Labview programme was used to write and read from the DDL. The DDL was adjusted from 0 to 60 ps and the observed FO-PMD was measured. The set FO-PMD ($\tau_{set\text{-}DDL}$) of the DDL was compared to the observed FO-PMD ($\tau_{obs\text{-}DDL}$) and is shown in Fig. 6.12 (c). The gradient of the slope is 0.99 and y-intercept is 0.19 (close to zero) which shows there is a negligible difference between $\tau_{set\text{-}DDL}$ and $\tau_{obs\text{-}DDL}$. Thus, $\tau_{set\text{-}DDL}$ and $\tau_{obs\text{-}DDL}$ are equivalent and will be referred to as the DDL FO-PMD (τ_{DDL}). The observed FO-PMD is wavelength-independent (Fig. 6.12 (a)) due to finite mode coupling, while SO-PMD is stochastic (Fig. 6.12 (b)) over a small range which is likely due to PSP rotations enhanced by internal mechanical changes occurring in the DDL.

Figure 6.12 (c) shows that the DDL has low residual SO-PMD (residual-τ_ω) present. This is similar to what would be obtained in a single PMF section of arbitrary FO-PMD magnitude. The low SO-PMD is ascribed due to finite mode coupling. Though low, the behaviour of the SO-PMD of the DDL is important in this study due to its application in the design of the PMD emulator in Section 6.4. The residual mean SO-PMD (residual-$\langle\tau_\omega\rangle$) was non-uniform for $\tau_{DDL} \leq 18$ ps, while the residual-$\langle\tau_\omega\rangle$ remains fairly constant at 0.24 ± 0.07 ps^2 for 20 ps $\leq \tau_{DDL} \leq 60$ ps. This non-uniformity in SO-PMD is likely due to the manufacturing imperfections of the DDL. It should be noted that the behaviour of residual SO-PMD in other delay lines does not necessarily follow this trend.

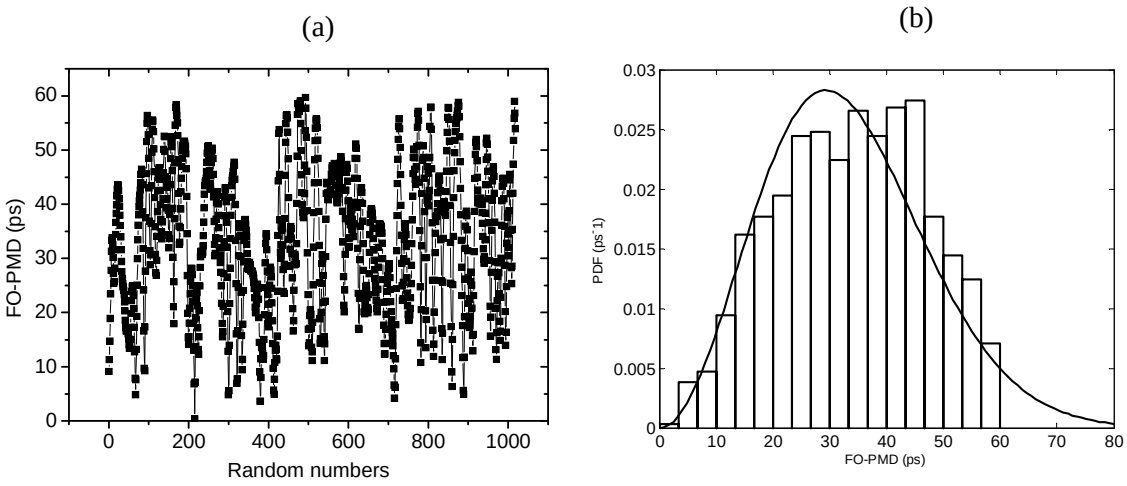

Fig. 6.13: The statistical distribution of the DDL observed FO-PMD after randomly generating 1018 DDL set FO-PMD ($\tau_{set\text{-}DDL}$) values. The solid line in (b) is the Maxwellian distribution fit. GINTY was used to measure the FO-PMD.

In this study, 1018 values between 0 and 60 ps were randomly generated using Labview to give a variation similar to that in Fig. 6.13 (a).These 1018 random values were written to the DDL to adjust it and the resulting FO-PMD values are those shown in Fig 6.13 (a). These FO-PMD values were measured using GINTY. The FO-PMD variation in Fig. 6.13 (a) gives a histogram approaching Maxwellian (Fig. 6.13 (b)), although not well populated on the tail. This therefore means the DDL alone can be controlled to generate a distribution approximating the Maxwellian distribution over a large sample size. Take note that the FO-PMD values generated by the DDL are independent of wavelength as illustrated in Fig. 6. 12 (a).

6.3 Emulator with fixed birefringent sections and rotatable polarization orientations

Polarization state and PMD changes in aerial fibres are due to varying environmental effects such as temperature, wind speed and direction changes as highlighted in sections 5.1.2 and 5.2. Polarization state and PMD changes experienced along a buried fibre length are due to birefringence and mode coupling changes (Musara *et al.* 2009). The emulator presented in this section, controls mode coupling through electro-optic polarization rotators, which act as half waveplates. These half waveplates (HWPs) enable SOP and PMD adjustments. For more information and specifications on the HWPs the reader is referred to Section 3.3.2 I and Appendix III. The insertion loss for the emulator is 3.87 dB. The disadvantage of some emulators like those described in Section 6.1 is that they give a fixed PMD statistics which can mimic only a particular fibre link or plant. However, this emulator seeks to address this limitation. The aim of the emulator design is to tune the PMD statistics with wavelength and time. SOPs will also be adjusted and then measured using the Adaptif A1000 polarization analyser with time as the emulator is varied in a similar way to the aerial fibre in Section 5.2.

6.3.1. Emulator design and its operation

This subsection focuses on the principle operation of the emulator and its components. The discussion will make it easier for one to rebuild a similar type of emulator. The emulator design is shown as a schematic diagram and then as a photograph (Fig. 6.14). Of the eight HWPs shown on Fig. 6.14 (b), only seven will be used due to a high loss from one of the HWPs. In order to get a mean FO-PMD equal to 13.3 ps and stochastic PMD spectra, PMFs of different FO-PMD magnitudes were randomly distributed as shown in Fig. 6.14 (a). The PMFs and HWPs are interconnected using single mode fibre (SMF) patchcords with negligible PMD (Fig. 6.14 (b)). Each PMF section has SO-PMD approximately 0.31 ps^2. The loop diameter of each PMF sections was $\geq$ 13.5 cm to minimise the introduction of insertion loss and PDL (Section 6.5).

(a)

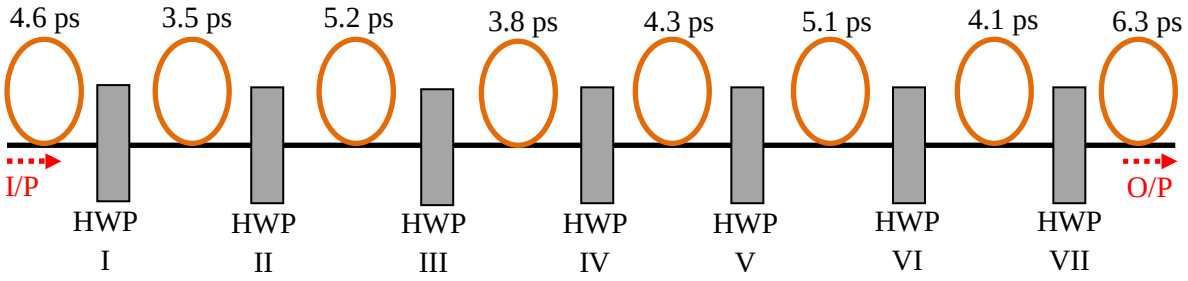

(b)

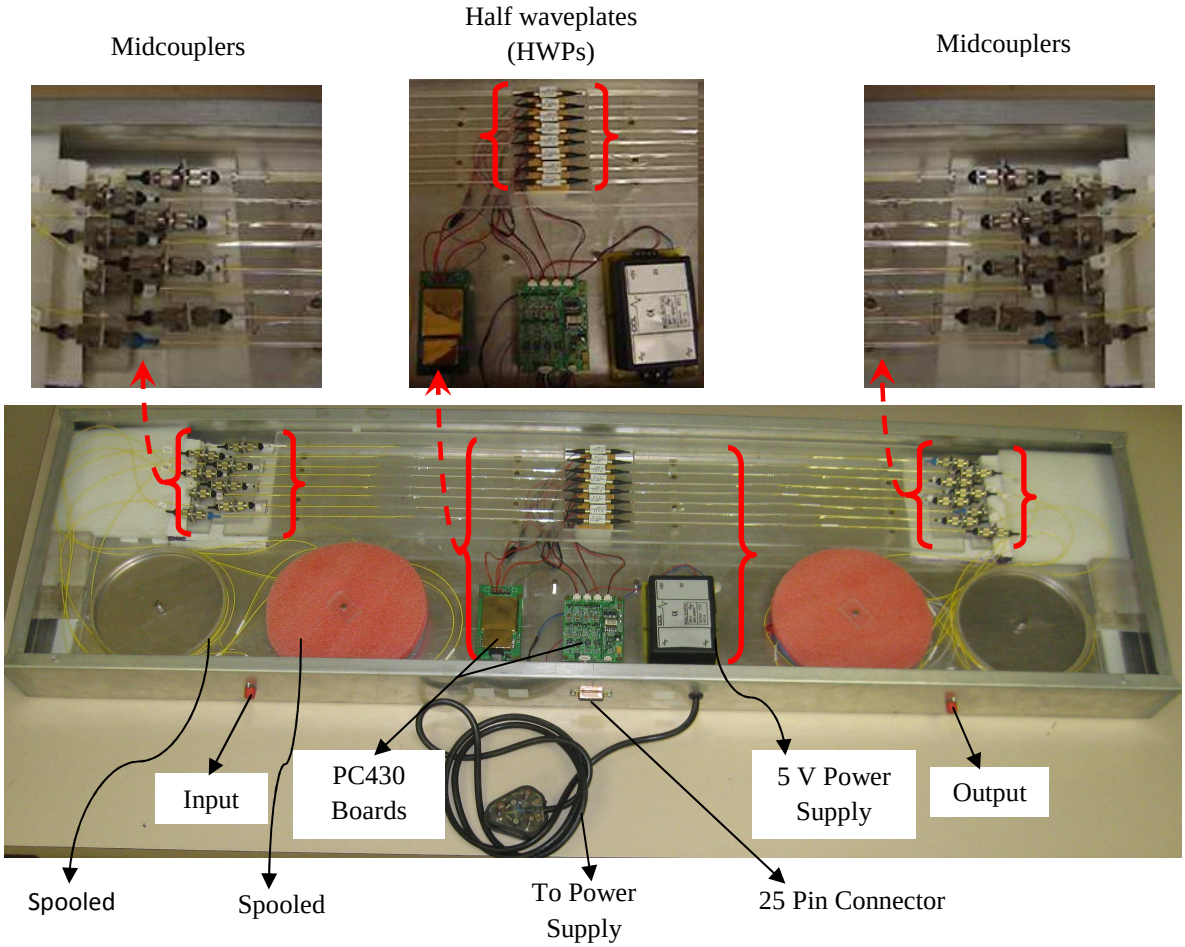

Fig. 6.14: The (a) Schematic and (b) Photographic layout of the emulator. The orange circles in (a) denote the PMF sections. The yellow fibres appearing in the photograph are single mode patchcords used to connect the HWPs and the PMFs. The FO-PMD values of each PMF section are provided. I/P stands for input and O/P for output.

Each HWP tunes between 0 to 180^{o} by supplying voltages between 0 – 4 V from the computer through the PC430 board (refer to Fig. 6.14 (b)). Voltage above 4 V will damage the HWPs. Before assembling the emulator each HWP had the 0 to 180^{o} range experimentally determined using two arbitrary PMFs (see Fig. 6.15, for HWP II), though they are from the

same manufacturer. This is required since the alignment axes of PMF sections might vary after the introduction of the SMF patchcords and also due to imperfections in the manufacturing of the HWPs. The SMF patchcords enable easy flexible attachment and removal of the PMF section(s) to the HWP via mounted midcouplers.

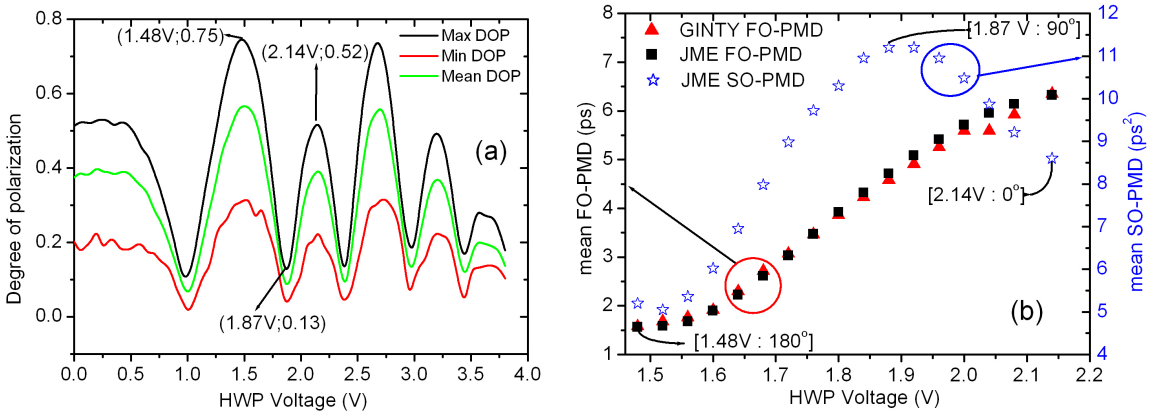

Fig. 6.15: Two arbitrary PMF sections were coupled using HWP II. The applied voltage to the HWP was varied between 0 and 3.8 V. (a) Variation of DOP with voltage and (b) Calibrating voltage to angles using FO- and SO-PMD.

Calibration of HWPs between 0 and 180^o were performed by monitoring FO-PMD, SO-PMD and DOP (min, man and mean) as the voltage to the HWP was varied between 0 to 3.8 V in steps of 0.2 V. The maximum applied voltage was set at 3.8 V as a safety measure to reduce the possibility of voltage overshoot. The C+L band light source (after polarization scrambling) was used in the calibration process. Fig. 6.15 shows the calibration results when HWP II interconnected two arbitrary PMF sections. The max, min and mean DOP cycle upwards and downwards as the HWP voltage varies (Fig. 6.15 (a)). A complete peak to peak cycle indicates the 0 to 180^o range; when the max DOP is at its minimum, the angle between the two FO-PMD vectors provided by the two arbitrary PMF sections is 90^o. The 1.48 V to 2.14 V range was selected as the operating range and a voltage of 1.87 V indicates 90^o. At an applied voltage of 2.14 V the FO-PMD was maximum (~ 6.3 ps) and minimum (~ 1.6 ps) at 1.48 V (Fig. 6.15 (b)), which corresponds to 0^o and 180^o respectively. The voltage giving maximum SO-PMD corresponds to 90^o (refer to concatenation equation 2.12), in this case it coincided with the expected voltage 1.87 V. There was a slight difference of at most 3.5% in the FO-PMD values obtained using the JME and GINTY methods, thus the two techniques compare well. All the other HWPs were also calibrated for voltage to angle using the above mentioned method, and are listed in Table 6.1.

Table 6.1: The seven half waveplates (HWPs) and a mapping of their voltage to angles.

HWP number ↓	0^o	90^o	180^o
I	1.85V	1.45V	1.21V
II	2.14V	1.87V	1.48V
III	2.35V	1.90V	1.15V
IV	2.26V	2.00V	1.62V
V	2.2V	1.85V	1.55V
VI	2.65V	2.20V	1.75V
VII	1.40V	1.20V	1.02V

For an adjustable PMD emulator to reproduce PMD statistics, it should be stable. In this study the emulator is tested for stability by measuring the output SOPs of light. SOP fluctuations were measured using a C+L broadband light source, linear polarizer and polarization analyser, over a 3 hour period at 1 second intervals. Fig. 6.16 (a) shows slight SOP changes (range of relative SOP angles = 0.32^o) on the Poincaré sphere. This meant the emulator was fairly stable under the laboratory environment (~ 20 ^{o}C). The slight SOP changes were probably due to lack of stability of the C+L broadband light source. If any significant temperature changes were to affect the emulator, every component making up the emulator would be affected. Since the emulator was stable in the laboratory, repeatability tests were conducted using the PMD (FO- and SO-PMD) measurements (Fig. 6.16 (b)).

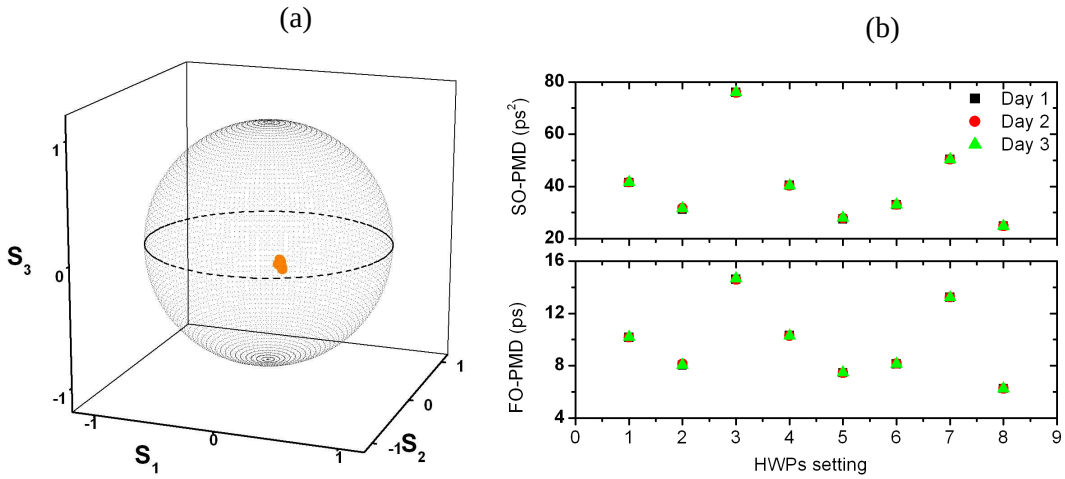

Fig. 6.16: Emulator (a) stability test through SOP monitoring and (b) repeatability test through PMD measurements. Eight different HWP settings (HWPs setting 1 - 8 in Table 6.2) were configured and repeated on three different days.

The PMD was adjusted by configuring the angles of the seven HWPs into 8 different combinations, HWPs setting 1 - 8 in Table 6.2. These adjustments were repeated on three different days as FO- and SO-PMD were measured. Fig 6.16 (b) shows that the PMD measurements were approximately equal on 3 different days, with a maximum difference of 0.02 ps for FO-PMD and 0.1 ps^2 for SO-PMD. The slight difference is most likely due to the error in the JME measurement method. This therefore means the emulator is able to reproduce PMD statistics either with wavelength or time.

6.3.2. PMD characteristics of the emulator with wavelength

This emulator, like the deployed buried fibres presented in Section 5.1.1, gives stochastic PMD statistics due to the presence of random mode coupling and birefringence distribution (Fig. 6.17). This subsection will first focus on adjusting the PMD spectra by controlling mode coupling angles and then investigate the reproducibility of PMD statistics using the emulator.

Table 6.2: Fourteen sets of HWP settings used to adjust the PMD statistics of the emulator. The voltage to angle mapping for each half waveplate (HWP) is given in Table 6.1.

HWPs setting ↓	***HWP I***	***HWP II***	***HWP III***	***HWP IV***	***HWP V***	***HWP VI***	***HWP VII***
1	0^o	90^o	0^o	0^o	0^o	0^o	0^o
2	0^o	90^o	90^o	90^o	90^o	90^o	90^o
3	90^o	0^o	0^o	0^o	0^o	0^o	0^o
4	0^o	90^o	90^o	0^o	0^o	0^o	0^o
5	0^o	90^o	90^o	90^o	90^o	90^o	0^o
6	0^o	90^o	0^o	90^o	90^o	90^o	90^o
7	90^o	0^o	90^o	90^o	90^o	90^o	0^o
8	0^o	0^o	0^o	90^o	0^o	90^o	0^o
9	0^o	90^o	0^o	90^o	0^o	90^o	0^o
10	0^o	0^o	0^o	90^o	90^o	0^o	0^o
11	90^o	90^o	0^o	0^o	90^o	90^o	0^o
12	0^o	0^o	90^o	90^o	90^o	90^o	0^o
13	90^o	0^o	0^o	0^o	0^o	90^o	0^o
14	90^o	90^o	0^o	0^o	0^o	90^o	90^o

In order to generate different PMD statistics using the emulator design in Fig. 6.14, the seven HWPs were configured to give a combination of different angles. Table 6.2 above gives some of the HWP settings (14) that were used to enable emulator tuneability. The table shows the combination of 0^o and 90^o angles used to control the HWPs, any of the combination of angles between 0^o and 180^o can be used. Figure 6.17 illustrates the resulting FO- and SO-PMD statistics at HWPs setting 8 and 14 using the JME method. Figure 6.17 (a) shows that the emulator can change both its mean PMD values and the shape of its spectrum. HWPs setting 14 results in more stochastic and rapid PMD changes with wavelength covering a wider range compared to the influence of HWPs setting 8. This is due to the difference in the degree of random mode coupling since the number of mode coupling sites is fixed.

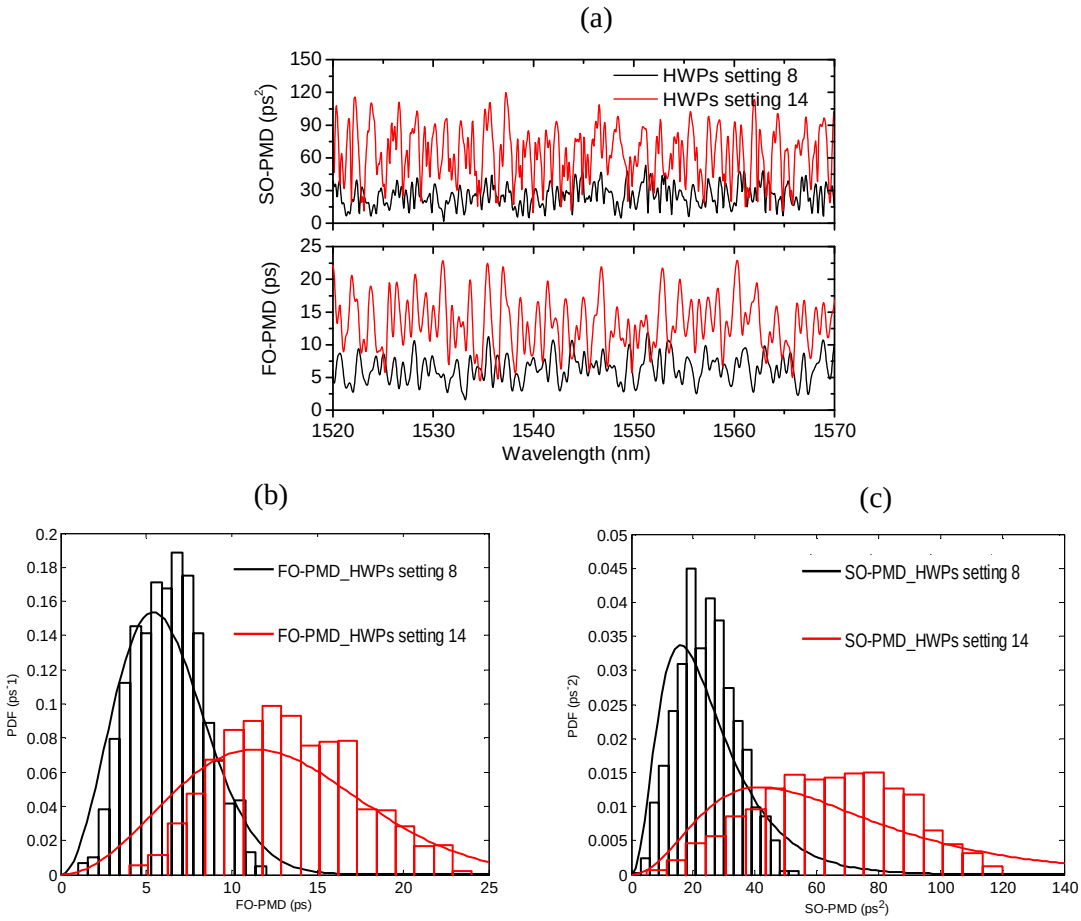

Fig. 6.17: (a) Illustration of the capability of the emulator to tune PMD statistics in the wavelength domain. The (b) FO-PMD and (c) SO-PMD statistical distribution when the HWPs settings are 8 and 14. The solid lines on the FO-PMD histograms are the Maxwellian distributions and those on the SO-PMD histograms are the theoretical distributions proposed by Foschini et al. (1999).

Fig. 6.17 shows the statistical distribution of the FO- and SO-PMD for HWPs setting 8 and 14. The FO-PMD statistics for HWPs setting 8 and HWPs 14 do not approximate the Maxwellian distribution fit (Fig. 6.17 (b)), some regions on the histograms are not well populated. However, the FO-PMD statistics for HWPs setting 8 approaches the Maxwellian better relative to that of the HWPs setting 14. This is due to the minimum FO-PMD value of HWPs setting 8 being close to zero (1.5 ps) and that of HWPs setting 14 away from zero (4.5 ps). In this study the HWP settings gave stochastic FO-PMD and minimum FO-PMD values either close or away from 0 ps. The SO-PMD statistics for HWPs setting 8 and 14 like the accompanying FO-PMD do not approximate to the SO-PMD theoretical distribution proposed by Foschini *et al.* (1999) (Fig. 6.17 (c)). The SO-PMD statistics of HWPs setting 8 approaches the SO-PMD theoretical distribution better relative to that of HWPs setting 14.

Increasing the number of PMF sections and HWPS on the emulator would make the PMD statistics better match the theoretical distributions.

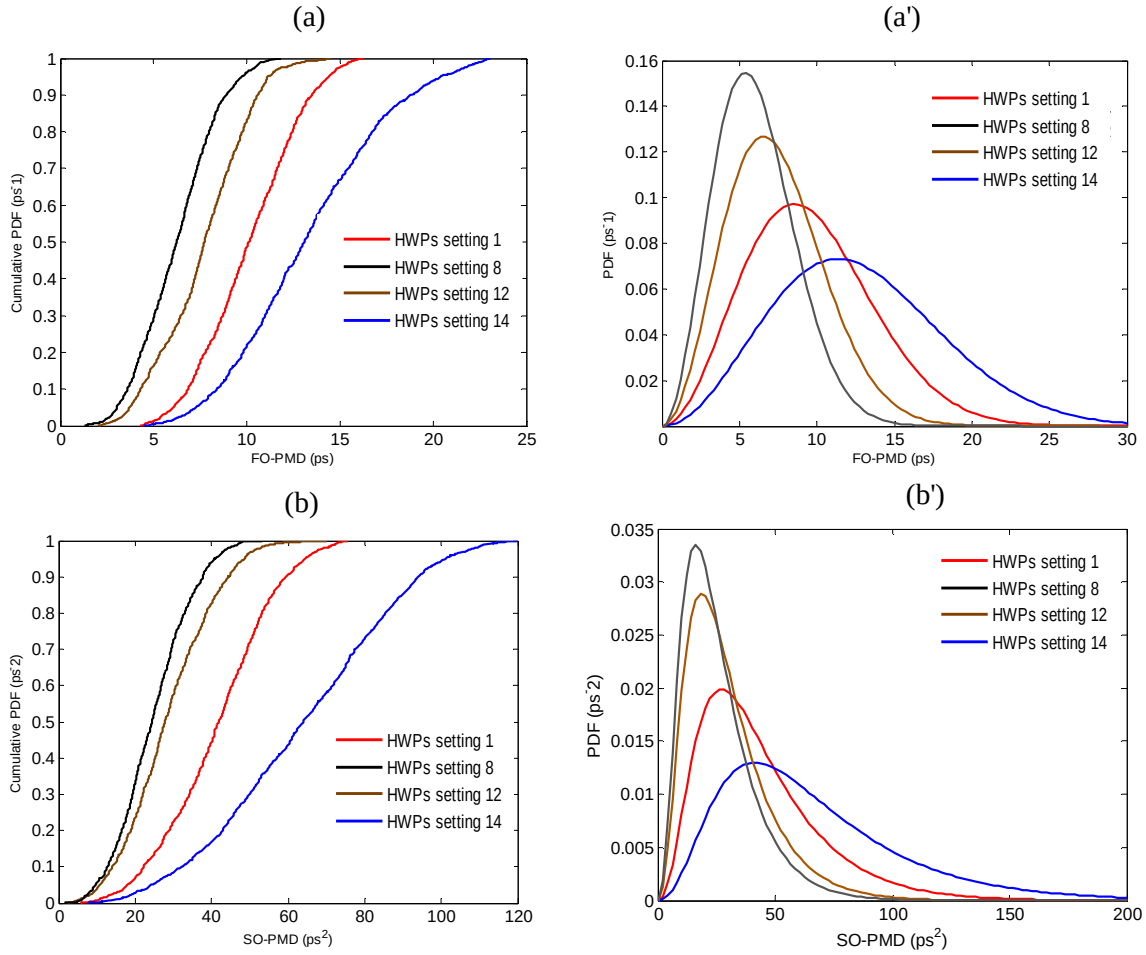

Fig. 6.18: ((a) and (b)) The cumulative probability density function (CPDF) of the PMD statistics provided by the emulator at different HWP settings. ((a') and (b')) The theoretical pdf fits on PMD statistics for different combinations of HWPs settings. The histograms of the PMD statistics are not shown in (a') and (b') for clear diagrammatic illustration but the PMD information is displayed in (a) and (b) respectively. Table 6.2 gives fourteen HWPs settings.

Figure 6.18 shows that HWPs setting 1, 8, 12, 14 give four different FO-PMD and SO-PMD statistics. There are many other different HWP configurations involving angles between 0^o and 180^o, only HWPs setting 1, 8, 12, 14 are used for illustration (Fig. 6.18)). The distributions in Fig. 6.18 (a') and (b') are the theoretical fits to the PMD histograms that are not shown to allow clear diagrammatic presentation. The cumulative probabilities of the four PMD statistics are shown in Fig. 6.18 (a) and (b). In order to view how the PMD statistics at different HWP configurations relate to theoretical distributions, refer to Fig. 6.17. The ability to reproduce these statistics depends on the stability of the emulator. Fig. 6.19 depicts a very slight deviation (histogram bins offset) of the PMD statistics of HWPs setting 1 on three

different days. This leads to the conclusion that under a stable laboratory environment, the PMD emulator design can reproduce the PMD statistics with wavelength. The slight difference in PMD statistics on the three different days as shown in the histograms in figures 6.19 (a') and (b') are most likely due to the JME instrumental error. The accuracy of the JME method can be influenced by fibre stability, optical source incremental wavelength accuracy, polarization analyser accuracy and the repeatability of the instrumental polarizations (Derickson 1998). Figures 6.19 (a) and (b) show that the slight difference in the PMD statistics on the three difference days does not affect the theoretical distribution fits.

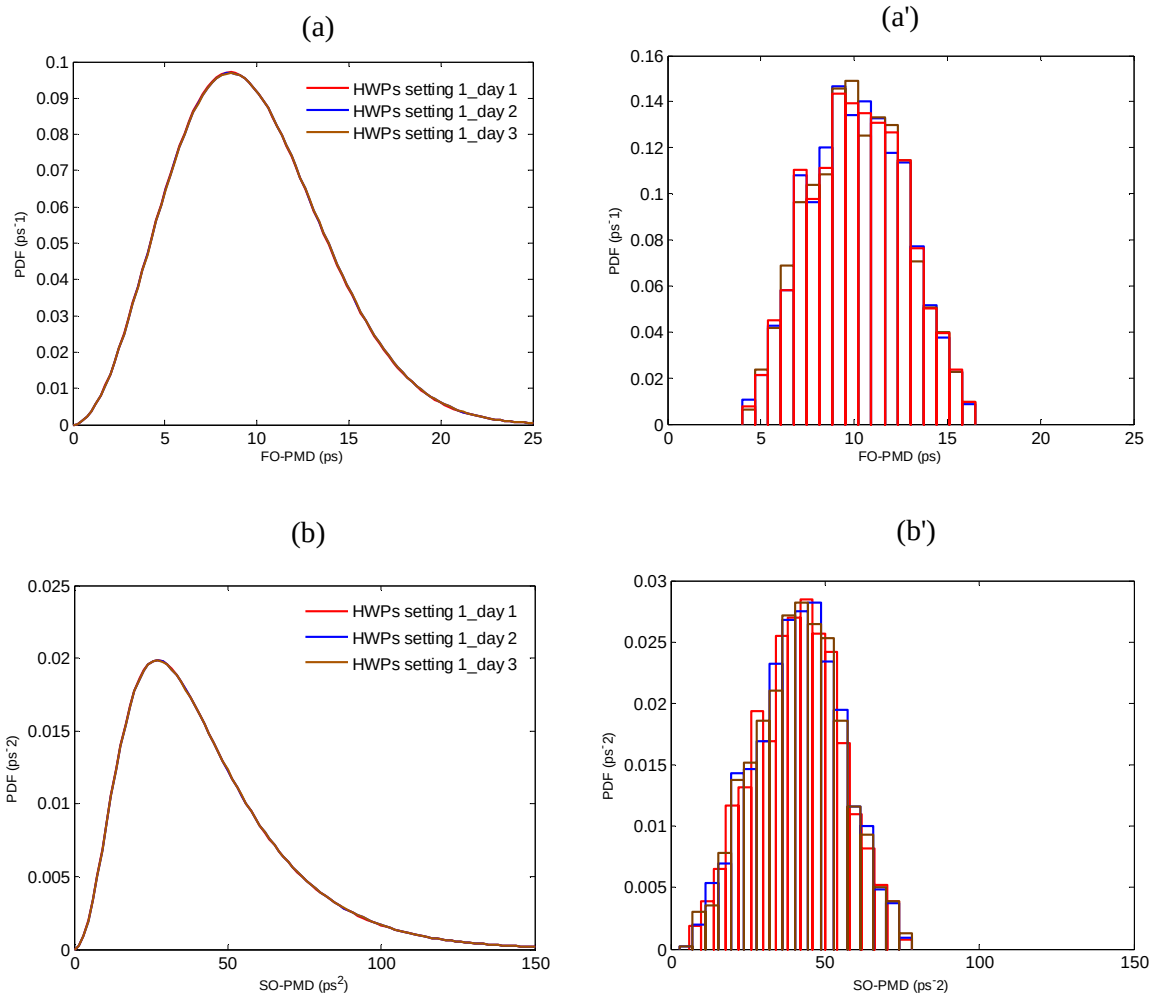

Fig. 6.19: (a) and (b) The theoretical PDF fits on the measured PMD statistics illustrated as histograms in (a') and (b'). The PMD measurements were carried out on three different days when the emulator was set at HWPs setting 1. These diagrams are used to investigate emulator reproducibility.

Thus instead of the application of importance sampling (IS) in the time domain, an emulator of this kind can be used for importance sampling in the frequency domain only if some its PMD values populate the low probability tail of the statistical distribution. The wavelengths

that have high PMD values that will lie in the tail of the theoretical probability density function are known to cause system outage and in such a case are highly likely to occur. For transmission in WDM systems, such wavelengths are not used for data transmission. In the time domain the high PMD values in the probability density function tail are known to occur in less than a minute per year (Kaminow 2002).

6.3.3. PMD characteristics of the emulator with time

FO-PMD and SOP changes experienced in aerial fibres can be mimicked by randomly adjusting the HWPs in the emulator relative to each other. The limitation with the emulator is that the PMFs have fixed birefringence. The FO-PMD and SOP changes in aerial fibres are due to simultaneous birefringence, mode coupling and fibre position changes whilst for the emulator FO-PMD and SOP changes are only due to mode coupling changes. The HWPs have a response time of < 10 ms but in this experiment to allow synchronisation between the Labview emulator control programme and GINTY, a 10 second interval was set between FO-PMD measurements. 1073 FO-PMD measurements were collected. During continuous output SOP measurements, light was supplied from a narrow band Agilent 8164A laser source set at 1550 nm, the polarization analyser recorded measurements over a time frame of 1000 s at 30 ms intervals. The 30 ms time interval was used due to it being the maximum response time of the polarization analyser.

The control of the HWP angles between 0^o and 180^o resulted in stochastic FO-PMD changes (Fig. 6.20 (a)) similar in behaviour to those experienced in aerial fibres during the day when there are drastic and significant environmental changes. The FO-PMD statistics approaches the Gaussian distribution (Fig. 6.20 (a')), similar to what was observed for the aerial fibre presented in Section 5.1.2. Due to the emulator being stable and reproducible as discussed before, the time-varying FO-PMD statistics can be reproduced. It should be noted that for FO-PMD values less and greater than 13.3 ps, the expected root-mean-square-sum, depends on the nature of mode coupling. The expected root-mean-square-sum is applied considering there is random mode coupling. However, the degree of random mode coupling can differ. The emulator gave FO-PMD values, using the 1075 HWP configurations, spanning from 2.61 ps to 14.75 ps (see Fig. 6.20).

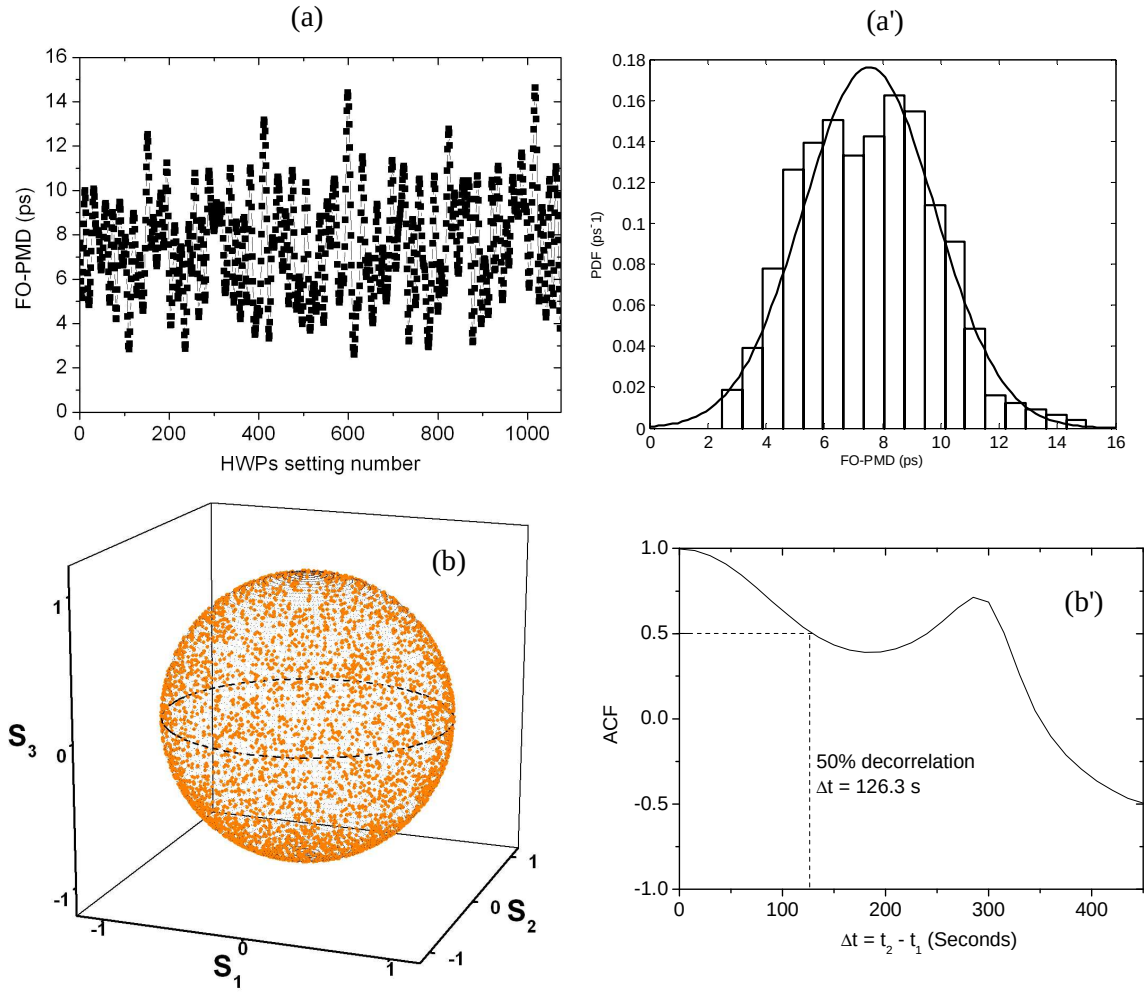

Fig. 6.20: (a) The FO-PMD variation with random adjustments in the HWPs on the emulator, (a') The FO-PMD histogram and Maxwellian PDF fit, (b) A Poincaré sphere showing the variation of the output SOPs and (b') The ACF for the emulator over the first 450 seconds.

SOP changes generated by the emulator covered many polarization states on the Poincaré sphere as shown in Fig. 6.20 (b), although they were mostly on the surface of the sphere (with DOP > 0.9) since a highly polarized narrow band laser source was used. The random adjustments in the HWPs switched the SOPs from one polarization state to the other; changes depended on the degree of random mode coupling changes. In order to measure the degree of SOP change as the HWPs changed, a time ACF was calculated using equation (2.24). The emulator decorrelation time was 126.3 s as shown in Fig. 6.20 (b'), it falls within the decorrelation time range (between 13.62 s and 600s) given by Waddy *et al.* (2001) for aerial fibres. It should be noted that the ACF of the emulator can either be above or below 126.3 s

depending on the degree of random changes introduced by the HWPs. Each HWP has a response time < 10 ms.

6.4 Emulator with fixed birefringent sections plus tuneable delay element and rotatable polarization orientation

PMD emulators exhibiting both FO-PMD and SO-PMD have been designed and implemented (Wegmuller *et al.* 2000, Zeng 2003, Yan *et al.* 2004). These types of emulators were found to be necessary due to the coexistence of FO- and SO-PMD in optical network links. Due to the interaction between these two effects, the impact of SO-PMD on FO-PMD has been investigated (Bruyére 1996, Nelson *et al.* 2000, Gupta *et al.* 2007). By definition, SO-PMD is dependent on the magnitude of the FO-PMD vector ($\vec{\tau}$). The reverse impact of FO-PMD on SO-PMD should therefore also be looked into experimentally. To investigate this phenomenon, presented in this section is a PMD emulator design having a fixed mean SO-PMD but varying mean-FO-PMD. The emulator had insertion losses of 1.55 and 1.95 dB. Firstly, the design considerations for the emulator are considered, followed by the characteristics of the emulator.

6.4.1. Design considerations for the emulator

The emulator comprises a sub-emulator, a computer controlled polarization controller (PC) and a digital delay line (DDL) as shown in Fig. 6.21. The sub-emulator generates fixed SO-PMD and the DDL controls the FO-PMD. The sub-emulator has 8 PMF segments, with random birefringence and mode coupling distributions. The length of each PMF segment lies within 20% standard deviation (Gaussian distribution) of the mean length (~ 4 m) of the sub-emulator. The FO-PMD values of the 8 segments are: 4.35, 6.6, 4.95, 5.4, 6.3, 5.7, 7.1 and 7.8 ps in sequence, resulting in the sub-emulator mean FO-PMD being 18.1 ps (see sub-emulator PMD statistics in Fig. 6.22). These PMF segments were fusion spliced together without any intentional alignment of the birefringent axes; it is assumed that the mode coupling angles are randomly distributed. The PC is computer adjusted to an angle θ such that the angle β between the sub-emulator and the DDL FO-PMD vectors is equal to 0^o. This means the FO-PMD vectors of the sub-emulator and the DDL are parallel. The angle β was obtained using the method previously discussed in section 6.3.

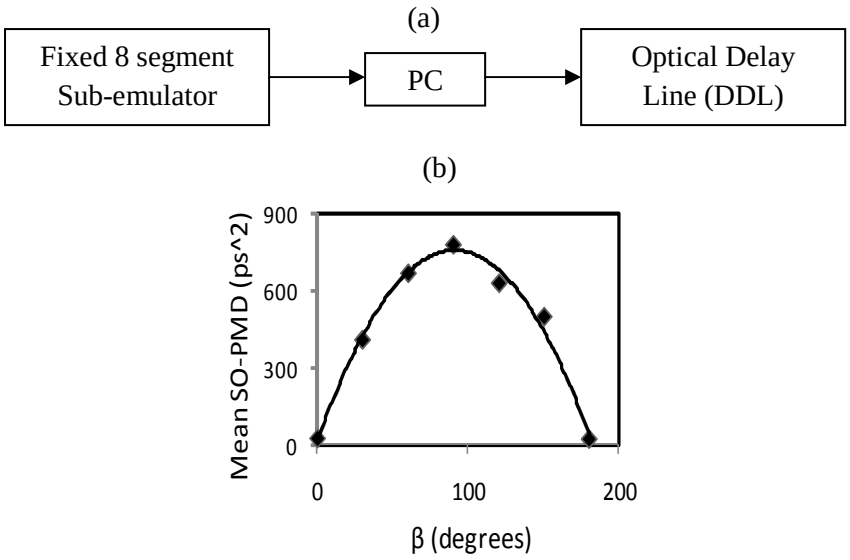

Fig. 6.21: (a) Block diagram for fixed SO-PMD but varying FO-PMD emulator. The polarization controller (PC) angle θ alters to always ensure β is always equal to 0^o as wavelength changes. (b) The SO-PMD of the emulator when the β is varied from 0 to 180^o. The solid line is a guide to the eye. The DDL FO-PMD is fixed at 26 ps, resulting in the emulator mean FO-PMD remaining fairly uniform at 38.8 ± 0.8 ps. PC stands for polarization controller.

The choice of the angle $\beta = 0^o$ emanated from the concatenation equations of Eq. (6.1) and (6.2), as highlighted in Section 2.1.3 IIIa. The mean emulator FO- and SO-PMD can be expressed in vector form by:

$$\vec{\tau}_{\text{mean}} = \vec{\tau}_{\text{DDL}} + \mathbf{R}_{\text{DDL}}\vec{\tau}_{\text{sub}} \tag{6.1}$$

$$\vec{\tau}_{\omega\_\text{mean}} = \vec{\tau}_{\omega\_\text{DDL}} + \mathbf{R}_{\text{DDL}}\vec{\tau}_{\omega\_\text{sub}} + \vec{\tau}_{\text{DDL}} \times \vec{\tau}_{\text{mean}} \tag{6.2}$$

where $\vec{\tau}_{\text{DDL}}$ and $\vec{\tau}_{\text{sub}}$ are the FO-PMD vectors of the DDL and the sub-emulator respectively, $\mathbf{R}_{\text{DDL}}$ is the rotational matrix of the DDL, $\vec{\tau}_{\omega\_\text{DDL}}$ and $\vec{\tau}_{\omega\_\text{sub}}$ are the SO-PMD vectors for the DDL and the sub-emulator, respectively. In order to make the mean SO-PMD of the emulator independent of the DDL FO-PMD $\vec{\tau}_{\text{DDL}}$, the last term of Eq. (6.2), $\vec{\tau}_{\text{DDL}} \times \vec{\tau}_{\text{mean}}$, should be set to zero. This is achievable only if $\vec{\tau}_{\text{DDL}}$ and $\vec{\tau}_{\text{mean}}$ are collinear (either the vectors are parallel or anti-parallel), that is the angle between the two vectors are 0 and 180^o. When $\beta = 0^o$, $\vec{\tau}_{\text{sub}}$ is parallel to $\vec{\tau}_{\text{DDL}}$, Eq. (6.1) then reduces to

$\vec{\tau}_{mean} \sim \vec{\tau}_{DDL}$ when the DDL is the dominant FO-PMD vector contributor for the emulator. In summary, to make the SO-PMD independent of the DDL FO-PMD, β has to be 0^o. Since the PMD at each wavelength is represented by a unique vector, the PC needs to be adjusted for each wavelength to ensure the angle $\beta = 0^o$ (obeying the condition $\vec{\tau}_{DDL} \times \vec{\tau}_{mean} = 0$) for that wavelength.

Fig. 6.21 (b) provides an insight into the behaviour of the FO-PMD τ and SO-PMD $\vec{\tau}_{\omega}$ of the emulator when the PC angle is altered, enabling β to rotate between 0^o and 180^o. The SO-PMD output reaches minimum close to that of the sub-emulator when $\beta = 0^o$ or 180^o, and maximum when $\beta = 90^o$. The mean FO-PMD is always fairly constant at 38.8 ± 0.8 ps due to the dominance of the DDL FO-PMD vector. Adjusting the DDL FO-PMD (τ_{DDL}) whilst $\beta = 0^o$ will always give a SO-PMD outcome almost equivalent that of the sub-emulator alone and the mean FO-PMD approximates τ_{DDL}. Thus controlling the PC angle changes the SO-PMD statistics but still maintains a fairly uniform mean FO-PMD.

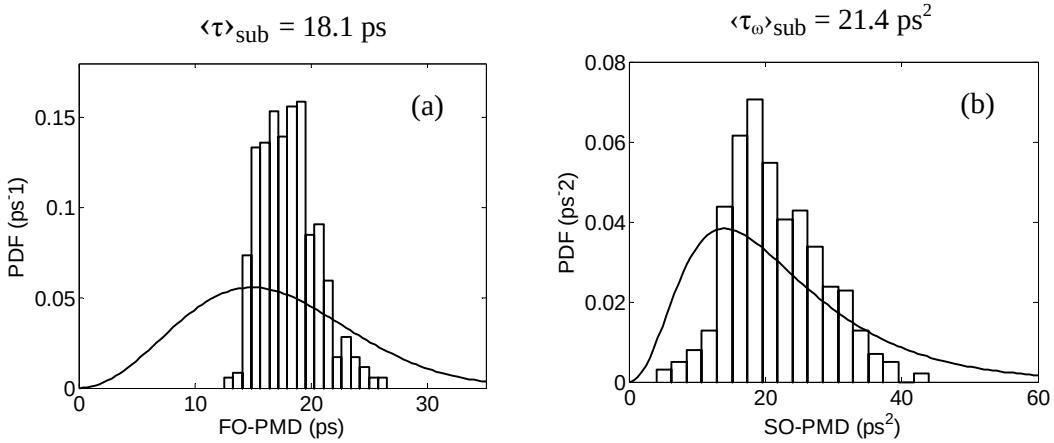

Fig.6.22: The (a) FO-PMD (τ) and (b) SO-PMD (τ_{ω}) statistical distribution for the 8 segment sub-emulator. The solid line on the FO-PMD histogram is the ideal Maxwellian distribution and that on the SO-PMD histogram is the ideal SO-PMD theoretical distribution. ‹τ›sub stands for the mean FO-PMD of the sub-emulator and ‹τω›sub stands for the mean SO-PMD of the sub-emulator.

Although the main aim of this experiment was to control the mean PMD values, the PMD statistics of the emulator cannot be ignored. The emulator can also be used as a statistical emulator which scans PMD conditions whilst changing wavelength or the polarization controller. Fig. 6.22 (a) illustrates the histogram of the sub-emulator FO-PMD, which does not approach the Maxwellian distribution. The corresponding SO-PMD statistics of the sub-

emulator (Fig. 6.22 (b)) does not approach the SO-PMD theoretical distribution. Failure of the sub-emulator to approximate PMD theoretical distributions is most likely due to the limited number of randomly distributed birefringent segments (8 segments only). Therefore, further additions of random birefringent segments and mode coupling on the sub-emulator as highlighted in Section 6.1 could result in its PMD statistics approaching the well known ideal PMD theoretical distributions.

6.4.2. Characteristics of the PMD emulator

In this subsection the PMD emulator is controlled in the presence of the sub-emulator (Fig. 6.21 (a)) and for comparison, the sub-emulator is replaced with a single PMF segment. Initially, the FO-PMD of the DDL was calibrated to ensure experimental accuracy as discussed in Section 6.2. The residual mean SO-PMD (residual-$\langle\tau_\omega\rangle$) of the DDL remained fairly constant at 0.24 ± 0.07 ps^2 for 20 ps $\leq \tau_{DDL} \leq$ 60 ps, thus making this the preferred experimental range. By ensuring $\tau_{DDL} \geq 20$ ps, the DDL is the dominant contributor to the FO-PMD vector ($\vec{\tau}$) of the emulator. This condition together with $\beta = 0^o$, allowed the adjustment of only the emulator FO-PMD (emulator-τ) and not the two $\vec{\tau}_\omega$ components, which remain constant. If $\tau_{DDL} \leq \langle\tau\rangle_{sub}$ and $\beta \neq 0^o$ or 180^o, then changes in τ_{DDL} will enhance emulator-τ change, and hence affect the emulator-τ_ω. The DDL is implemented in Chapter 7 to investigate the impact a high FO-PMD (HiFO-PMD) segment has on PMD, output SOPs and system performance at different values of β.

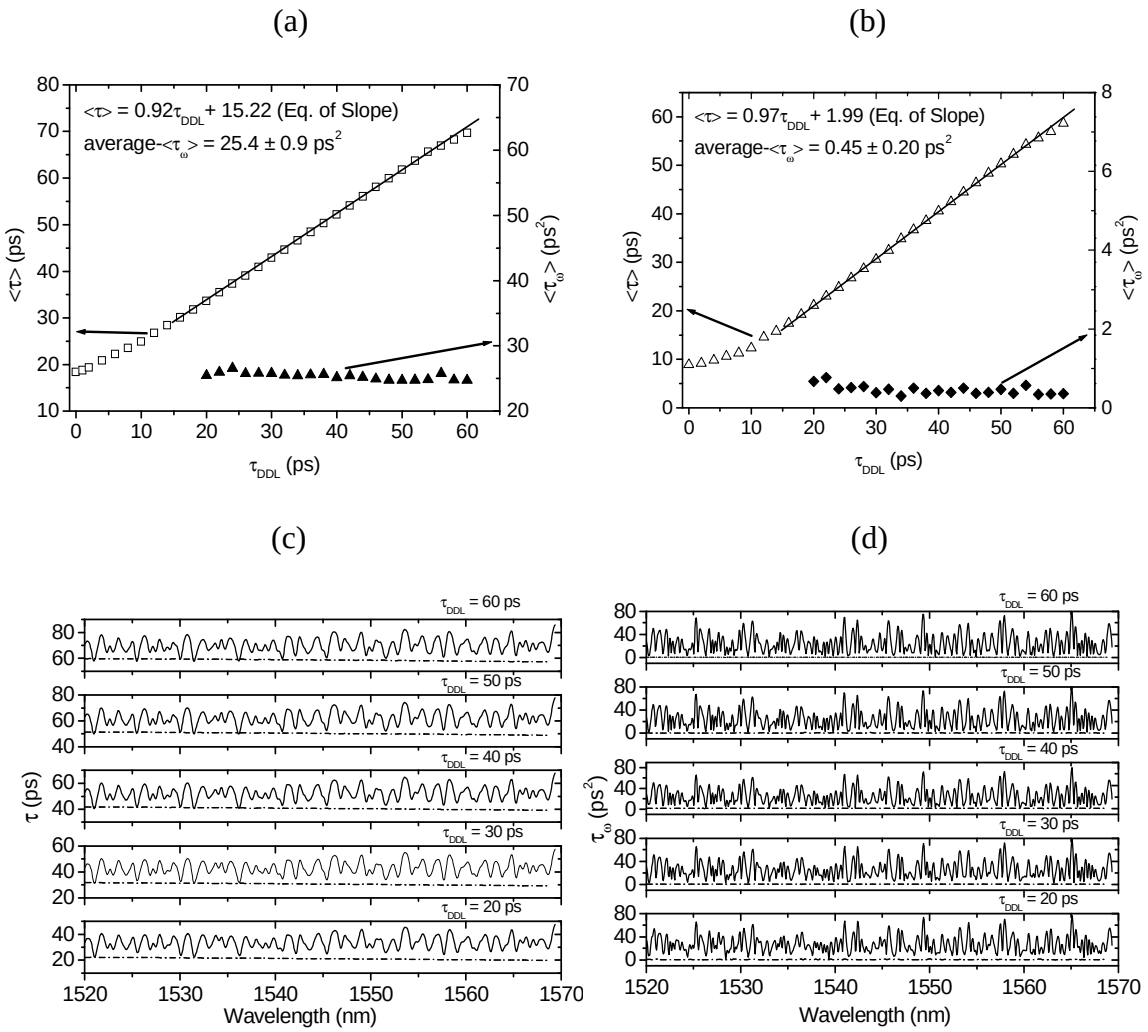

Fig. 6.23: Emulator characteristics for various τ_{DDL} values when (a) the sub-emulator and (b) the PMF segment (8.15 ps) are attached to the DDL. The gradient of the slope and SO-PMD (τ_ω) measurements were obtained between 20 ps $\leq \tau_{DDL} \leq$ 60 ps. The FO-PMD (τ) wavelength spectra (c) and τ_ω wavelength spectra (d) when τ_{DDL} is at 20, 30, 40, 50 and 60 ps for the sub-emulator (solid line) and for the 8.15 ps single PMF segment (dashed line) coupled to the DDL.

The FO- and SO-PMD characteristics of the emulator incorporating the sub-emulator, and the sub-emulator substituted with a PMF equivalent are shown in Fig. 6.23. Fig. 6.23 (a) illustrates how $\langle\tau_\omega\rangle$ can be maintained constant for a range of $\langle\tau\rangle$ values. This is achieved by keeping the sub-emulator configurations (mode coupling and birefringence distribution) fixed and the coupling angle β always at 0^o with wavelength change, as τ_{DDL} was varied from 20 to 60 ps. DDL settings therefore provide the dominant $\vec{\tau}$ such that the emulator-$\langle\tau\rangle$ is biased towards τ_{DDL}. SO-PMD is maintained fairly constant as τ_{DDL} is altered (with an average-$\langle\tau_\omega\rangle$ ($\langle\tau_\omega\rangle_{avg}$) = 25.4 ± 0.9 ps^2 for the 20 ps $\leq \tau_{DDL} \leq$ 60 ps range). What is only affected is the emulator-$\langle\tau\rangle$, while the shapes of the FO-PMD spectra remain unaffected (Fig. 6.23 (c)). The

PCD therefore remained constant. A gradient of 0.92 and cut-off ‹τ› of 15.22 ps (Fig. 6.23 (a)) suggests why ‹τ› is always ~ 13 ps above τ_{DDL}. The FO-PMD range around the emulator-‹τ› was always maintained at ±11.7 ps throughout the entire experiment. Each individual wavelength on the sub-emulator side possess a unique $\vec{\tau}$, each $\vec{\tau}$ is therefore always considered to be resolved together with the wavelength-independent dominant DDL $\vec{\tau}$ at a coupling angle $\beta = 0^o$.

Since the mode coupling angles are fixed and in this case are assumed to be uncorrelated (random), PSP-depolarization was unaffected throughout the experiment. Therefore since both PCD and PSP-depolarization were unaffected, the emulator-τ_ω is unaffected as shown in Fig. 6.23 (d). During SO-PMD measurements, PSP-depolarization and PCD were proportional, and always changed simultaneously (not shown). The slight change on emulator-τ_ω is likely due to the slight changes in residual-τ_ω presented by the DDL, as shown in Fig. 6.12 (c), although its contribution is minimal.

As a comparison to the emulator, the sub-emulator was replaced with a single PMF segment with ‹τ› = 8.15 ps and ‹τ_ω› = 0.33 ps^2, whilst maintaining the coupling angle $\beta = 0^o$ as wavelength changed. In this case the single segment 8.15 ps fibre had a wavelength-independent $\vec{\tau}$. The FO-PMD and SO-PMD spectra of the emulator are shown in Fig. 6.23 (c) and (d) for various τ_{DDL} settings. It can be seen that the emulator-‹τ› is fairly close to τ_{DDL}. This is evident in the almost unity gradient (Fig. 6.23 (b)), with an y-intercept ‹τ› close to zero (~ 2 ps) for the range 20 ps ≤ τ_{DDL} ≤ 60 ps. The single mode coupling site and angle $\beta = 0^o$ resulted in the emulator-‹τ_ω› remaining low, see Fig. 6.23 (d), due to negligible PCD and little PSP-depolarization from limited PSP rotations with wavelength. The emulator average-‹τ_ω› for 20 ps ≤ τ_{DDL} ≤ 60 ps is 0.45±0.2 ps^2.

The difference in emulator-‹τ› at each τ_{DDL} value between Fig. 6.23 (a) and (b) is approximately 13 ps. This agrees closely to the difference between the y-intercepts when the single 8.15 ps segment was attached (= 1.99 ps) and that when the sub-emulator was attached (= 15.22 ps). In order to successfully design the type of emulator presented in this section, one should ensure $\beta = 0$ or 180^o.

In summary, in order to successfully design the emulators presented in this Chapter one should have an understanding of the PMD equations (see Chapter 2). These equations

together with the background information on the PMD phenomenon guides one to come up with the appropriate configurations (mode coupling and birefringence configurations) for a particular emulator design. An emulator comprising a single birefringent section (Section 6.2) gives a certain amount of FO-PMD but negligible SO-PMD. Emulators that are made from coupled birefringent sections have both FO- and SO-PMD coexisting. However, those emulators comprising a HiFO-PMD section have a mean FO-PMD biased towards that of the HiFO-PMD section. The SO-PMD from the emulators comprising a HiFO-PMD section solely depends on the coupling angle β and is best explained using the concatenation equations.

6.5 Impact of PDL in PMD emulators

In this section we will first investigate the design consideration that may result in the introduction of PDL. Later, focus will be on the impact of PDL on the PMD statistics of PMD emulators. Emulator designs in Section 6.1 to 6.4 had PDL values less than 0.08 dB which we considered negligible. PDL measurements were made using the JME.

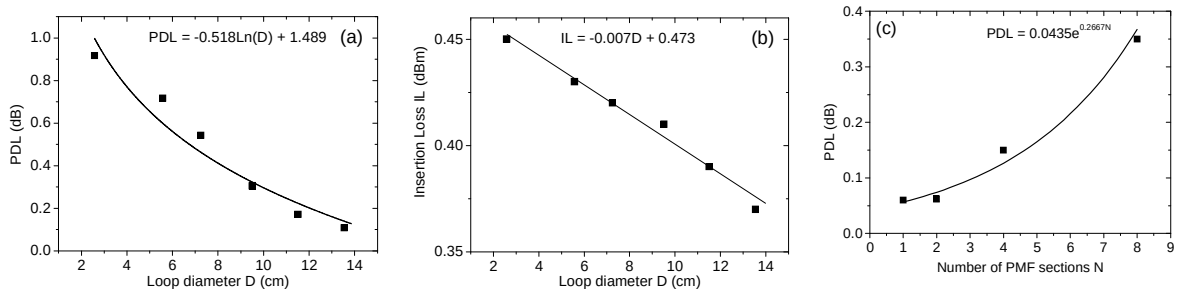

Fig. 6.24: Investigating the effects of (a) looping on the PDL, (b) looping on the insertion loss, and (c) bad fusion splicing using a 10 meter PMF length. The solid lines are the best fits using the equations given.

Using a 10 metre PMF fibre length with a FO-PMD = 13.3 ps and SO-PMD = 0.31 ps^2, the fibre was spooled on cylinders of different diameters. Five turns were made around each diameter. Fig. 6.24 (a) shows that the PDL decreases as a logarithm function with increasing loop diameter and Fig. 6.24 (b) shows the insertion loss decreases linearly with increasing loop diameter. These observations were used as a guide in designing PMD emulators in this study, especially the one discussed in Section 6.3 (Fig. 6.14). The design shown in Fig. 6.14 had loop diameters at least 13.5 cm in order to minimise the introduction of PDL and limit insertion loss. The 10 m PMF was then subdivided into 2, 4 and then 8 sections in sequence

and spliced using the Sumitomo fusion splicer. The fusion splicer was used in such a way as to intentionally create bad splices, which gave losses between 0.3 dB and 2 dB. Fig. 6.24 (c) shows that if there is bad splicing at mode coupling sites, the PDL increases exponentially. This was the other precautionary measure taken in designing PMD emulators in this study. During the design of PMD emulators, splicing losses introduced were less than 0.01 dB.

PDL effects on PMD statistics can best be observed through emulation. In order to show the implications PDL has on the PMD statistics, a 35 PMF section emulator was designed from pre-existing emulators. The emulator had a PDL value of 0.06 dB which we consider negligible. The PMD statistics of the 35-sections emulator alone approached theoretical distributions as shown by figures 6.25 (a) and (b). The introduction of PDL was done through coupling a PDL emulator and four 3 dB couplers in series. The PDL emulator had a PDL = 4.5 dB and each of the couplers had a PDL = 0.13 dB. An insertion loss of 12.85 dB was obtained when the 35-sections were interconnected to all the PDL components. Each coupler had an insertion loss of 3.153 dB.

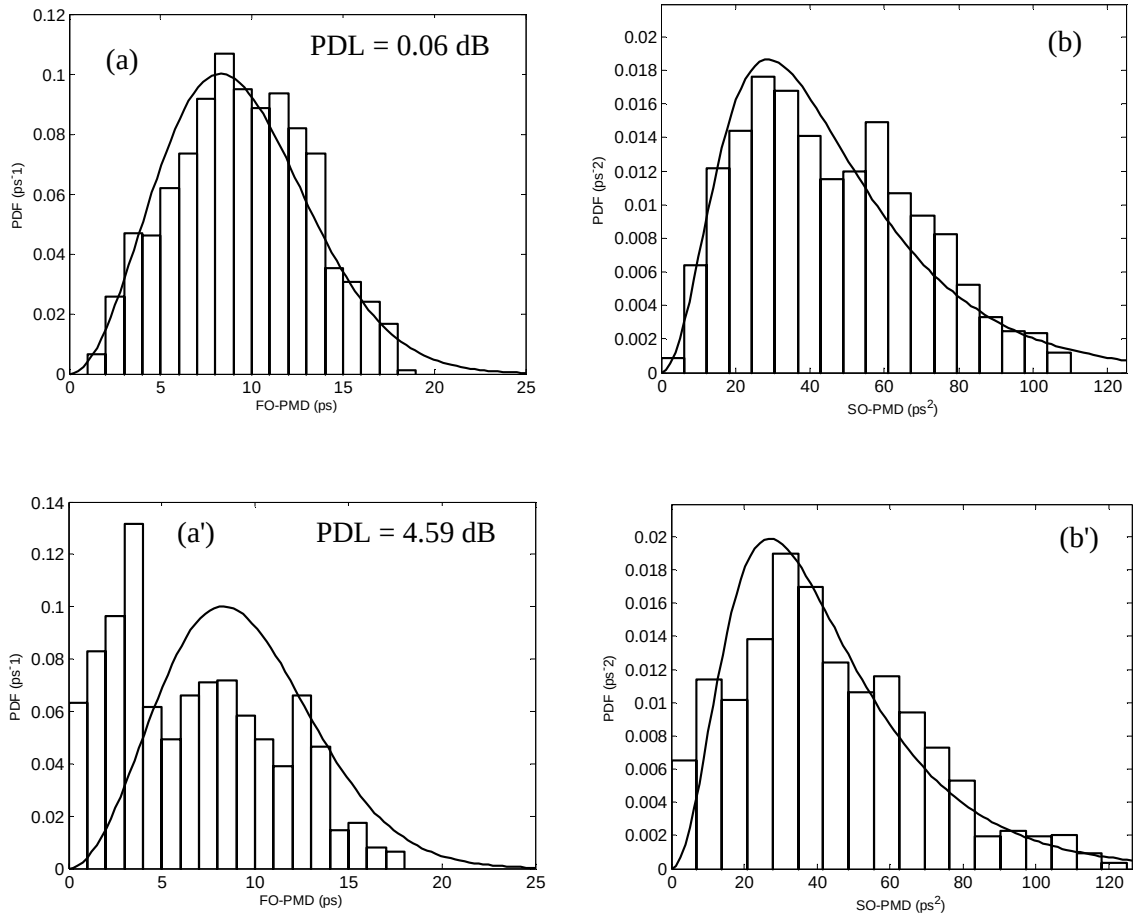

Fig. 6.25: Statistical distribution of FO- and SO-PMD in the absence of PDL ((a) and (b)) and the statistical distribution in the presence of PDL ((a') and (b')). The solid line on FO-PMD histograms is the Maxwellian probability density function (PDF) fit and that on SO-PMD histograms is the theoretical fit proposed by Foschini et al. (1999).

Fig. 6.25 (a') shows that PDL distorts FO-PMD statistics away from the Maxwellian theoretical distribution even in the presence of a high number of random mode coupling sites; This agrees with findings by Willner *et al.* (2004) and Pelaelo (2008). Under these conditions the PSPs of the fibre are no longer orthogonal to each other as illustrated in Fig. 2.12. There is also increased probability density on the low FO-PMD side (Fig. 6.25 (a')), this agrees with findings by Steinkamp and Voges (2007) that large values of PDL cause an increased probability of very high and/or low instantaneous FO-PMD.

Fig. 6.25 also shows that SO-PMD statistics is affected (evidenced by the unpopulated regions on the histogram) and the probability of low SO-PMD increases with the introduction of PDL. This is likely due to the abrupt interchange of the PSPs as was discovered by

Steinkamp and Voges (2007). The maximum SO-PMD on the low probability events tail shifted to 122 ps^2 from 115 ps^2 (Fig. 6.25) after the PDL components were introduced. This was probably due to mode coupling between the polarization components (PDL components) which promoted PSP and FO-PMD rotations with varying frequency. Thus emulators with no or negligible PDL give PMD statistics approaching theoretical distributions in the presence of large random mode coupling. The presence of PDL in PMD emulators would require the addition of more PMF sections compared to when PDL is absent, thus making the emulator costly.

CHAPTER 7

THE IMPACT OF A HIGH FIRST-ORDER PMD SECTION IN OPTICAL NETWORK SYTEMS

Deployed optical fibres are modelled as hundreds to thousands of randomly mode coupled birefringence fibre sections. Each fibre section possesses a certain amount of FO-PMD, assumed to be non-correlated to that of the other sections. Findings by Rogers (1981), Galtarossa *et al.* (2000) and Conibear *et al.* (2005) indicate on some fibre cables the presence of fibre sections having higher FO-PMD (HiFO-PMD) contributions than others, through the use of the polarization-optical time domain reflectometry technique (P-OTDR) (see Appendix II). Removal of such HiFO-PMD sections reduces the overall FO-PMD. In this chapter, the impact of a HiFO-PMD section on the overall FO- and SO-PMD, output state of polarization (SOP) of light and network system performance will be looked into. System performance will be evaluated by monitoring the bit error rate (BER). The impact of a HiFO-PMD section on the PMD statistical distribution was investigated in Section 6.1.3 III through emulation. Besides the JME and GINTY being used to measure the overall FO- and SO-PMD, they can provide an indication of the presence of a HiFO-PMD section through analysing the GINTY interferogram and JME spectrum.

7.1 Impact of a HiFO-PMD section on PMD

In this section, the impact of a HiFO-PMD (represented by a digital delay line (DDL)) on the overall FO- and SO-PMD is investigated as well as its effects on the resulting GINTY interferograms and JME spectra. The JME was tuned from 1520 – 1569 nm at a wavelength resolution of 0.3 nm during FO- and SO-PMD measurements. GINTY was used for FO-PMD measurements only. The experimental setup is illustrated in Fig. 7.1. Two of the buried fibre links (Link 61-62 /78-80) reported in Chapter 5 and a DDL were used for this part of the experiment. Link 61-62 had FO-PMD = 3.4 ps and SO-PMD = 4.98 ps^2, while Link 78-80 had FO-PMD = 11.2 ps and SO-PMD = 30.57 ps^2.

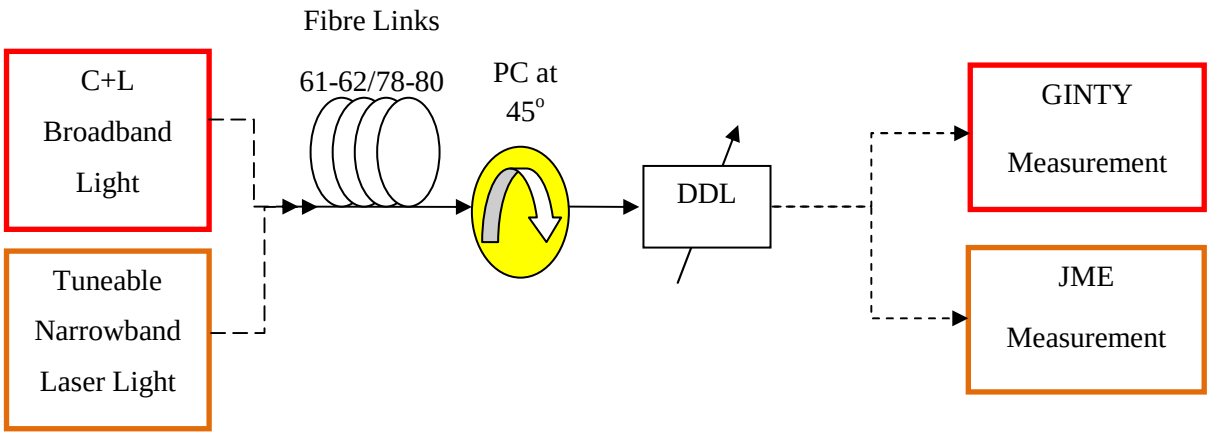

Fig. 7.1: Schematic setup for PMD measurements. The entire link is a concatenation of the fibre Link (61-62/78-80) and the digital delay line (DDL). For FO-PMD each entire fibre link was measured twice, using GINTY then the JME method. SO-PMD was measured using the JME only. The DDL was varied from 0 – 60 ps. PC stands for polarization controller.

Fig. 7.1 is a sketch showing the concatenation between a 28.4 km fibre link and a DDL (Section 3.3.1 III) via a polarization controller (Section 3.3.2) fixed at 45°. The DDL emulates the HiFO-PMD section present in the network. FO-PMD and SO-PMD were measured at each DDL FO-PMD setting ($\tau_{set\text{-}DDL}$) up to 60 ps.

7.1.1 FO- and SO-PMD

Focus will firstly be on FO-PMD, followed by SO-PMD in this subsection. Fig. 7.2 presents results for FO- and SO-PMD measured for various $\tau_{set\text{-}DDL}$ values. Fig. 7.2 (a) shows that as $\tau_{set\text{-}DDL}$ increases, the mean FO-PMD of the entire fibre link (τ_{mean}) is biased towards $\tau_{set\text{-}DDL}$. When this happens, the FO-PMD vector from the DDL ($\vec{\tau}_{DDL}$) exceeds that provided by Link 61-62 ($\vec{\tau}_{61\text{-}62}$) or 78-80 ($\vec{\tau}_{78\text{-}80}$). This means $\tau_{set\text{-}DDL} > 3.4$ ps for Link 61-62 and $\tau_{set\text{-}DDL} > 11.2$ ps for Link 78-80. Thus the ratio between $\tau_{set\text{-}DDL}$ and the mean FO-PMD (τ_{mean}) of the entire link is approximately equal to one, in the region 15 ps $\leq \tau_{set\text{-}DDL} \leq$ 60 ps, giving a gradient of 0.97 (~ 1) and a small y-intercept equal to 1.48 ps (Fig. 7.2 (a)). It is found that there is little deviation between GINTY and the JME measurements. Considering the experimental findings from the emulator designs in Sections 6.1.3 and 6.4 and those from this subsection, a HiFO-PMD section biases the mean FO-PMD of a fibre link towards its mean FO-PMD value for all polarization controller angles ranging from 0° to 180°.

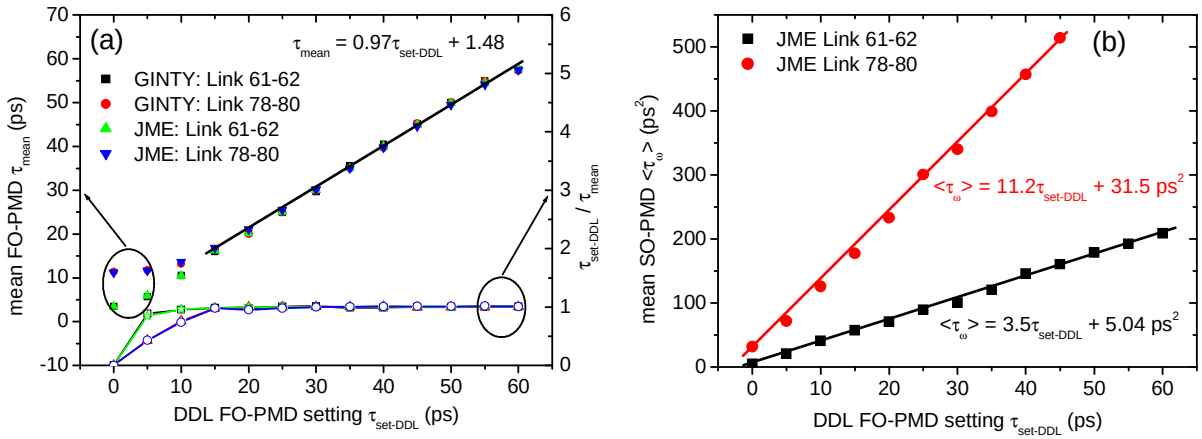

7.2: Measured (a) FO-PMD using JME and GINTY and (b) SO-PMD using JME as the DDL FO-PMD ($\tau_{set\text{-}DDL}$) was varied from 0 to 60 ps. The linear equation in (a) was obtained from 15 ps $\leq \tau_{set\text{-}DDL} \leq$ 60 ps and those in (b) were obtained from 0 ps $\leq \tau_{set\text{-}DDL} \leq$ 60 ps.

Fig. 7.2 (b) shows that as $\tau_{set\text{-}DDL}$ increases, the SO-PMD also increases. Consider the concatenation rule expressed by equation 2.12, with Link 61-62 or 78-80 providing the FO-PMD vector $\vec{\tau}_{link}$ and the DDL providing a FO-PMD vector $\vec{\tau}_{DDL}$ (or $\vec{\tau}_{HiFO\text{-}PMD}$). The SO-PMD then increases as a function of the cross product between $\vec{\tau}_{DDL}$ and the overall FO-PMD vector of the entire link $\vec{\tau}_{mean}$. This corresponds to the linear relationships shown in Fig. 7.2 (b). When $\tau_{set\text{-}DDL}$ = 0 ps, the mean SO-PMD is slightly above that provided by the fibre link alone due to contributions from the residual SO-PMD of the DDL. A similar trend in SO-PMD as in Fig. 7.2 (b) will be observed if the coupling angle between $\vec{\tau}_{DDL}$ and $\vec{\tau}_{mean}$ is not equal to 0^o or 180^o. It has been previously shown in Section 6.4 that having a 0^o or 180^o coupling angle between $\vec{\tau}_{DDL}$ and $\vec{\tau}_{mean}$ results in a fixed mean SO-PMD but changing mean FO-PMD.

7.1.2 GINTY interferogram and JME spectrum in the presence of a HiFO-PMD section

In this subsection an analysis into the GINTY interferogram and JME spectrum is carried out from FO-PMD measurements obtained as $\tau_{set\text{-}DDL}$ was adjusted from 0 to 60 ps. As stated before, the DDL emulates the HiFO-PMD section in a network (in this case for Links 61-62 and 78-80). Focus in this subsection is only given to FO-PMD because of the nature of the GINTY interferogram and JME spectrum which easily indicate the presence of a HiFO-PMD section.

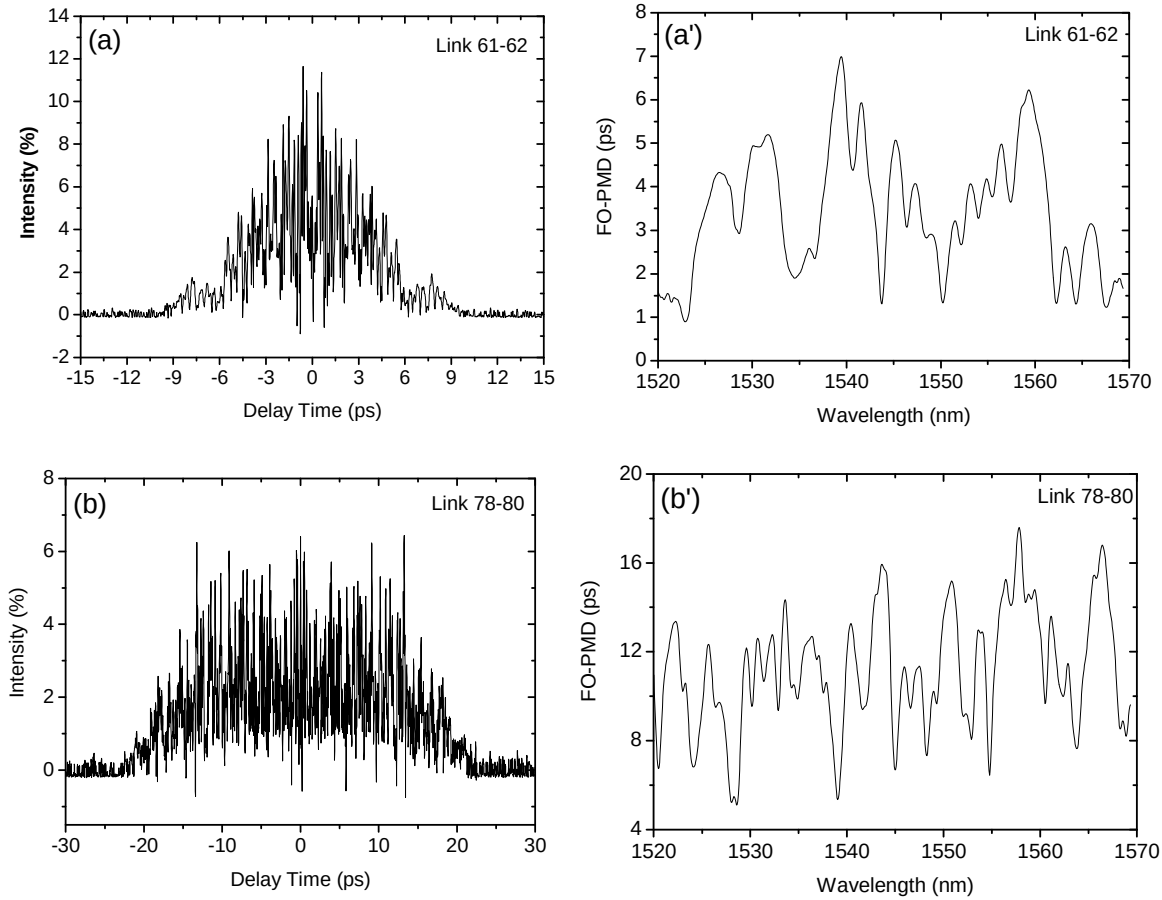

Fig. 7.3: GINTY interferograms for Links (a) 61-62 and (b) 78-80. The JME spectra for Links (a') 61-62 and (b') 78-80. Measurements were taken for $\tau_{set\text{-}DDL}$ *= 0 ps.*

Fig. 7.3 shows the FO-PMD measured on Links 61-62 and 78-80, with DDL set to 0 ps, i.e. the resulting GINTY interferogram envelope and JME spectrum show only the effect of the two links. Link 61-62 was found to be less random mode coupled as compared to Link 78-80. This is evidenced by the lower number of interference peaks or limited changes of FO-PMD with wavelength in Link 61-62 (Fig. 7.3 (a - a')) as compared to those of Link 78-80 (Fig. 7.3 (b - b')). In the absence of mode coupling or weak mode coupling, the resulting GINTY interferogram has three interference peaks similar to what is shown in Fig. 4.3 (b).

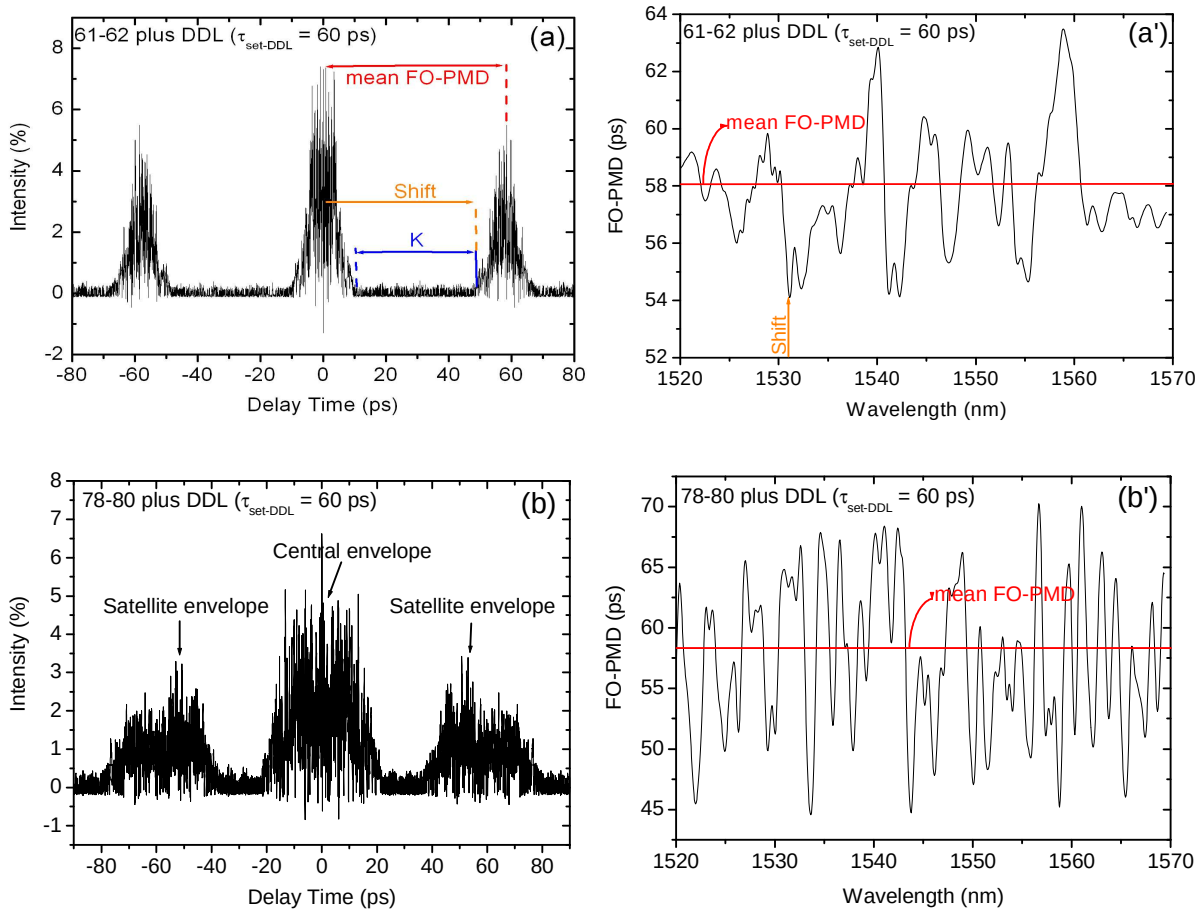

Fig. 7.4: GINTY interferograms (left) and JME spectra (right) for $\tau_{set\text{-}DDL}$ = 60 ps. The DDL is attached to fibre Links 61-62 and 78-80.

It is found that when $\tau_{set\text{-}DDL}$ is non-zero the GINTY interferogram widens, and a central and two satellite interferogram envelopes appear (Fig. 7.4 (a - b)). These envelopes maintained their shapes throughout as $\tau_{set\text{-}DDL}$ was increased, with the two satellite envelopes shifting in opposite directions by an equal amount whilst the central envelope remained fixed in position (Fig. 7.4 and Fig 7.5). 0 ps was used as the reference point when the shift of the satellite envelopes was measured. The three interferogram envelopes are visible for Link 61-62 when $\tau_{set\text{-}DDL} \geq 15$ ps, and for Link 78-80 when $\tau_{set\text{-}DDL} \geq 20$ ps. For the other settings, $\tau_{set\text{-}DDL} < 15$ ps (Link 61-62) and $\tau_{set\text{-}DDL} < 20$ ps (Link 78-80), there was a single interferogram as those in Fig. 7.3. On the other hand, the JME spectrum shifted upwards and the shape of the FO-PMD spectrum changed with its mean FO-PMD value biasing towards that of the HiFO-PMD value (Fig. 7.4 (a' and b')) as was discussed in Section 7.1.1. Fig. 7.5 shows an increase in shifts for the JME spectra and GINTY satellite envelopes as $\tau_{set\text{-}DDL}$ increases.

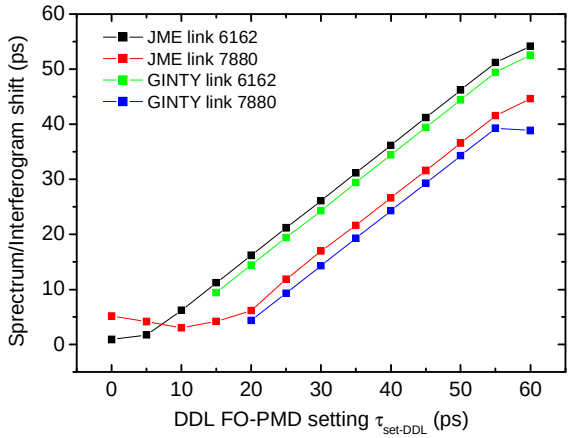

Fig. 7.5: The shifts in GINTY interferogram and JME spectrum. Refer to Fig. 7.4 to see how the shifts were obtained.

The numerous interference peaks on the central and satellite envelopes (Figures 7.4 (a) and (b)) are proof that fibre Links 61-62 and 78-80 are random mode coupled. The region with almost null intensity, indicated as K in Fig. 7.4 (a), implies the presence of a wavelength-independent FO-PMD vector. The bigger $\tau_{set\text{-}DDL}$ is, the longer the region K becomes. It should be noted that the distance from the centre of the central envelope to the centre of the satellite envelop is the mean FO-PMD of the entire link, which is similar in concept to how the FO-PMD is measured for a single PMF section (refer to Fig. 4.3 (b)). Findings in this subsection show that the nature of the GINTY inteferogram and the JME spectrum can inform one of the presence of a HiFO-PMD section along a network. However, this does not give the exact location of the HiFO-PMD section, in contrast to the P-OTDR.

7.2 Impact of a HiFO-PMD section on the output SOP

In this section, the impact of a HiFO-PMD section (in this case the DDL) on the output state of polarization (SOP) of light will be investigated. The experimental setup is similar to that in Fig. 7.1; in this case the tuneable narrow band laser source is used. The PMD measurement devices were replaced by an Adaptif A1000 polarization analayser. The buried fibre link(s) together with the DDL represented an entire fibre link as was discussed in Section 7.1. The tuneable laser was tuned from 1520 to 1570 nm in steps of 0.3 nm for each measurement DDL FO-PMD setting ($\tau_{set\text{-}DDL}$). $\tau_{set\text{-}DDL}$ was tuned from 0-60 ps. The evolution of the three SOP components (normalized Stokes parameters) as a function of wavelength was monitored using the polarization analyser. The FO-PMD of the entire fibre links were measured using the JME and GINTY techniques (Fig. 7.1).

Fig. 7.6 depicts the range of SOP spread for $\tau_{set\text{-}DDL}$ up to 60 ps. The cosine rule was used to find the relative angles between the output SOPs from one wavelength to the other, which was then used to find the range covered by the relative SOP angles. The range covered by the relative SOP angles (i.e. see figures 7.7 (a"), (b") and (c")) represents the relative SOP spread over the entire 1520-1570 nm wavelength range. The increase in FO-PMD dominancy by a fibre section through increasing $\tau_{set\text{-}DDL}$ gives rise to a reduction in the SOP spread (Fig. 7.6) and a mean FO-PMD value approximately equal to $\tau_{set\text{-}DDL}$ (Fig. 7.2 (a)).

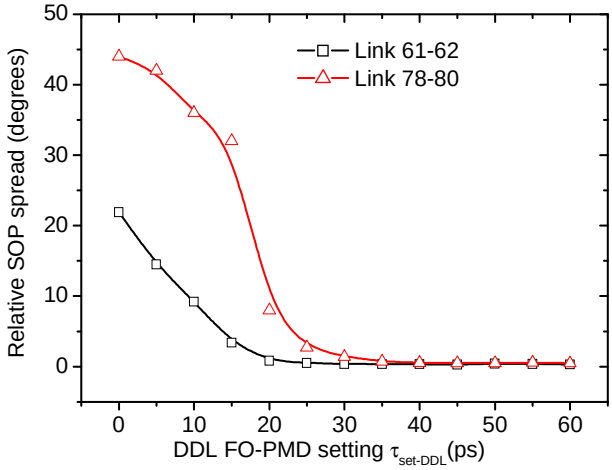

Fig. 7.6: The behaviour of the output SOP from an entire fibre link as the variable DDL is adjusted from 0 - 60 ps. The DDL is concatenated to fibre Links 61-62 (FO-PMD = 3.5 ps) and 78-80 (FO-PMD = 11.2 ps).

When $\tau_{set\text{-}DDL}$ = 0 ps, the range of SOP spread is maximum; this is evidenced by the stochastic evolution of the Stokes parameters (S_1, S_2, S_3) each spanning between -1 to 1 as shown in Fig. 7.7 (a). When these SOPs are mapped to the Poincaré sphere as in Fig. 7.7 (a'), numerous polarization states are attained. However, an increase of $\tau_{set\text{-}DDL}$ to 5 ps resulted firstly in S_1 randomly evolving between negative and positive values whilst the random evolutions of S_2 and S_3 were predominantly positive (Fig. 7.7 (b)). These resulting SOPs cover mainly in the upper hemisphere on the Poincaré sphere (Fig. 7.7 (b')). This implies that for $\tau_{set\text{-}DDL} > \tau_{link}$ (FO-PMD of Link 61-62/78-80), there is a reduction in the SOP spread until $\tau_{set\text{-}DDL} > 35$ ps, after which it remains constant at ~ 0.35^o. When these SOPs are mapped on the Poincaré sphere they cover a narrow range of closely spaced states of polarization as in Fig. 7.7 (c'), similar to that obtained for the DDL alone. The associated normalised Stokes parameters are independent of each other and wavelength, i.e. as shown in Fig. 7.7 (c) when $\tau_{set\text{-}DDL}$ = 60 ps.

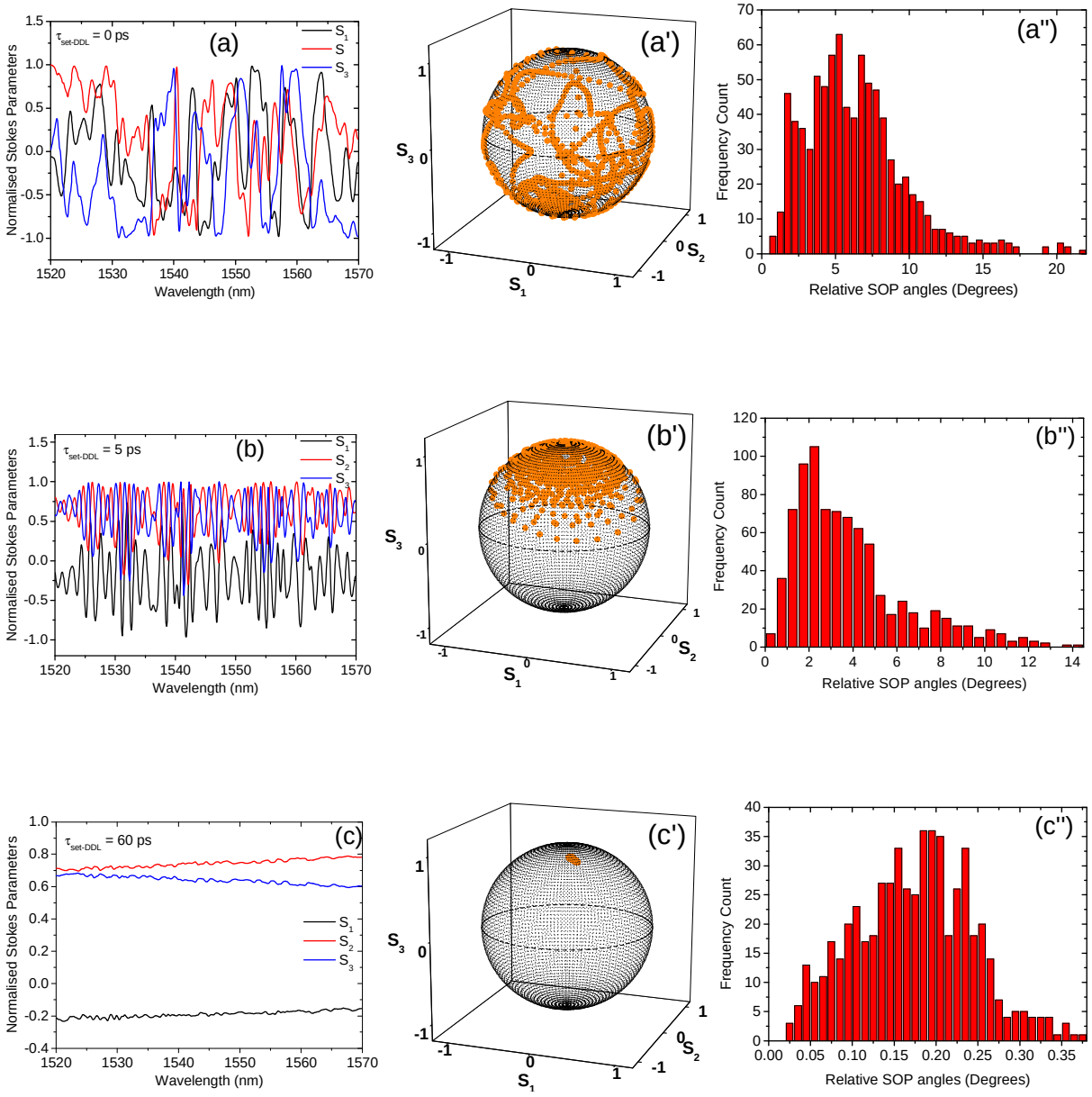

Fig. 7.7: The evolution of the output SOP as a function of wavelength when the DDL is attached to deployed fibre Link 61-62, for the DDL set at a FO-PMD value ($\tau_{set\text{-}DDL}$) equal to (a) 0 ps, (b) 5 ps and (c) 60 ps. (a'), (b') and (c') are the mapping of the SOPs on the Poincaré sphere whilst (a''), (b'') and (c'') are the histograms of the relatives angles between the output SOPs as wavelength changes.

In order to draw conclusively the impact of the HiFO-PMD section on the output SOP, the HiFO-PMD section (i.e. DDL) should be placed at different locations along the fibre network length to investigate whether the same outcomes are observed. Such verification testing will be conducted in this study through the use of PMD emulators.

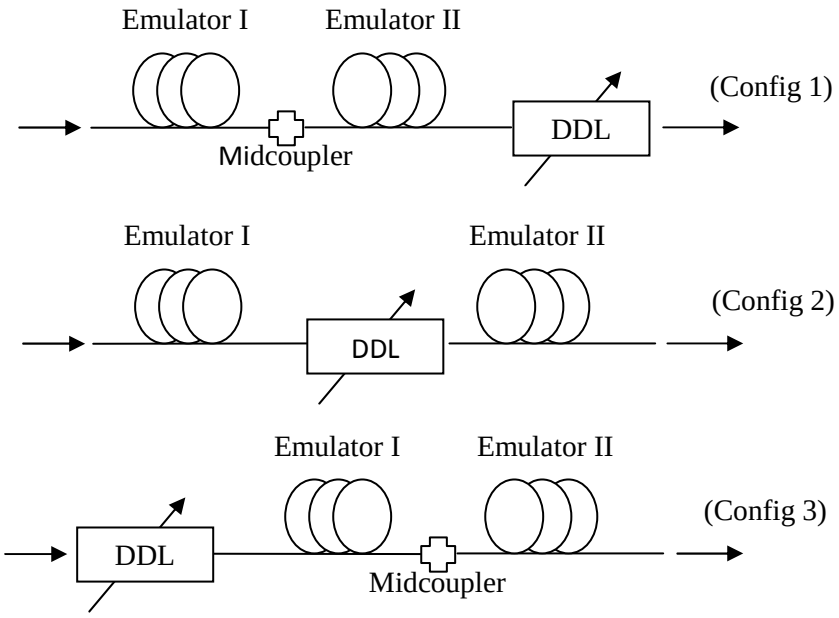

Fig. 7.8: Measurement setup for SOPs when the DDL is (Config 1) at the output of the emulators, (Config 2) in between the emulators and (Config 3) at the input of the emulators. These emulators are coupled through a midcoupler. Config stands for configuration.

Each of the emulators shown in Fig. 7.8 represent a fibre link. Emulator I (FO-PMD = 6.1 ps) and II (FO-PMD = 4.2 ps) each have ten randomly coupled PMF sections. When the two emulators are concatenated they give a mean FO-PMD of 7.1 ps. The combination of the two emulators and the DDL represent an entire fibre link. As in the previous case, the DDL represents the HiFO-PMD section; it is tuned from 0 - 60 ps in steps of 5 ps. For each configuration in Fig. 7.8, the relative SOP spread and mean FO-PMD were extracted and plotted in Fig. 7.9.

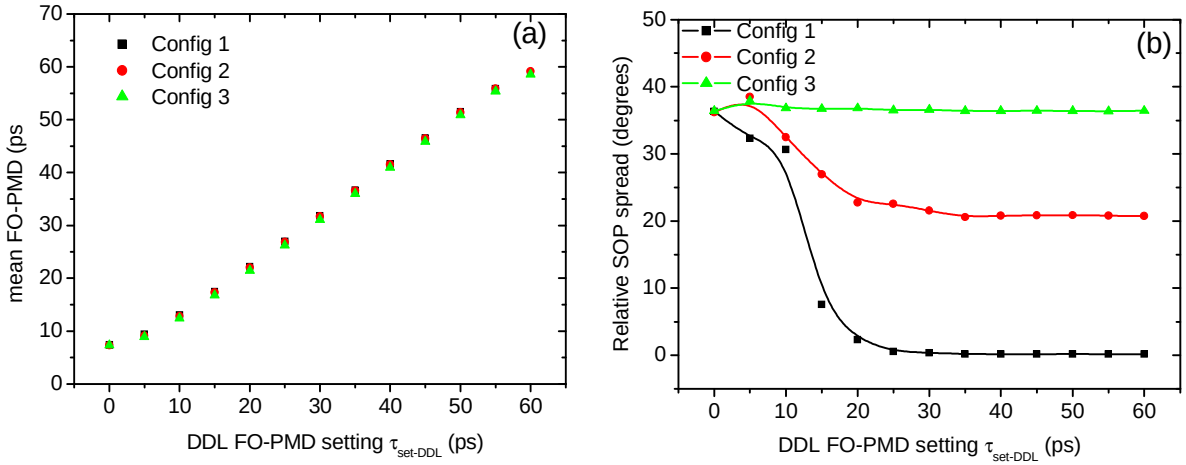

Fig. 7.9: The behaviour of (b) the output SOP spread with (a) increasing FO-PMD dominancy provided by the variable DDL. The three configurations in Fig. 7.8 were used.

With reference to figures 7.8 and 7.9 (a), $\tau_{set\text{-}DDL}$ provides a dominant FO-PMD vector thus biasing the overall FO-PMD values of the entire link towards $\tau_{set\text{-}DDL}$. This is similar to what was observed previously in Fig. 7.2 (a). In the case of Config 1, there is a reduction in SOP spread as $\tau_{set\text{-}DDL}$ increases and it become fairly constant around 0.15^{o} for $\tau_{set\text{-}DDL} \geq 35$ ps (Fig. 7.9 (b)). When the accompanying SOPs are mapped to a Poincaré sphere, they cover limited polarization states described by a spot similar to that occurring for the DDL alone. However, using Config 2 and the results in 7.9 (b), it is found that when $\tau_{set\text{-}DDL} = 0$ ps the SOP spread is similar to that provided by the two coupled emulators (36.5^{o}) but when $\tau_{set\text{-}DDL} \geq 35$ ps the SOP spread or distribution is that of Emulator II (20.7^{o}). At this stage the output SOPs at the end of the DDL populates a portion similar to that populated by Emulator II. Lastly, placing the DDL at the input of the coupled emulators (Config 3) ensures all SOPs entering the input of Emulator I are those due to the DDL. All the SOPs from the DDL output have a minute SOP spread. Thus the output SOP distribution observed at the output of the emulator shown in Fig. 7.8 (Config 3) is due to the random nature of the concatenated Emulators, I and II. The SOP spread remained around 36.5^{o} when $\tau_{set\text{-}DDL} \geq 10$ ps. Therefore, considering the region after the HiFO-PMD section as the "last mile", it means the output SOP distribution or spread is that due to the last mile. The HiFO-PMD section reduces the states of polarization (SOP) coverage or spread of the propagating light.

7.3 Impact of a HiFO-PMD section on system performance

In this section the impact of a HiFO-PMD on the bit error rate (BER) is investigated. Huttner *et al.* (2000) refers to the BER as the most important parameter characterising network

performance. The reader is referred to Section 2.1.7 Id for more information on the BER. The Virtual Photonics Inc. (VPI) simulation software (Version 8) was used in showing the impact the HiFO-PMD has on propagating signals from a 10 Gb/s non-return-to-zero (NRZ) light source using the eye diagram and BER tester. The eye diagram is a superposition of pseudo-random patterns of zeros and ones of the transmitted bits. The simulation setup is shown is Fig. 7.10. The PMD emulator is controller by Emulator I, polarization controller and Emulator II. Emulator I is a FO- and SO-PMD emulator in which the PMD values are specified by choosing the emulator length, FO- and SO-PMD values. The polarization controller is controlled to adjust the coupling angle β between 0^o and 180^o. Emulator II is a delay block that is controlled to induce a certain amount of delay between the two propagating orthogonal modes of light, similar in behaviour to the DDL. The delay block like the DDL in Sections 7.1 and 7.2 represents the HiFO-PMD section. In this section, three cases on the effect of the HiFO-PMD section will be presented.

Case I: The HiFO-PMD section biases the mean FO-PMD of the link towards its fixed FO-PMD value and changes the SO-PMD.

Case II: The HiFO-PMD section biases the mean FO-PMD of the link towards its varying FO-PMD whilst SO-PMD remains constant.

Case III: The HiFO-PMD section biases the overall FO-PMD of the link towards its varying FO-PMD resulting in SO-PMD changing.

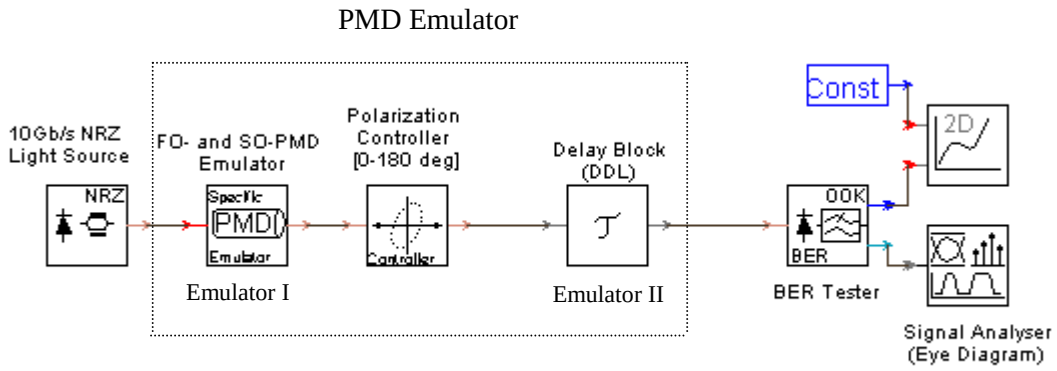

Fig. 7.10: Schematic layout used to investigate the impact the HiFO-PMD section has on system performance. Emulator II (similar to a digital delay line (DDL)) represents the HiFO-PMD on the network. Emulator I, polarization controller and Emulator II mimic an optical fibre network system.

In Case I, the FO-PMD of the emulator was fixed at 30 ps by Emulator II (representing the HiFO-PMD section) the dominant FO-PMD contributor. The PC was set at a fixed angle equal to 45^{o} as the SO-PMD on Emulator I was tuned. Emualtor I was set to give a FO-PMD equal to 5 ps. The behaviour of the PMD emulator under these configurations is similar to that of the emulator presented in Section 6.1.3. Results in Fig. 7.11 (a) show that the BER increases from 2.57×10^{-12} to 4.10×10^{-2} as the SO-PMD on Emulator I adjusted from 2 to 60 ps^2. This is supported by a reduction in the area of the eye opening of the eye diagram in Fig. 7.11 (a' - a").

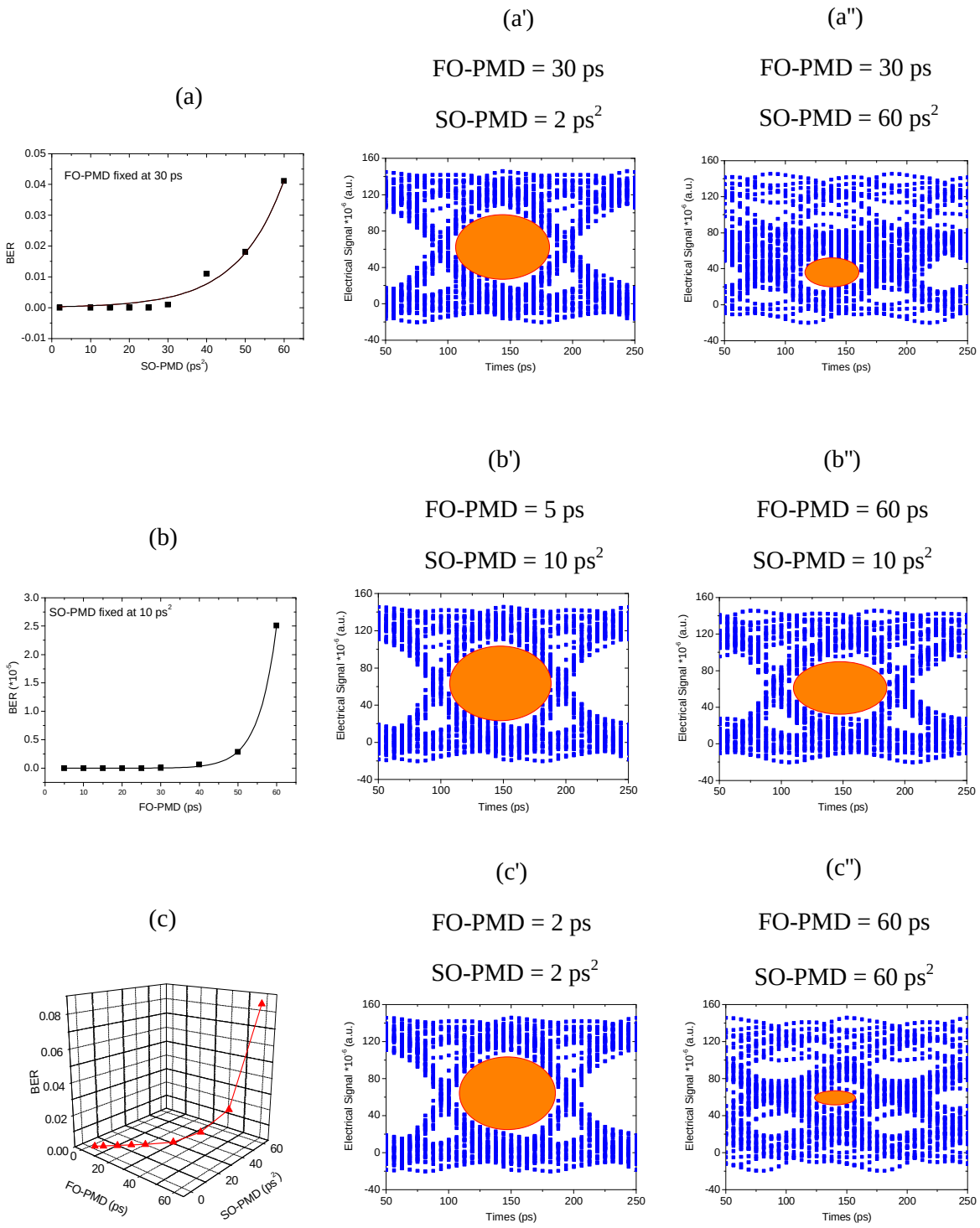

Fig. 7.11: (a) The variation of the BER when (a) FO-PMD is fixed at 30 ps and SO-PMD is varying (PC angle = 45^o), (b) SO-PMD is fixed at 10 ps^2 and FO-PMD is varying (β = 0^o), and (c) both FO- and SO-PMD are varying (β = 45^o). β is the angle between the HiFO-PMD vector $\vec{\tau}_{\text{HiFO-PMD}}$ and FO-PMD vector of the entire link $\vec{\tau}_{\text{mean}}$. The orange ellipses show the regions of the eye diagrams which are open.

Case II involved keeping the SO-PMD fixed at 10 ps^2 and varying FO-PMD. This was achieved by making the FO-PMD vector $\vec{\tau}_{\text{HiFO-PMD}}$ of Emulator II (HiFOPMD section) the dominant FO-PMD contributor and controlling the PC to ensure the FO-PMD vector of the entire fibre link $\vec{\tau}_{\text{mean}}$ and $\vec{\tau}_{\text{HiFO-PMD}}$ were always parallel (the coupling angle β between the two vectors was 0^o). Emulator I was kept set to give a FO-PMD equal to 5 ps. The method used to determine the coupling angles between two vectors is highlighted in Section 6.3. The network system in Fig. 7.10 under these configurations behaved like the emulator presented in Section 6.4. Fig. 7.11 (b) shows that as the FO-PMD increases from 5 to 60 ps, the BER increases from 2.4 x 10^{-12} to 2.5 x 10^{-5}. This is evidenced by an eye closer from Fig. 7.11 (b') to (b''). However, the eye in Fig. 7.11 (b'') is less closed than that in Fig. 7.11 (a''). This shows that SO-PMD has more profound effect on the propagating NRZ signals compared to FO-PMD. The emulator design in Section 6.1.3 showed that SO-PMD causes fluctuations around the mean penalty of FO-PMD.

In Case III, both FO-PMD and SO-PMD were increased simultaneously by adjusting Emulator I and Emulator II in Fig. 7.10. The PC angle was adjusted to ensure β was equal to 45^o. Results in Fig. 7.11 (c) show an increase in BER from 2.6 x 10^{-12} to 8.5 x 10^{-2}. The maximum BER was above that experienced in Case I (see Fig. 7.11 (a)). This means that although SO-PMD has a profound effect on the propagating NRZ signals compared to FO-PMD, its effects are less than those when both FO- and SO-PMD are simultaneously changing. With reference to Fig. 7.10, removal of the HiFO-PMD section (Emulator II) reduced the BER to only the BER due to Emulator I, indicating that the removal of the HiFO-PMD section not only results in FO-PMD reduction but also SO-PMD which was found to cause more severe system impairments.

In summary, the presence of a HiFO-PMD section biases the mean FO-PMD of the entire fibre link to its mean FO-PMD. The acompanying mean SO-PMD of the entire fibre link can either remain fixed (when $\beta = 0^o$ or 180^o) or increase (when $\beta \neq 0^o$ or 180^o). In the case were SO-PMD is introduced, the BER increases. A HiFO-PMD section results in reduction in the output SOP spread. The reduction in output SOP spread solely depends on the amount of FO-PMD the HiFO-PMD section has and the region after the HiFO-PMD section “last mile”.

CHAPTER 8

CONCLUSIONS

The purpose of this thesis was to bring about an understanding of the complex nature and effects of PMD to the telecommunication industry and research groups through characterising the PMD of deployed fibres, designing and implementing PMD emulators under a stable laboratory environment and investigating the impact of high FO-PMD (HiFO-PMD) in optical network systems.

8.1 Deployed fibre characterisation

PMD field measurements on deployed buried fibres showed that the PMD variation over the 1520 to 1570 nm wavelength was stochastic. The PMD variation over the 98-hour period for each wavelength was directional and limited; they are due to the presence of random mode coupling along the fibre length and limited influence from extrinsic perturbations over time respectively. PMD variation in the wavelength domain showed that the mean FO-PMD value is independent of whether the FO-PMD statistics of a fibre link approaches the Maxwellian theoretical distribution; the key factor is sufficient random mode coupling. The accompanying SO-PMD statistics, with FO-PMD statistics approaching Maxwellian, followed the PDF given by Foschini *et al.* (1999). The FO- and SO-PMD statistics at a given wavelength gave non-stochastic PMD distributions with time.

FO-PMD and SOP measurements with time on aerial fibres were more stochastic in nature compared to those of buried fibres. These FO-PMD and SOP changes were due to the aerial fibres being directly exposed to varying extrinsic perturbation changes as opposed to buried fibres that are secured in ducts, with significantly more FO-PMD and SOP changes experienced during the day than night. It was evidenced by a faster decorrelation time over the aerial fibre (in this case 107 s) compared to a buried fibre which decorrelates over a longer time span. The FO-PMD statistics for the aerial fibre over the 14 day period approached the Gaussian distribution and those of the SOPs over 30 minutes were skewed to low rates of SOP change. PMD characteristics and SOP variations experienced in deployed fibres can be better understood through PMD emulation.

8.2 PMD emulators

8.2.1 Emulator with an increase in both FO- and SO-PMD

This emulator shows that increased random mode coupling and PMF sections, in this case 30 PMF sections, give FO-PMD statistics approaching the Maxwellian distribution and SO-PMD statistics approaching the theoretical distribution proposed by Foschini *et al.* (1999). This is only valid when the length of each of the PMF segments lies within 20% standard deviation of the mean emulator length. Quantification of the FO-PMD statistics of the emulator using the frequency ACF showed that the BACF decreases towards zero with increasing numbers of randomly coupled PMF sections. The amount of BACF informs the designer of the number of birefringent sections and their distribution. The RMS FO-PMD of the emulator increased as PMF sections were added but fell short of the direct summation of the FO-PMD contributions from the individual PMF sections due to FO-PMD vector cancellation. The corresponding SO-PMD increase was mainly due to mode coupling increase which promoted PSP and DGD variation with wavelength.

8.2.2 Emulator with inverse trend in FO- and SO-PMD

This emulator confirmed that the magnitude of the mean FO-PMD is independent of whether its FO-PMD statistics approaches Maxwellian or not. It was shown that FO-PMD is not always proportional to SO-PMD but can be inversely proportional in behaviour. The increase in both the number of PMFs and mode coupling increased the range of the PMD statistics. Results also show that the BACF decreased with increasing number of PMF sections from 1 to 31 although the emulator length was fixed at 22 metres. This means the BACF is independent of the mean FO-PMD but depends on the properties of the emulator or fibre link.

8.2.3 Emulator with fixed FO-PMD but varying SO-PMD

This emulator was designed using only a combination of PMFs and a polarization controller. Thus the emulator design is cost effective compared to other emulators of similar characteristics. The RMS FO-PMD remained fixed at around 31 ps due to the HiFO-PMD section providing a dominant wavelength-independent FO-PMD vector compared to the FO-PMD contribution from the sub-emulator. The novelty of this emulator is that it tunes the PMD statistics both horizontally (FO- and SO-PMD changes with wavelength) and vertically (the FO- and SO-PMD range). This emulator showed that irregular fluctuations that occur around the RMS FO-PMD penalty are enhanced by SO-PMD. SO-PMD can be adjusted by

either changing mode coupling angles or, not completely in real time, by altering the number of mode coupling sites.

8.2.4 Tuneable delay element

The FO-PMD of the digital delay line (DDL) is wavelength-independent and so is its FO-PMD vector. The residual SO-PMD of the DDL is very small though it is uneven in the region ≤ 18 ps, this is likely due to manufacturing imperfections. The DDL was controlled to generating stochastic FO-PMD statistics that approach the Maxwellian distribution. Concatenating several of these types of DDL will make the FO-PMD wavelength-dependent and will result in SO-PMD.

8.2.5 Emulator with fixed birefringent sections and rotatable polarization orientations

This emulator was successfully built using eight randomly distributed PMF sections interconnected via seven half waveplates (HWPs) which rotate from 0 to 180^{o}. Random adjustments of the seven HWPs gave different PMD statistics in the wavelength domain, making the PMD emulator tuneable. The emulator was found to be fairly stable under the laboratory environment, enabling it to be repeatable. Configuring the same HWPs setting on three different days gave close PMD statistics and similar probability density function (pdf) fits. This shows that the emulator can reproduce PMD statistics. Random variations of the HWPs over a large sample size gave a stochastic FO-PMD variation which approached the Gaussian distribution just as the characterised aerial fibre in this study. The output SOPs of the emulator with time covered different polarization states as the HWPs were randomly changed. The polarization states covered had at least DOP > 0.9 since a highly polarized narrow band light source was used. The SOP decorrelation time of the emulator is 126 s; this decorrelation time can be reduced or increased depending on the degree of random SOP changes introduced by the HWPs.

8.2.6 Emulator with fixed SO-PMD and varying FO-PMD

The principle of operation of this emulator is based on mode coupling ($\beta = 0^{o}$ for all wavelengths, random sub-emulator coupling angles), birefringence distribution and the presence of a dominant wavelength-independent $\vec{\tau}$ provided by the DDL. This FO-PMD vector ($\vec{\tau}$) is greater than the total sub-emulator $\vec{\tau}$ thus making it the main contributor to the emulator-‹τ›. SO-PMD can be adjusted by controlling the FO-PMD, either by ensuring the FO-PMD becomes wavelength-dependent or by changing the range of wavelength-dependent

FO-PMD spectrum. This arises from either an increase or decrease in the number of mode coupling sites or mode coupling angle variations (i.e. $\beta \neq 0^o$ or 180^o).

8.3 The impact of PDL in PMD emulators

PDL is found to distort PMD statistics away from theoretical distributions even in the presence of large random mode coupling. This is due to the loss of orthogonality between the two principal states of polarization (PSP) and the abrupt changes in the PSPs with wavelength. It was shown that having a large loop diameter ($\geq$ 13.5 cm) and good fusion splices, each with a loss less than 0.01 dB, ensures a PMD emulator has negligible PDL.

8.4 The impact of a HiFO-PMD section in optical network systems

This work shows that in the presence of a HiFO-PMD section, the mean FO-PMD of the entire link is biased towards the FO-PMD provided by the HiFO-PMD section and SO-PMD can either increase ($\beta \neq 0^o$ or 180^o) or remain constant ($\beta = 0^o$ or 180^o) depending on the coupling angle β between the HiFO-PMD section and the rest of the fibre link. This is in agreement with the concatenation equations. Investigations show that SO-PMD introduces higher bit error rate (BER) compared to FO-PMD, with simultaneous changes in FO- and SO-PMD causing higher BER compared to any of the two (FO- and SO-PMD) in isolation. Removal of the HiFO-PMD section reduces the BER due to reduction in both the FO-PMD and SO-PMD. Besides a HiFO-PMD section affecting the mean PMD values, the emulator in Section 6.1.3 showed that the HiFO-PMD PMF section shifts the FO-PMD statistics of the sub-emulator to approach unpredictable statistical distributions instead of the anticipated predictable Maxwellian distribution, even in the presence of high random mode coupling. The accompanying SO-PMD statistics still followed the theoretical distribution due to its strong dependence on the PSP-depolarization, which is mode coupling dependent. The emulator (Section 6.1.3) showed that the presence of a HiFO-PMD section on a deployed fibre link results in higher likelihood of high FO-PMD values occurring, with higher possibilities of system impairments.

The relative SOP spread reduced with an increase in the FO-PMD on the HiFO-PMD section to a constant minimum value. At this stage there is small polarization state coverage and all the three normalised Stokes parameters become wavelength-independent. The application of PMD emulators in this investigation showed that the relative SOP spread depends on the position of the HiFO-PMD section along the fibre link and its associated FO-PMD magnitude.

Therefore, considering the region after the HiFO-PMD section as the “last mile”, it means the output SOP distribution or spread is that due to mode coupling contributions from the “last mile”. In this study it happened when HiFO-PMD $\geq$ 35 ps.

An analysis into GINTY and JME PMD measurement methods showed that as the amount of FO-PMD in the HiFO-PMD section increases, a central interferogram envelope and two symmetric satellite interferogram envelopes develop in a GINTY scan. Further increases in the FO-PMD of the HiFO-PMD section resulted in the satellite envelopes drifting in opposite directions by an equal amount whilst the central interferogram envelope remained fixed in position. The JME spectrum shifted upwards with changes in the FO-PMD statistics as the FO-PMD of the HiFO-PMD section was increased. This therefore means an observation of the GINTY interferogram and JME spectrum can indicate the presence of a HiFO-PMD section.

In summary, the findings of this thesis show that the PMD phenomenon that occurs in deployed fibres is better explained through PMD emulation. The presence of PDL distorts the PMD statistics of PMD emulators. A HiFO-PMD section in an optical network system does not only result in high FO-PMD but also introduces SO-PMD when $\beta \neq 0^o$ or 180^o. SO-PMD has more profound signal degradation effects compared to FO-PMD. However, the HiFO-PMD section only affects the FO-PMD statistics and not the SO-PMD statistical distribution.

APPENDIX I

POINCARÉ SPHERE AND STOKES PARAMETERS

This appendix will focus on the Poincaré sphere and Stokes parameters. Light is an electromagnetic (EM) wave with time varying electric and magnetic fields that are perpendicularly aligned. The polarization of an EM wave, considering the electric field, describes the behaviour of the electric field vector as light propagates through the fibre. The magnitude and orientation of the electric field vector is referred to as the state of polarization (SOP) of light. Light can either be elliptically, linearly or circularly polarized. The SOP is represented best using the Stokes parameters and easily mapped on a Poincaré sphere. Information presented in this appendix has been obtained from Derickson (1998) and Rochford (2004).

In 1852, G. G. Stokes introduced a Stokes vector to represent the polarization states of a beam of light. The four components of the Stokes vector (Eq. A1.1) were driven from the optical power at different polarization settings. The Stokes parameters are given by:

$$\begin{bmatrix} s_0 \\ s_1 \\ s_2 \\ s_3 \end{bmatrix} = \begin{bmatrix} E_{0x}^2 + E_{0y}^2 \\ E_{0x}^2 - E_{0y}^2 \\ 2E_{0x}E_{oy}\cos\delta \\ 2E_{0x}E_{oy}\sin\delta \end{bmatrix} = \begin{bmatrix} P_{total} \\ P_{LH} - P_{LV} \\ P_{L+45^o} - P_{L-45^o} \\ P_{RC} - P_{LC} \end{bmatrix} \qquad \text{(A1.1)}$$

where P_{LH}, P_{LV}, P_{L+45^o}, P_{L-45^o}, P_{RC} and P_{LC} denotes the power through the polarizers in linear horizontal, linear vertical, linear $+45^o$, linear -45^o, right circular and left circular orientations, respectively. δ is the phase difference.

The relationship governing Stokes parameters is:

$$s_0^2 = s_1^2 + s_2^2 + s_3^2 \qquad \text{(A1.2)}$$

and hence only three Stokes parameters (s_1, s_2 and s_3) are independent. The amount of optical power contained in the polarized part of light is:

$$P_{polarized} = \sqrt{s_1^2 + s_2^2 + s_3^2} \qquad \text{(A1.3)}$$

Normalised Stokes parameters are:

$$S_1 = \frac{s_1}{s_0},\ S_2 = \frac{s_2}{s_0},\ S_3 = \frac{s_3}{s_0} \qquad \text{(A1.4)}$$

The above (Eq. A1.4) form coordinates of a point which lies on the Poincaré sphere and ranged from -1 to +1 (Fig. A1.1). The Poincaré sphere is a graphical tool or display device for instrumentation, convenient three dimensional (3D) aid for representing different polarization states. This sphere visualises different SOPs. Any SOP is uniquely represented by a point on or within a unit sphere centred on a rectangular xyz-coordinate system. That is any fully polarized state on the surface of the sphere can be found using Cartesian coordinates. Partially polarized states map to a point within the sphere and unpolarized light is represented by the origin.

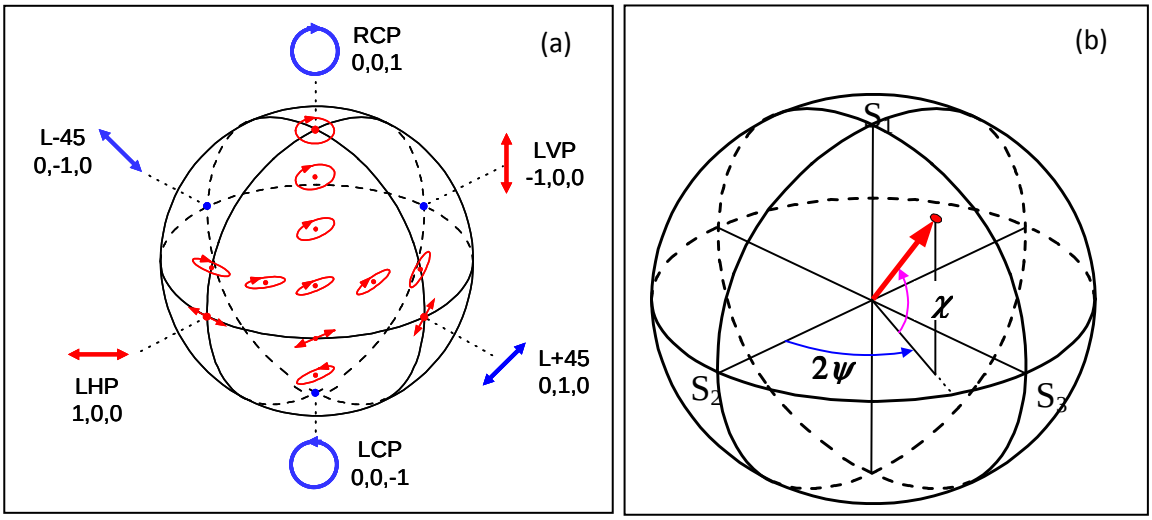

Fig. A1.1: (a) Poincaré sphere representing various SOPs of polarized light. (b) Stokes parameters shown on the Poincaré sphere. RCP and LCP stand for right and left circular polarization respectively, LHP and LVP stand for linear horizontal and vertical polarization respectively whilst L+45 and L-45 stand for linear polarization at +45^o and -45^o.

Each of the ellipse on the Poincaré sphere yields a set of unique Stokes parameters, refer to Fig. A1.1 (b):

$$S_1 = S_0 \cos 2\chi \cos 2\psi \quad \text{(A1.5a)}$$

$$S_2 = S_0 \cos 2\chi \sin 2\psi \quad \text{(A1.5b)}$$

$$S_3 = S_0 \sin 2\chi \quad \text{(A1.5c)}$$

where ψ specifies the orientation of the ellipse and χ is the ellipticity.

The distance of a point from the centre of the Poincaré sphere, is the degree of polarization (DOP). The DOP can be expressed in terms of Stokes parameters:

$$\text{DOP} = \frac{\sqrt{s_1^2 + s_2^2 + s_3^2}}{s_0} = \sqrt{S_1^{\,2} + S_2^{\,2} + S_3^{\,2}} \quad \text{(A1.6)}$$

Considering the source to be a Gaussian spectrum, the lowest DOP which results from differential group delay $(\Delta\tau)$ is expressed as:

$$\text{DOP} = \exp -1/4 \ln 2 \left(\frac{\pi c \Delta\tau \Delta\lambda^2}{\lambda^2} \right) \quad \text{(A1.7)}$$

where c is speed of light, λ is the wavelength and $\Delta\lambda$ is the full width-half maximum (FWHM) of the light source. The DOP for non polarized (natural) light in zero (DOP = 0), totally polarized light has a DOP = 1 and partially polarized light (real optic beams) has a DOP lying in the range 0 < DOP < 1. Partially polarized light is due to the superposition of non-polarized and totally polarized light.

APPENDIX II

POLARIZATION-OPTICAL TIME DOMAIN REFLECTOMETRY METHOD

This is a time domain PMD measurement technique that measures FO-PMD with distance, covering the entire optical fibre length. The NMMU Fibre Optic Unit found out that not all fibre segments contribute equally to the overall FO-PMD measured after tests on South African Telkom optical fibre networks (Sibaya 2004, Conibear *et al.* 2005). This had also been observed by Huttner *et al.* (1999), Rogers (1981), and Galtarossa and Palmieri (2004 and 2004b) on other fibre networks. Although the polarization-optical time domain reflectormetry (P-OTDR) technique is not used in this study, an understanding of this technique and how it works provides one an insight of how the exact location of the high birefringent (HiBi) section(s) is qualitatively determined. Parts of Chapter 7 show how the presence of HiBi (or HiFO-PMD) sections can be detected through the use of GINTY and the JME, although this could not determine were the HiFO-PMD section is situated along the fibre link length.

The unequal contributions of birefringence along the fibre length meant that HiFO-PMD fibre sections contributed much to the FO-PMD value of that link. Therefore, in order to measure the amount of birefringence (or FO-PMD) for each fibre segment the P-OTDR was designed. The well known non-destructive events locator, optical time domain reflectometry (OTDR) was consequently modified to give the polarization-OTDR (P-OTDR), which was pioneered in 1981 by Rogers (Rogers 1981) and was intended for measurements in a weak mode coupling regime. In 1998, Corsi *et al.* extended the theory of the P-OTDR into the strong mode coupling regime. Huttner *et al.* (1998) also developed a polarization-dependent optical frequency domain reflectometry (P-OTFR) which has a higher resolution than the P-OTDR, but works over shorter distances. The qualitative P-OTDR is commercially available (EXFO P-OTDR 1100), while a quantitative P-OTDR (FTB5700) which measures the cumulative PMD with distance is currently under test in optical networks around the world (Roberge 2009).

The P-OTDR involves measuring the spatial distribution of the FO-PMD; this consists of measuring the spatial distribution of both the beat and coupling lengths. The P-OTDR technique is based on the Rayleigh backscattered light signals to infer the FO-PMD. In actual sense the P-OTDR measures the evolution of the backscattered-field polarization state

(Galtarossa and Palmieri 2004). The longitudinal evolution of the backward-travelling polarization state $\vec{s}_B(z)$ at location z obeys a precession rule about the round-trip birefringence vector $\vec{\beta}(z)$ such that (Corsi *et al*. 1998):

$$\frac{\partial \vec{s}_B}{\partial z} = \vec{\beta}(z) \times \vec{s}_B(z) \qquad \text{(A2.1)}$$

This equation is similar to Eq. 2.13 (a). The analysis by Corsi *et al.* (1998) was only able to deduce the fibre beat length through the use of a small pulse width. Wuilpart *et al.* (2007) provided a new analysis of the Rayleigh backscattered signals based on a level-crossing rate analysis. This analysis enabled the quantification of the spatial distribution of the beat length, the coupling length and FO-PMD along an optical link using large 500 ns pulses in order to improve measurement dynamics. The P-OTDR measurement setup is shown below (Fig A2.1).

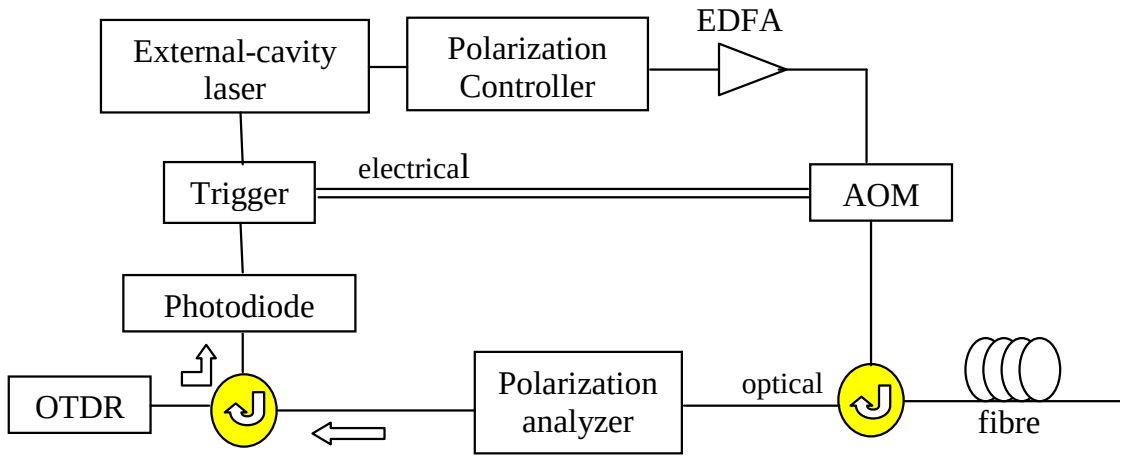

Fig. A2.1: The P-OTDR setup (after Galtarossa et al. 2000).

Fig. A2.1 shows a P-OTDR proposed by Galtarossa *et al.* (2000). The commercial OTDR output is detected by the photodiode and triggers the external-cavity short-pulse laser. To ensure the laser pulse is highly polarized the pulse goes past a polarization controller. The pulse is then amplified using the EDFA and launched into the fibre under investigation. The acoustic-optic modulator (AOM) transmits the pulse and blocks the amplified spontaneous emission (ASE) noise outside of the pulse time slot. The pulse is then analysed by a polarization analyser and returned to the OTDR for further analysis.

APPENDIX III

SPECIFICATIONS OF COMPONENTS USED IN EXPERIMENTAL WORK

Components	Specifications
Half Waveplate (HWP)	Response time: < 10 ms Insertion loss: 0.43 dB(1) PDL: 0.03 dB(1) Powered by: 0 to 4 V only
Polarization controller/scrambler (Adaptif A3200)	SOP switching time: < 10 µs PDL: < 3 dB(2) FO-PMD: < 0.1 ps(2)
Polarization analyser (Adaptif A1000)	Wavelength range: 1460-1620 nm Sampling rate < 1kHz
Digital delay line (DDL)	FO-PMD range: -65 ps to 65 ps Insertion loss: < 1.5 dB(1)
PCM430 board	Powered by: 5 V Inputs/outputs: 4
PDL emulator	Wavelength range: 1510 to 1590 nm PDL dynamic range: 0.05dB to 5 dB(1) Insertion loss: < 0.6 dB(1) Optical return loss: > 50 dB(1)
1x2 50:50 Beam splitter or 2x1 Coupler	Insertion loss: 3.153 dB PDL: 0.13 dB(1)

(1)At 1550 nm

(2)For the wavelength range 1520-1580 nm

APPENDIX IV

RESEARCH OUTPUTS OF THE AUTHOR

2009

Vitalis Musara, Lorinda Wu and Andrew W. R. Leitch, "*Patent: Polarization Mode Dispersion Emulator Apparatus*," World Intellectual Property Organization, Pub. No. WO/2010/026541, Publication Date 11 March 2010.

Vitalis Musara '*Fibre Optics Technology*,' Department of Science and Technology 2009 Awards, Cape Town, South Africa, 21-22 October 2009. (Certificate of Achievement: Finalist in the THRIP Best Black or Female Science Student 2009 category.)

Vitalis Musara, Lorinda Wu and Andrew W. R. Leitch *'A polarization mode dispersion emulator with tuneable first-order PMD and constant second-order PMD,'* Optics Communications **282**, pp. 3270–3274, May 2009.

Vitalis Musara, Lorinda Wu, Gaoboelwe Pelaelo and Andrew W. R. Leitch '*PMD emulation using polarization maintaining fibres: Fixed root-mean-square DGD but varying second-order PMD*,' Review of Scientific Instrument **80**, pp. 1-5, May 2009.

Vitalis Musara, Selma Younsi, Lorinda Wu, Mourad Zghal and Andrew W. R. Leitch, '*Statistical characterization of combined first and second-order polarization mode dispersion in a deployed fibre cable*', Proc. of IEEE AFRICON (*IEEE Xplore Release*), Kenya, pp. 1-6, 23-25 September 2009.

Vitalis Musara, Winston T. Ireeta, Lorinda Wu and Andrew W. R. Leitch, "*Detecting the dominance of PMD from a fibre segment on a fibre network system through state of polarization monitoring*," Proc. of Southern African Telecommunication Network and Application Conference (SATNAC), Swaziland, 30 August-2 September 2009.

2008

Gibion Makiwa, Vitalis Musara, Lorinda Wu and Andrew W. R. Leitch, '*Polarization mode dispersion and polarization dependent loss in single-mode optical fibre systems*,' Poster presentation at the African Laser Centre (ALC) Kariega conference, Eastern Cape, South Africa, 7-9 May 2008.

Vitalis Musara, Gaoboelwe Pelaelo, Lorinda Wu and Andrew W. R. Leitch, '*The impact of a high birefringence fibre Section in an optical network system through emulation*,' Proc. of

Southern African Telecommunication Network and Application Conference (SATNAC), Cape Coast, South Africa, 7-10 September 2008.

Gaoboelwe Pelaelo, Lorinda Wu, Vitalis Musara and Andrew W. R. Leitch, '*Impact of polarization dependent loss in the presence of polarization mode dispersion on the optical network,*' Proc. of Southern African Telecommunication Network and Application Conference (SATNAC), Cape Coast, South Africa, 7-10 September 2008.

Vitalis Musara, Lorinda Wu, Andrew W. R. Leitch, '*A fixed differential group delay but varying second-order polarization mode dispersion emulator,*' Proc. of 3rd International Conference on Broadband Communication, Information Technology & Biomedical Applications (appearing in *IEEE Xplore Release 2.5*), Pretoria, South Africa, pp. 468-472, 23-26 November 2008.

2007

Vitalis Musara, Selma Younsi, Mourad Zghal and Andrew W. R. Leitch, '*An investigation into optimum design conditions of a second-order polarization mode dispersion emulator,*' Poster presentation at the 52nd South African Institute of Physics (SAIP) conference, Johannesburg, South Africa, 3-7 July 2007.

Gaoboelwe Pelaelo, Lorinda Wu, Vitalis Musara and Andrew W. R. Leitch, '*Characterization of polarization dependent loss in optical fibres in the presence of polarization mode dispersion,*' Oral presentation at the 52nd South African Institute of Physics (SAIP) conference, Johannesburg, South Africa, 3-7 July 2007.

Selma Younsi, Vitalis Musara, Tim B. Gibbon, Lorinda Wu, Mourad Zghal, Andrew W. R. Leitch, '*Frequency Domain Characterization of an experimental and simulated polarization mode dispersion emulator design,*' Proc. of Southern African Telecommunication Network and Application Conference (SATNAC)**,** Mauritius, 8-13 September 2007.

2006

Lorinda Wu, Vitalis Musara, M. Comfort and Andrew Leitch, "*Making reliable PMD measurements: The importance of polarization scrambling,*" Proc. of Southern African Telecommunication Network and Application Conference (SATNAC), Cape Town, South Africa, 3-6 September 2006.

Vitalis Musara, Maphuti C. Mankga, Lorinda Wu, M. Mathuthu and Andrew W. R. Leitch, "*An investigation of scrambling effects on buried optical cables,*" Poster presentation at the 51th South African Institute of Physics (SAIP) Conference, Cape Town, South Africa, 3-7 July 2006.

REFERENCES

A

Adaptif Photonics, "*User Guide*," Adaptif Photonics GmbH **Rev. 1.3**, (2004).

Alexandra P. and W. Thomas, "*On the potential of Faraday anomalous optical filter as high resolution edge filters*," Laser Phys. **15**, pp. 55-60 (2007).

Allen C. T., P. K. Kondamuri, D. L. Richards and D. C. Hague, "*Measured temporal and spectral PMD characteristics and their implications for network-level mitigation approaches*,"J. Lightwave Technol. **21**, pp. 79-86 (2003).

Andresciani D., F. Curti, F. Matera and B. Diano, "*Measurement of the group-delay difference between the principal staes of polarization on a low-birefringence terrestrial fiber cable*," Opt. Lett. **12**, pp. 844-846 (1987).

Antonelli C., C. Colamarino, A. Mecozzi and M. Brodsky, "*A Model for Temporal Evolution of PMD*," IEEE Photon. Technol. Lett. **20**, pp. 1012-1014 (2008).

Antonelli C., A. Mecozzi, "*Theoretical chracteristics and system impact of the Hinge model of PMD*," J. Lightwave Technol. **24**, pp. 4064-4074 (2006)

B

Barlow A. J., J. J. Ramskov-Hansen, and D. N. Payne, "*Birefringence and polarization mode-dispersion in spun single-mode fibers*," Appl. Opt. **20**, pp. 2962-2968 (1981).

Bogoni A., A. Orlandini and L. Poti, "*A deterministic emulator for the statistical reproduction of a real fiber with accurate PMD statistics up to the third order*," IEEE Photon. Technol. Lett. **14**, pp. 1085-1087 (2002).

Boston Applied Technologies, "*Acrobat^{TM} Polarization Rotator: Model PRM00111 Description and User Instructions*,' Boston Applied Technology Inc. (BATi), (2008).

Brinkmeyer E., "*PMD compensation*," Proc. of European Conf. Optical Communication (ECOC), paper.9.3.1 (2002).

Brodsky M., P. Magill and N. J. Frigo, "*Polarization-mode dispersion in installed recent vintage fiber as a parametric function of temperature*," IEEE Photon. Technol. Lett. **16**, pp. 209-211 (2004).

Bruyère F. and O. Audouin, "*Penalties in long-haul optical amplifier systems due to polarization dependent loss and gain*," IEEE Photon. Technol. Lett. **6**, pp. 654-656 (1994).

Bülow H., "*System outage probability due to first- and second-order PMD on the presence of chromatic dispersion*," Proc. of European Conf. Optical Communication (ECOC), paper WdC5 (1998).

C

Cameron J., B. Diano, G. De Marchis and F. Matera, "*Time evolution of polarization mode dispersion in optical fibers*," IEEE Photon. Technol Lett. **10**, pp 1265-1267 (1998).

Chen L., Z. Zhang and X. Bao, "*Polarization dependent loss vector measurement in a system with polarization mode dispersion*," Opt. Fiber Technol. **12**, pp. 251-254 (2005).

Chou P. O., J. M. Fini and H. A. Haus, "*Real-time principal states characterization for use in PMD compensators*," IEEE Photon. Technol. Lett. **13**, pp. 568-570 (2001).

Conibear A. B., A. W. R. Leitch, N. A. Sibaya, T. B. Gibbon and L. Viljoen, "*Study of polarization mode dispersion in a South African optical fibre network*," S. Afr. J. Sci. **101**, pp. 275-277 (2005).

Corsi F., A. Galtarossa and L. Palmeiri, "*Polarization mode dispersion characterization of single-mode optical fiber using backscattering technique*," J. lightwave Technol. **16**, pp. 1832-1843 (1998).

Curti F.,B. Daino, G. D. Marchis and F. Matera, "*Statistical treatment of the evolution of the principal states of polarization in single-mode fibers*," J. Lightwave Technol. **8**, pp. 1162-1166 (1990).

Cyr N., "*Polarization mode dispersion measurements: Generalization of the interferometric method to any mode coupling regime*," J. Lightwave Technol. **22**, pp. 794-805 (2004).

Cyr N., A. Girard and G. W. Schinn, "*Stokes parameter analysis method, the consolidated test method for PMD measurements*," Proc. of National Fiber Optics Engineers Conf. (NFOEC) **2**, p. 280 (1999).

D

Dal Forno A. O., A. Paradisi, R. Passy and J. P. von der Weid, "*Experimental and theoretical modelling of polarization-mode dispersion in singe-mode fibers*," IEEE Photon. Technol. Lett. **12**, pp. 296-298 (2000).

Damask J. N., "*Polarization Optics in Telecommunication*," first edition, Springer New York, (2005).

De Angelis C., A. Galtarossa, G. Gianello, F. Matera and M. Schiano, "*Time evolution of polarization mode dispersion in long terrestrial links*," J. Lightwave Technol. **10**, pp. 552-555 (1992).

De Lignie M. C., H. G. J. Nagel and M. O. van Deventer, "*Large polarization mode dispersion in fiber optic cables*," J. lightwave Technol. **12**, pp. 1325-1329 (1994).

Derickson D. (editor), "*Fibre optics test and measurement*," Prentice Hall Inc. UK, (1998).

E

Elbers J.-P., C. Glingener, M. Düser and E. Voges, "*Modelling of polarization mode dispersion in single mode fibres*," Electron. Lett. **33**, pp. 1894-1895 (1997).

Eyal A. and M. Tur, "*Measurement of polarization mode dispersion in systems having polarization dependent loss or gain*," IEEE Photon. Technol. Lett. **9**, pp. 1256-1258 (1997).

F

Fitzgerald J. and A. Dennis, "*Business Data Communications and Networking*," 7th Edition, John Wiley & Sons Incl. USA, (2002).

Forestieri E. and L. Vincetti, "*Exact evaluation of the Jones matrix of a fiber in the presence of polarization mode dispersion of any order*", J. Lightwave Technol. **20**, pp. 2204-2219 (2002).

Forestieri E. "*A fast and accurate method for evaluating joint second-order PMD statistics*," J. Lightwave Technol. **21**, pp. 2942-2952 (2003).

Foschini G. J., R. M. Jopson, L. E. Nelson and H. Kogelnik, "*The statistics of PMD-induced chromatics fiber dispersion*," J. Lightwave Technol. **17**, pp. 1560-1565 (1999).

Foschini G. J., L. E. Nelson, R. M. Jopson and H. Kogelnik, "*Probability density of second-order polarization including polarization chromatic fiber dispersion*," IEEE Photon. Technol. Lett. **12**, pp. 293-295 (2000).

Foschini G. J., L. E. Nelson, R. M. Jopson and H. Kogelnik, "*Statistics of second-order PMD depolarization*," J Lightwave Technol. **19**, pp. 1882-1886 (2001).

Foschini G. J. and C. D. Poole, "*Statistical theory of polarization mode dispersion in single mode fibres*," J. Lightwave Technol. **9**, pp. 1439-1456 (1991).

Francia C., F. Bruyére, D. Penninckx and M. Chbat, "*PMD second-order effects on pulse propagation in single-mode optical fibers*," IEEE Photon. Technol. **10**, pp. 1739-1741 (1998).

G

Gaillard P., M. Carratt, A. Gouronnec and G. Vuillaume, "*Extensive cabling effect analysis and determination of the PMD limit*," Proc. of International Wire and Cable Symposium (IWCS), November (1995).

Gallagher D, K. Emig, M. Ashby and M. Feodoroff, "*Cable and system PMD prediction*," Proc. of International Wire and Cable Symposium (ICWS), November (1995).

Galtarossa A., G. Gianello, C. G. Somade and M. Schiano, "*In field comparison among polarization mode dispersion measurement techniques*," J. Lightwave Technol. **14**, pp. 42-49 (1996).

Galtarossa A., D. Grosso, L. Palmieri and L. Schenato, "*Reflectometric chracterization of Hinges in Optical Fiber Links*," IEEE Photon. Technol. Lett. **20**, pp. 854-856 (2008).

Galtarossa A. and C. R. Menyuk (Editors), "*Optical Fiber Communication Reports*," Springer, New York, ISBN 0-387-23193-5, (2005).

Galtarossa A. and L. Palmieri, "*Relationship between pulse broadening due to polarisation mode dispersion and differential group delay in long singlemode fibres*," Elect. Lett. **34**, pp. 492-493 (1998).

Galtarossa A. and L. Palmieri, "*Theoretical analysis of reflectometric measurements in optical fiber links affected by polarization-dependent loss*," J. Lightwave Technol. **21**, pp. 1233-1241 (2003).

Galtarossa A. and L. Palmieri, "*Spatially resolved PMD measurements*," J. Lightwave Technol. **22**, pp. 1103-1115 (2004).

Galtarossa A. and L. Palmieri, "*Reflectometric measurements of polarization properties in optical-fiber links*," IEEE Trans. On Instrumentation and Measurement **53**, pp. 86-94 (2004b).

Galtarossa A. and L. Palmieri, A. Pizzinat, M. Schiano and T. Tambosso, "*Measurement of local beat length and differential group delay in installed single mode fibers*," J. Lightwave Technol. **18**, pp. 1389-1394 (2000).

Gibbon T. B., "*Polarization mode dispersion compensation in an optical fibre*," PhD Thesis, Nelson Mandela Metropolitan University (NMMU), (2007).

Gisin N., "*Polarization mode dispersion: Definitions, measurements and statistics*," Proc. of Symposium for Optical Fiber Measurement (SOFM), pp. 149-154 (1994).

Gisin N. and B. Huttner, "*Combined effects of polarization mode dispersion and polarization mode dispersion lossess in optical fibres*," Opt. Commun. **142**, pp. 119-125 (1997).

Gisin N., B. Gisin, J. P. Von Der Weid and R. Passy, "*How accurately can one measure a statistical quantity like polarization-mode dispersion?*," IEEE Photon. Technol. Lett. **8**, pp. 1671-1673 (1996).

Gisin N., R. Passy, J. C. Bishoff and B. Perny, **"***Experimental investigations of the statistical properties of polarization mode dispersion in single mode fibers*," IEEE Photon. Technol. Lett. **5**, pp. 819-821 (1993).

Gisin N. and J. P. Pellaux, "*Polarization mode dispersion: time versus frequency domains*," Opt. Commun. **89**, pp. 316-323 (1992).

Gisin N., J. P. von der Weid and J. P. Pellaux, "*Polarization mode dispersion of short and long single-mode fibers*," J Lightwave Technol. **9**, pp. 821-827 (1991).

Gleeson L., E. Sikora and M. J. O'Mahoney, "*Experimental and numerical investigation into the penalties induced by second order polarization mode dispersion at 10 Gb/s*," Proc. of European Conf. Optical Communication (ECOC) **1**, pp. 15-18 (1997).

Gordon J. P. and H. Kogelnik, "*Polarization mode dispersion in optical fibers*," Proc. of Natl. Acad. Sci. USA. **97**, pp. 4541-4550 (2000).

Gouronnec A., R. Goarin, M. Auvray and G. Le Moigne, "*Characterization of the environmental effects on the polarization mode dispersion (PMD) meausurements on G. 652 single mode,*" Proc. of International Cable and Wire Symposium (ICWS), November (1995).

Gregory L., "*Testing polarization mode dispersion (PMD) in the field*," JDSU whitepaper, (2006).

Gupta D., A. Kumar and K. Thyagrarajan, "*Effect of second-order polarization mode dispersion on the performance of polarization mode dispersion emulators*," Opt. Eng. **46**, pp. 085006-1 to 085006-6 (2007).

H

Hakki B. W., "*Polarization mode dispersion in a single mode fiber*," J. Lightwave Technol. **10**, pp. 2202-2208 (1996).

Hauer M. C., Q. Yu, E. R. Lyons, C. H. Lin, A. A. Au, H. P. Lee and A. E. Willner, "*Electrically controllable all-fiber PMD emulator using a compact array of thin-film microheaters*," J. Lightwave Technol. **22**, pp. 1059-1065 (2004).

Hayashi I., M. B. Oanish, P. W. Poy and S. Sumski, "*Junction lasers which operate continuosly at room temperature*," Appl. Phys. Lett. **17**, pp. 109-111 (1970).

Heffner B. L., "*Automated measurement of polarization mode dispersion using Jones matrix eigenanalysis*," IEEE Photon. Technol. Lett. **4**, pp. 1066-1069 (1992).

Hetch J., "*Understanding fibre optics*," third edition, Prentice Hall Inc. UK, (1999).

Hui D., W. Chong-Qing and F. Song-Nian, "*General demonstration of principal states of polarization and real-time monitoring of polarization mode dispersion in optical fibres*," Chin. Phys. Soc. and IOP Publ. Ltd **13**, pp. 1291-1295 (2004).

Huttner B., C. D. Barros, B. Gisin and N. Gisin, "*Polarization-induced pulse spreading in birefringent optical fibers with zero differential group delay*," Opt. Lett. **24**, pp. 370-372 (1999).

Huttner B., C. Geiser and N. Gisin, "*Polarization-induced distortions in optical fiber networks with polarization-mode dispersion and polarization-dependent losses*," IEEE J. Quantum Electron. **6**, pp. 317-329 (2000).

Huttner B. and N. Gisin, "*Anomalous pulse spreading in brifringent optical fibers with polarization-dependent loss*," Opt. Lett. **22**, pp. 504-507 (1997).

Huttner B., J. Reecht, N. Gisin, R. Passy, and J. von der Weid, "*Local birefringence measurements in single-mode fibers with coherent optical frequency-domian reflectometry*," IEEE Photon. Technol. Lett. **10**, pp. 1485-1460 (1998).

I

ITU G.691 Standard, "*G.691 optical interfaces for single-channel STM-64, STM-256 and other SDH systems with optical interfaces*," (1997).

J

Jopson R. M., L. E. Nelson and H. Kogelnik, "*Measurement of second-order polarization-mode dispersion vectors in optical fibers*," IEEE Photon. Technol. Lett. **11**, pp. 1153-1155 (1999).

K

Kaminow I., "*Polarization mode dispersion*," Optical Fiber Communications **IVB**, Academic Press USA, pp. 745-762 (2002).

Kapron F. P., D. B. Keck and R. D. Maurer, "*Radiation losses in glass optical waveguides*," Appl. Phys. Lett. **17**, pp. 423-425 (1970).

Karlsson M., "*Polarization mode dispersion-induced pulse broadening in optical fibres*," Opt. Lett. **23**, pp. 688-690 (1998).

Karlsson M. "*Probability density function of differential group delay in optical fiber communication systems*," J. Lightwave Technol. **19**, pp. 324-331 (2001).

Karlssom M. "*Geometrical interpretation od second-order PMD*," J. Lightwave Technol. **24**, pp. 643-651 (2006)

Karlsson M. and J. Brentel, "*Autocorrelation function of the polarization-mode dispersion vector*," Opt. Lett. **24**, pp. 939-941 (1999).

Karlsson M., J. Brentel and P. A. Andrekson, "*Long-term measurement of PMD and polarization drift in installed fibers*," J. Lightwave Technol. **18**, pp. 941-951 (2000).

Kasap S. O., "*Optoelectronics and Photonics: Principles and Practices*," Prentice Hall Inc. UK, (2001).

Kogelnik H., R. M. Jopson and L. E. Nelson, "*Polarization-mode dispersion*," Optical Fiber Telecommunications **IV B**, edited by I.P. Kaminow and T.Li, Academic Press USA, (2002).

Kogelnik H., P. J. Wizner, L. E. Nelson, R. M. Jopson, M. Borodisky, and M. Brodsky, "*First-order PMD outage for the Hinge model*," IEEE Photon. Technol. Lett., **17**, pp. 1208-2499 (2005).

Khosravani R., Jr. I. T. Lima, P. Ebrahimi, E. Ibragimov, A. E. Willner and C. R. Menyuk, "*Time and frequency domain characteristics of polarization-mode dispersion emulators*," IEEE Photon. Technol. Lett. **13**, pp. 127-129 (2001).

L

Lee J. H., M. S. Kim and Y. C. Chung, "*Statistical PMD emulator using variable DGD elements*," IEEE Photon. Technol. Lett. **15**, pp. 54-56 (2003).

Lefevre H. C., "*Single-mode fibre fractional wave devices and polarization controller*," Electron. Lett. **16**, pp. 778-780 (1980).

Leitch A. W. R., A. B. Conibear, T. Kroon and H. Coetzer, "*Polarization mode dispersion: A limiting factor os transmission rates through an optical fibre*," Proc. of Sothern African Telecommunication Networks and Applications Conference (SATNAC), 2-5 September (2001).

Li L., C. Wei and R. Yang, "*Effect of cabling process and installation on polarization mode dispersion*," Proc. of International Wire and Cable Symposium (IWCS), November (2000).

Lima I. T., R. Khosravani, P. Ebrahimi, E. Ibragimov, C. R. Menyuk and A. E. Willner, "*Comparison of polarization mode dispersion emulators*," J. Lightwave Technol. **19**, pp. 1872-1881 (2001).

Lizé Y., P. Lavoie, N. Godbout, S. Lacroix, R. Kashyap and L. Palmer, "*Novel first and second order polarization mode dispersion emulator*," Proc. of Optical Fiber Communication Conf. (OFC), paper OThT1 (2004).

M

Mabrouki A., M. Gadonna, A. Guoronnec, R. Goarin and R. Le Naour, "*Analysis of polarization mode dispersion of single mode elliptic-core optical fibers*," Opt. Commun. **149**, pp. 255-260 (1998).

Mecozzi A. and M. Shtaif, "*The statistics of polarization-dependent loss in optical communication systems*," IEEE Photon. Technol. Lett. **14**, pp. 313-315 (2002).

Marks B. S., I. T. Lima, C. R. Menyuk, "*Autocorrelation function for PMD emulators with rotators*," Proc. of Conf. on Lasers and Electro Optics (CLEO), paper CWH5 (2002).

Merker T., A. Scwarzbeck and P. Meissner, "*PMD compensation up to second order by tracking the principle states of polarization using a two-Section compensator*," Opt. Commun. **198**, pp. 41-47 (2001).

Mimura Y., "*A programmable second-order PMD emulator and precision PMD measurement system based on a variable Faraday rotator*," Digest of the Laser Elctro-Optics Soc. (LEOS) Summer Topical Meetings, paper TUB3.3 (2003).

Mimura Y., K. Ikeda, T. Hatano, T. Takagi, S. Wako and H. Matsuura, "PMD compensator and PMD emulator," Furukawa Rev. **24**, pp. 23-28 (2003).

Mudau E. A., "*Characterization of polarization effects on deployed aerial optical fibres in South Africa*," MSc Thesis, Nelson Mandela Metropolitan University (NMMU), (2008).

Muga N., A. Pinto and M. Ferreira," *The development of a PMD emulator*, Proc. of Confele'05, Tomar Portugal, (2005).

Musara V., "*Polarization studies of a light wave through an optical fibre*," MSc Dissertation, University of Zimbabwe, (2006).

Musara V., L. Wu, A. Leitch, S. Younsi and M. Zghal, "*Statistical characterization of first-order and second order polarization mode dispersion in a deployed buried optical fibre cable*," Proc. of IEEE Africon, pp. 1-6, September (2009).

Musara V., L. Wu and A. W. R. Leitch, "*A polarization mode dispersion emulator with tunable first-order PMD and constant second-order PMD*," Opt. Commun. **282**, pp. 3270-3274 (2009a).

Musara V., L. Wu, G. Pelaelo and A. W. R. Leitch, "*PMD emulation using polarization maintaining fibres: Fixed root-mean-square DGD but varying second-order PMD*," Rev. Sci. Instrum. **80**, pp. 1-5 (2009b).

N

Nelson L. E. and R. M. Jopson, "*Introduction to polarization mode dispersion in optical systems*," J. Opt. Fiber. Commun. **Rep. 1**, pp. 312-344 (2004).

Nelson L. E., R. M. Jopson, H. Kogelnik, and G. J. Foschini, "*Measurement of depolarization and scaling associated with second-order polarization mode dispersion in optical fibers*," IEEE Photon. Technol. Lett. **11,** pp. 1614-1616 (1999).

Nelson L. E., R. M. Jopson and H. Kogelnik, "*Polarization mode dispersion penalties associated with rotation of principal states of polarization in optical fiber*," Proc. of Optical Fiber Communication Conf. (OFC), paper ThB2 (2000).

Nelson L. E., M. Karlsson and D. Q. Chowdhury, "*Special issue on Polarization-Mode Dispersion*," J. Lightwave Technol. 22, pp. 951-952 (2004).

Noda J., K. Okamoto and Y. Sasaki, "Polarization-*maintaining fibers and their applications*," J. Lightwave Technol. **4**, pp. 1071-1089 (1986).

Noé R., D. Sandel, M. Yoshida-Dierolf, S. Hinz, V. Mirvoda, "*Polarization mode dispersion compensation at 10, 20 and 40 gb/s with various optical equalizers*," J. Lightwave Technol. **17**, pp. 1602-1616 (1999).

O

Odlysko A M. "*Internet traffic growth: Sources and implications*," University of Minnesota Digital Technology Centre (DTC) research report, pp.1-15 (2003).

Okoshi T. and K. Kukuchi, "*Coherent Optical Communications*," Tokyo-Dordrecht: KTK-Reidel Publishing Company, (1986).

Olson N. A., "*Lightwave systems with optical amplifiers*," J. Lightwave Technol. **7**, pp. 1071-1082 (1989).

Ono T., S. Y. Yamazaki, H. Shimizu and S. Emura, "*Polarization control method for suppressing polarization mode dispersion influence in optical transmission systems*," J. Lightwave Technol. **12**, pp. 891-898 (1994).

P

Palmer L., S. D. Dods and P. M. Farrell, "*Broad-band concatenated-Section PMD emulator design for low interchannel correlation*," IEEE Photon. Technol. Lett. **17**, pp. 1019-1021 (2005).

Pelaelo G., "*Characterization of polarization depent loss in optical fibres and optical components in the presence of polarization mode dispersion*," MSc Thesis, Nelson Mandela Metropolitan University, (2008).

Phua P. B. and H. A. Haus, "*Variable second-order PMD module without first-order PMD*," J Lightwave Technol. **20**, pp. 1951-1956 (2002).

Phua P. B. and E. P. Ippen, "*Combinatorial polarization scramblers for many-segment PMD emulator*," IEEE Photon. Technol. Lett. **17**, pp. 405-407 (2005).

Poole C. D. and D. L. Favin, "*Polarization-mode dispersion measurements based on transmission spectra through a polarizer*," J. Lightwave Technol. **12**, pp. 917-929 (1994).

Poole C. D. and C. R. Giles, "*Polarization-dependent pulse compression and broadening due to polarization dispersion in dispersion-shifted fiber*," Opt. Lett. **13**, pp. 155-157 (1988).

Poole C. D., J. H. Winters and J. A. Nagel, "*Dynamical equation for polarization dispersion*," Opt. Lett. **16**, pp. 372-374 (1991).

Poole C. D. and J. A. Nagel, "*Polarization effects in lightwave systems*," Optical Fiber Telecommunication **IIIA**, edited by I. P. Kaminow and K. T. Koch, Academic Press USA, (1997).

Poole C. D. and R. E. Wagner, "*Phenomenological approach to polarization dispersion in long single-mode fibres*," Electron. Lett., **22**, pp. 1029-1030 (1986).

R

Raja M. Y. A. and S. K. Arabasi, "*Design and simulations of a dynamic polarization-mode dispersion compensator for long-haul optical networks*," Opt. Exp. **11**, pp. 1166-1174 (2003).

Rashleigh S. C., "*Origins and control of polarization effects in single-mode fibers*," J. Lightwave Technol. **1**, pp 312-331 (1983).

Rashleigh S. C. and Ulrich R, "*Polarization mode dispersion in single-mode fibre*," Opt. Lett. **3**, pp. 60.62 (1978).

Roberge R. "*Case Study: PMD Measurement on aerial fiber under wind-induced oscillations and vibrations*," Next Generation Network Assessment, EXFO Technical Note **039**, (2009).

Rochford K., "*Polarization and Polarimetry*," third edition, Encyclopaedia of Physical Science and Technology, (2004).

Rogers A. J., "*Polarization-optical time domain reflectometry: A technique for the measurement of field distribution*," Appl. Opt. **20**, pp. 1060-1074 (1981).

S

Schinn G. W., "*Polarization and the patchcord*," EXFO Technical Note **008**, (2003).

Shtaif M., A. Mecozzi, M. Tur and J. A. Nagel, "*A compensator for the effects of high-order polarization mode dispersion in optical fibers*," IEEE Photon. Technol. Lett. **12**, pp.434-436 (2000).

Sibaya N. A., "*Evaluation of polarization mode dispersion in the South African optical fibre network*," MSc Dissertation, Nelson Mandela Metropolitan University, (2004).

Steinkamp A. and E. Voges, "*Higher order polarization-mode dispersion in the presence of polarization-dependent loss in optical fiber systems*," IEEE Photon. Technol. Lett. **19**, pp. 124-126 (2007).

Sunnerud H., X. Chongjin, M. Karlsson, R. Samuelsson and P. A. Andrekson, "*A comparison between different PMD compensation techniques*," J. Lightwave Technol. **20**, pp. 368-378 (2002).

T

Tomita A. and R. Y. Chiao, "*Observation of Berry's topological phase by use of an optical fiber*," Phys. Rev. Lett. **57**, pp. 937-940 (1986).

Tomita S., M. Kawase, T. Shinohara, H. Fuchigami, "*Suppression of galloping oscillations for a self-supporting optical fibre*," J. Lightwave Technol. **6**, pp.186-190, (1988)

TIA/EIA-455-157, "*Measurement of polarization dependent loss (PDL) of single mode fibre optics components*," Telecommunications Industry Association (TIA) Std., (1995).

TIA/EIA 455-124-A (FOTP-124A), "*Polarization mode dispersion measurement for single mode optical fibres by interferometry*," Telecommunciation Industry Association (TIA) Std., (2004).

U

Ulrich R., S. C. Rashleigh and W. Eickhoff, "*Bending induced birefringence in single mode fibers*," Opt. Lett. **5**, pp. 273-275 (1980).

V

Van Antwerpen U., A. B. Conibear and A. W. R. Leitch, "*On the variability of polarization mode dispersion*," Proc. of South African Telecommunication Networks and Application Conference (SATNAC), September (2002).

Van Antwerpen U., "*The influence of cabling on the polarization mode dispersion of an optical fibre*," MSc Dissertation, Nelson Mandela Metropolitan University, (2004).

W

Waddy D. S., L. Chen and X. Bao, "*Polarization effects in aerial fibers*," Opt. Fiber Technol. **11**, pp. 1-19 (2005).

Waddy D. S. , P. Lu, L. Chen, X. Bao, "*Fast state of polarization changes in aerial fiber under different climatic conditions*," Photon. Technol. Lett. **13**, pp. 1035-1037 (2001).

Wegmuller M., S. Demma, C. Vinegoni and N. Gisin, "*Emualtor of first- and second-order polarization mode dispersion*," IEEE Photon. Technol. Lett. **14**, pp. 630-632 (2002).

Williams P. A., "*Mode-coupling artifact standard for polarization-mode-dispersion: design, assembly, and implementation*," Appl. Opt. **38**, pp. 6498-6507 (1999).

Williams P. A., "*Modulation phase-shift measurement of PMD using only four launched polarization states: a new algorithm*," Electron. Lett. **35**, pp. 1578-1579 (1999a).

Williams P. A., "*PMD measurement techniques and how to avoid pitfalls*," J. Opt. Fibre. Commun. **Rep. 1**, pp. 84-105 (2004).

Willner A. E. and M. C. Hauer, "*PMD emulation*," J. Opt. Fiber. Commun. **Rep. 1**., pp. 181-200 (2004).

Willner A. E., S. M. R. M. Nezam, L. Yan, Z. Pan and M. C. Hauer, "*Monitoring and control of polarization-related impairments in optical fiber systems*," J. Lightwave Technol. **22**, pp. 106-125 (2004).

Winters J. H. and M. A. Santoro, "*Electrical signal processing techniques in long-haul fiber-optic systems*," IEEE Trans. Commun. **38**, pp. 1439-1453 (1990).

Wu L., V. Musara, M. C. Mangka and A. W. R. Leitch, "*Making reliable PMD measurements: The importance of polarization scrambling*," Proc. of SATNAC, September (2006).

Wuilpart M., C. Crunelle and P. Mégret, "*High dynamic polarization-OTDR for the PMD mapping in optical fiber links*," Opt. Commun. **269**, pp. 315-321 (2007).

Wuttke J., P. M. Krummrich and J. Rösch, "*Polarization oscillations in aerial fiber caused by wind and power-line current*," IEEE Photon. Technol. Lett. **15**, pp. 882-884 (2003).

Y

Yamamoto S., N. Edagawa, H. Taga, Y. Yoshida and H. Wakabayashi, "*Observation of BER degradation due to fading in long distance optical amplifier system*," Electron. Lett. **29**, pp. 209-210 (1989).

Yan L.-S., M. C. Hauers, C. Yeh, G. Yang, L. Lin, Z. Chen, Y. Q. Shi, X. S. Yao, A. E. Willner and W. L. Kath, "*High-speed, stable and repeatable PMD emulator with tunable statistics*," Proc. of Optical Fiber Communication Conf. (OFC), paper MF6 (2003).

Yan L., M. C. Hauer, Y. Shi, X. S. Yao, P. Ebrahimi, Y. Wang, A. E. Willner and W. L. Kath, "*Polarization-mode-dispersion emulator using variable differential-group-delay (DGD) elements and its use for experimental importance sampling*," J. lightwave Technol. **22**, pp. 1051-1058 (2004).

Yan L. –S., X. S. Yao and A. E. Willner, "*Enabling Hinge Model in polarization-mode-dispersion statistics using variable differential-group-delay-based emulator*," IEEE Photon. Technol. Lett. **18**, pp. 427-429 (2006).

Yan L., C. Yeh, G. Yang, L. Lin, Z. Chen, Y. Q. Shi, A. E. Willner and X. S. Yao, "*Programmable group-delay module using binary polarization switched*," J. Lightwave Technol. **21**, pp. 1676-1684 (2003a).

Yan L. S., Q. Yu, Y. Xie and A. E. Willner, "*Demonstration of in-line monitoring and compensation of polarization-dependent loss for multiple channels*," IEEE Photon. Technol. Lett. **14**, pp. 864-866 (2002).

Yan L. –S., B. Zhang, X. Steve Yao, A. E. Wilner, "*Reducing the number of polarization controllers in all-fiber polarization-mode-dispersion emulators using polarization maintaining fiber sub-Sections with unequal lengths*," Opt. Fiber Technol. **14**, pp. 172-175 (2008).

Yang S., L. Chen and X. Bao, "*Wavelength dependence study on the transmission characteristics of the concatenated polarization dependent loss and polarization mode dispersion elements*," Opt. Eng. **44**, pp. 115006-1 to 115006-5 (2005).

Younsi S., V. Musara, T. B. Gibbon, L. Wu, M. Zghal and A. W. R. Leitch, "*Frequency domain characterization of an experimental and simulated polarization mode dispersion emulator design*," Proc. of SATNAC, September (2007).

Yu Q., L. Yan, S. Lee, Y. Xie, M. Hauer, Z. Pan and A. E. Willner, "*Enhanced higher-order PMD compensation using a variable time delay between polarization*," Proc. of European Conf. Optical Communication (ECOC) **II**, pp. 47-48 (2000).

Z

Zalevsky Z. and V. Eckhouse, "*Polarization-mode dispersion manipulation using periodic polarization modulation,*"J. Opt. A: Pure Appli. Opt. **6**, pp. 862-864 (2004).

Zeng K. C. "*A PMD emulator with tunable second-order PMD and constant mean first-order DGD,*" IEEE Photon. Technol. Lett. **15**, pp. 1150-1152 (2003).

Zhang L., Y. Z. Xu, Q. G. Hu, S. Z. Zhao and S. H. Liu, "*Effect of chromatic dispersion and initial chip on the DOP feedback signal in PMD compensation,*" IEEE Photon. Technol. Lett. **17**, pp. 342-344 (2005).

Zheng Y., B. Yang and X. Zhang, "*Three-stage polarization mode dispersion compensator capable for compensating second-order polarization mode dispersion,*" IEEE Photon. Technol. Lett. **14**, pp. 1412-1414 (2002).